AD-A050 006 AIR FORCE INST OF TECH WRIGHT-PATTERSON AFB OHIO F/G 7/4
COMPARISON OF HEAVY ION-INDUCED K-ALPHA X-RAY SATELLITE SPECTRA--ETC(U)
DEC 77 J A DEMAREST
UNCLASSIFIED AFIT-CI-78-31 NL

1 OF 2
AD
A050 006

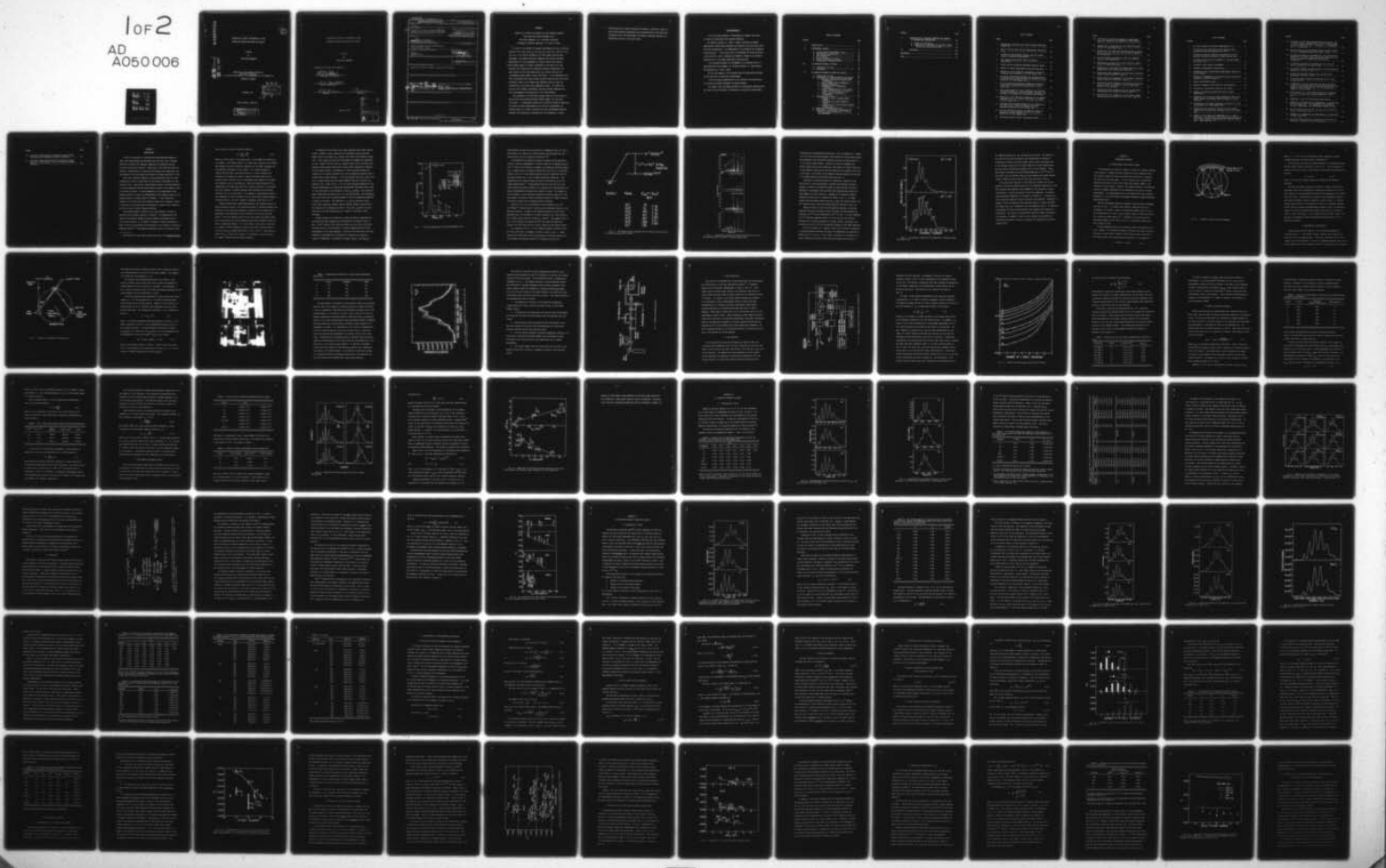

COMPARISON OF HEAVY ION-INDUCED Kα X-RAY SATELLITE SPECTRA FROM GASES AND SOLIDS

A Thesis

by

JOHN ALLEN DEMAREST

Submitted to the Graduate College of
Texas A&M University
in partial fulfillment of the requirement for the degree of

MASTER OF SCIENCE

December 1977

Major Subject: Chemistry

COMPARISON OF HEAVY ION-INDUCED Kα X-RAY SATELLITE SPECTRA FROM GASES AND SOLIDS

A Thesis

by

JOHN ALLEN DEMAREST

Approved as to style and content by:

R. L. Watson
(Chairman of Committee)

G. S. Mantell
(Head of Department)

R. B. Hedges
(Member)

J. Reading
(Member)

December 1977

UNCLASSIFIED
SECURITY CLASSIFICATION OF THIS PAGE (When Data Entered)

REPORT DOCUMENTATION PAGE

READ INSTRUCTIONS BEFORE COMPLETING FORM

1. REPORT NUMBER: CI-78-31
2. GOVT ACCESSION NO.
3. RECIPIENT'S CATALOG NUMBER
4. TITLE (and Subtitle): (6) Comparison of Heavy Ion-Induced K-alpha (Ka) X-Ray Satellite Spectra from Gases and Solids.
5. TYPE OF REPORT & PERIOD COVERED: (9) Master's thesis, Thesis
6. PERFORMING ORG. REPORT NUMBER: (14) AFIT-CI-78-31
7. AUTHOR(s): (10) [redacted] John A. Demarest
8. CONTRACT OR GRANT NUMBER(s)
9. PERFORMING ORGANIZATION NAME AND ADDRESS: AFIT/CI Student at Texas A&M University, College Station, Texas
10. PROGRAM ELEMENT, PROJECT, TASK AREA & WORK UNIT NUMBERS
11. CONTROLLING OFFICE NAME AND ADDRESS: AFIT/CI, WPAFB OH 45433
12. REPORT DATE: (11) December 1977
13. NUMBER OF PAGES: 112 Pages (12) 124 p.
14. MONITORING AGENCY NAME & ADDRESS (if different from Controlling Office)
15. SECURITY CLASS. (of this report): Unclassified
15a. DECLASSIFICATION/DOWNGRADING SCHEDULE
16. DISTRIBUTION STATEMENT (of this Report): Approved for Public Release; Distribution Unlimited
17. DISTRIBUTION STATEMENT (of the abstract entered in Block 20, if different from Report)
18. SUPPLEMENTARY NOTES: APPROVED FOR PUBLIC RELEASE AFR 190-17.
For James E. Skarstein MSgt USAF Deputy Director of Information
JERRAL F. GUESS, Captain, USAF
Director of Information, AFIT
19. KEY WORDS (Continue on reverse side if necessary and identify by block number)
20. ABSTRACT (Continue on reverse side if necessary and identify by block number)

012 200

DD FORM 1 JAN 73 1473 EDITION OF 1 NOV 65 IS OBSOLETE

UNCLASSIFIED
SECURITY CLASSIFICATION OF THIS PAGE (When Data Entered)

ABSTRACT

Comparison of Heavy Ion-Induced Kα X-ray Satellite Spectra from Gases and Solids.(December 1977)

John Allen Demarest, B.S., Syracuse University

Chairman of Advisory Committee: Dr. Rand L. Watson

A study of the effects of chemical environment on the Kα satellite spectra of Si, SiF_4, SiH_4, P_4, S_8, SF_6, SO_2, H_2S, NaCl, KCl(Cl), CCl_4, Cl_2, HCl, Ar and KCl(K) excited by 32.4 MeV oxygen ions has been performed. The present data were compared with earlier extensive measurements on solid compounds of silicon, sulfur and chlorine. The average degree of L-shell ionization at the time of Kα x-ray emission (as reflected by the satellite relative intensities) are much higher for the light gases SiH_4, H_2S, and HCl than for the corresponding heavy gases, solids, and liquid. It was determined from their correlation with local valence electron density that the L-shell ionization states do not depend upon physical state but upon the availability of electrons from neighboring atoms. For atoms with electron rich ligands, interatomic electron transfer dominates the fast rearrangement occurring prior to Kα x-ray emission.

The comparison of Kα satellite energy shifts with the results of Hartree-Fock calculations provided further support for the above conclusions. A theoretical prediction of multiple ionization employing the binary encounter approximation was found to overestimate the observed degree of L-shell ionization but that considerably improved agreement was obtained by accounting for the increases in L-shell

binding energy as L-shell electrons are removed. Various Kα satellite peak width broadening mechanisms were considered and it was found that broadening due to the distribution of M-shell vacancies accounts for a significant portion of the total width.

ACKNOWLEDGEMENTS

It is with great pleasure I acknowledge the support and advice of those who helped make this research possible.

My research advisor, Dr. Rand L. Watson, deserves my deepest appreciation without whose guidance and direction this work would never have been accomplished. My indebtedness to his guidance and friendship exceeds measure. I would also like to acknowledge the great privilege to have had Drs. John F. Reading and Richard M. Hedges on my graduate committee and to the great inspiration they provided.

I am sincerely grateful to the members of my research group, in particular Miss Alice Leeper, Mr. Jeffery Sjurseth, Mr. Mark Michael, and especially Dr. John R. White.

The aid and support I have received from the operations personnel at the Cyclotron is gratefully acknowledged.

I am particularly appreciative of the affection and perseverance of my wife and family throughout my degree program.

The support from the Energy Research and Development Administration and the Air Force Institute of Technology is gratefully acknowledged.

TABLE OF CONTENTS

LIST OF TABLES

LIST OF FIGURES

FIGURE Page

FIGURE Page

CHAPTER I

INTRODUCTION

Since the discovery of x radiation by Wilhelm-Konrad Röntgen in 1895, x-ray spectroscopy has developed over the years into a valuable method for studying the elemental composition of materials and the electronic structure of matter.[1] Early work in the 1920s and 1930s was aimed at a determination of inner-electron energy level separations and culminated in the x-ray energy-level tables of Bearden and Burr[2] in 1967.

Many other important aspects of x-ray spectroscopy have also been studied, one of which is the effect of the chemical environment on x-ray emission lines. Line shifts, called chemical shifts, have been observed in various compounds and have been directly related to the chemical state of the atoms involved. To give perspective to the magnitudes of the chemical shifts of x-rays, an understanding of the chemical shifts of the binding energies of atomic levels is helpful. In this discussion, elements of the third row of the periodic table are of principle interest so that the K- and L-shell may be considered to contain "core" electrons while the M-shell involves valence electrons.

The binding energy is defined as the work required to remove an electron from its atomic orbital to infinity.[3] To understand how the removal of peripheral valence electrons affects the binding energy of inner shell electrons, it is useful to consider a simple electrostatic model in which the electrons are distributed on the surfaces of concentric spherical shells.[4,5] The repulsive potential felt by an electron inside

---

The citations in this thesis follow the style of the Physical Review.

such a shell is given by classical theory as

$$U_i = \frac{1}{4\pi\varepsilon_o} \frac{ne^2}{r_i} \qquad (1.1)$$

where r_i is the radius of the sphere and n is the number of electrons on its surface. The binding energy of an inner shell electron is the difference between the sum of repulsive potentials of the other electrons and the attractive potential of the nucleus. If a valence electron is removed from the atom, the binding energy of a "core" electron will increase by the amount U/n (with r_i equal to the mean radius of the valence electron orbital) due to a decrease by this amount in the repulsive potential felt by the electron. Hence the binding energies of an ionized atom are larger than those for a neutral atom and it is expected that the increases in binding energies with ionization will be nearly identical for the K- and L-shell. For example, a photoelectron study of nine compounds of sulfur[4] indicate that the inner shell binding energies increase by about 7 eV over a change in oxidation state from 2^- to 6^+.

Whereas photoelectron spectroscopy measures the binding energies of bound electrons directly, x-ray emission involves a transition between two electronic levels and thus the photon is emitted with an energy that is determined by the difference in the energies of the inital and final states. Since the chemical shifts of the inner shells are nearly identical, x-ray chemical shifts are generally quite small (normally almost an order of magnitude smaller).[1] An illustration of this fact is provided by a study of sulfur compounds in which it was found that the chemical shift of the $K\alpha_{1,2}$ doublet varied from 0.14 to 1.19 eV.[6] Since chemical shifts of $K\alpha_{1,2}$ x-rays are so small it is difficult to use this effect as a means of characterizing chemical bonding.

In addition to the normal x-ray lines resulting from single vacancy states, a number of other satellite or non-diagram lines on the high energy side of the normal $K\alpha_{1,2}$ doublet also result from multiple ionization. X-ray satellites were first discovered by Siegbahn and Stenström[7] in 1916. Wenzel[8] was the first to interpret these lines as arising from multiply ionized states having one or more L-shell vacancies in addition to one K-shell vacancy. The absence of L-shell electrons reduces the screening of the nuclear potential felt by the remaining electrons and increases their binding energies. A Kα x-ray emitted from such a state will be at a higher energy than the normal diagram lines and is called a Kα satellite line. Shown in Fig. 1 is a Kα x-ray spectrum produced by 6 keV electron bombardment of Al which was reconstructed from data given in Ref. 9. The first peak in this spectrum is the $K\alpha_{1,2}$ doublet. Five satellite peaks (identified by arrows in Fig. 1) are also observed. The interpretation of the first set of satellite peaks as given by Kennard and Ramberg[10] is shown in the inset. The observed α', α_3, and α_4 satellite x-rays result from transitions between various multiplet states resulting from the coupling of two unpaired electrons. The α_5 and α_6 peaks are satellites due to initial configurations of single K- and double L-shell vacancies.

Recent studies of Kα satellites of various chemical compounds have indicated that their energies are influenced by the chemical environment. Chun[11] reported that chemical effects are more easily recognized by energy shifts in Kα satellites of fluorine compounds than by Auger measurements of the same compounds. Satellite line shifts have also been compared to semi-empirical calculations to determine the effective charge of phosphorus in compounds of NaH_2PO_2, Na_2HPO_3, and NaH_2PO_4.[11]

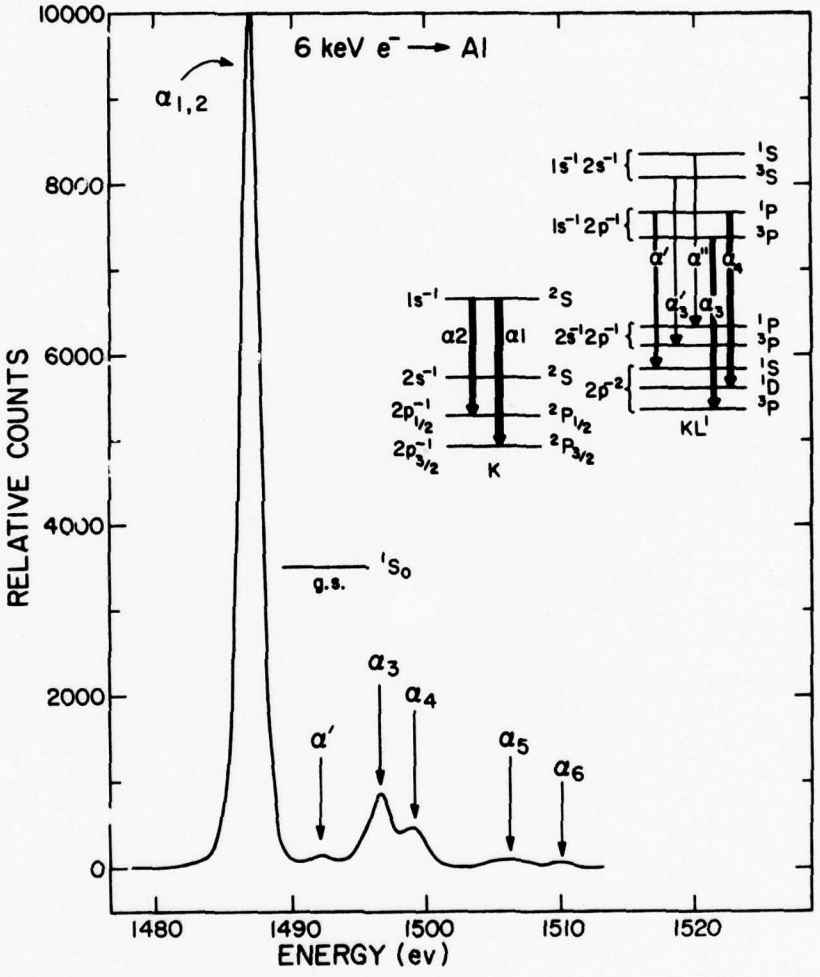

FIG. 1. Kα x-rays produced by electron bombardment of Al.

The multiplet structure of Kα satellites of compounds of Mg, Al, and Si were found to be sensitive to binding effects and displayed not only energy shifts but also intensity variations.[12,13]

The mechanism for producing multiple ionization during photoionization or electron bombardment is electron shake off or monopole excitation.[14] When a core electron is removed, the remaining electrons experience a sudden change in effective charge due to the loss of a shielding electron and this in turn induces another electron transition into the continuum (shake off) or into a higher bound state (shake up). The probabilities for electron shake off can be calculated by use of the sudden approximation.[15] These probabilities are quite low for inner shell electrons and hence studies of Kα satellites by photoionization or electron bombardment have been quite limited in scope. In contrast to the low degree of core ionization produced by electron shake off is the high degree of multiple L-shell ionization produced in K-shell ionizing collisions by heavy ions of energies around 1 MeV/amu.

Shown in Fig. 2 is an illustration of the production of a KL^n $[1s^{-1}(2s2p)^{-n}]$ vacancy state in sulfur and its subsequent decay by x-ray satellite emission. Because of the reduced screening of the nuclear potential due to the absence of nL-shell electrons, the x-ray satellite has a higher energy than the normal $K\alpha_{1,2}$ doublet. The example given in Fig. 2 also displays the energy shifts of the satellite peaks with respect to the KL^0 peak and the relative energy spacings between peaks.

Not considered in Fig. 2 is the complex multiplet structure of the KL^n x-ray satellites, an example of which is shown in Fig. 3. These spectra were constructed using the theoretical fluorescence yields and line energies calculated by Bhalla[16] by assuming that each KL^n

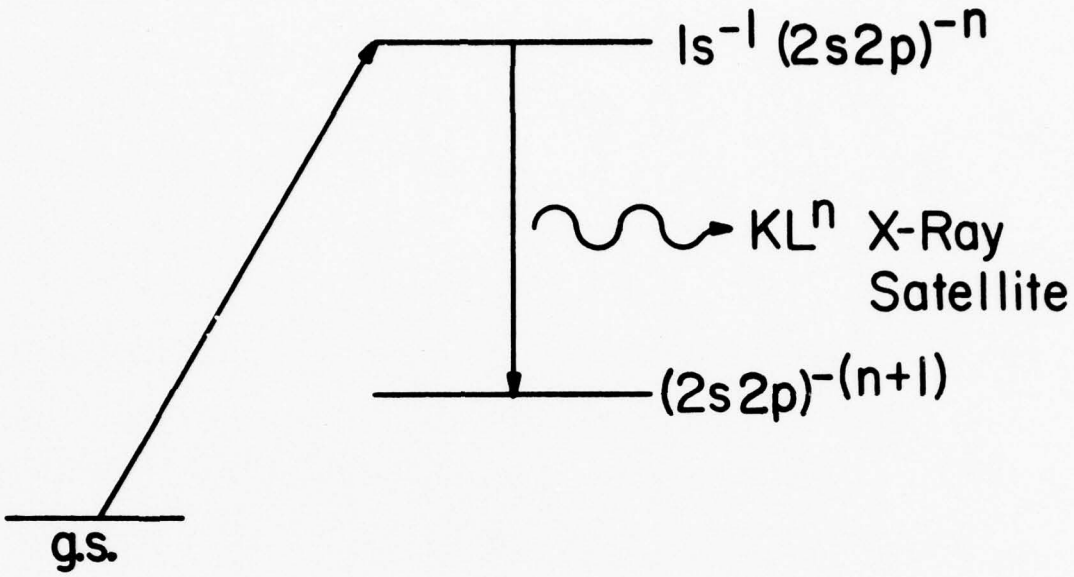

Sulfur:	Peak	$E_{KL^n} - E_{KL^0}$ (eV)	
	KL^1	15	] 16
	KL^2	31	] 18
	KL^3	49	] 18
	KL^4	67	] 20
	KL^5	87	] 21
	KL^6	108	] 24
	KL^7	132	

FIG. 2. KL^n vacancy state production and Kα satellite peak energies and relative spacings for sulfur.

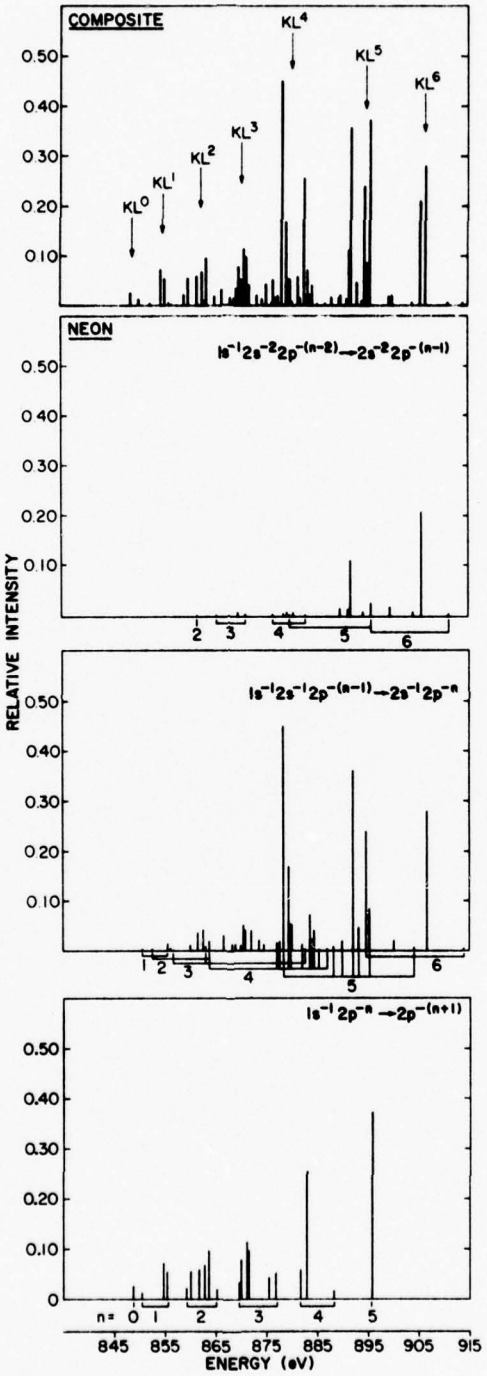

FIG. 3. Theoretical relative intensity distribution of the Kα satellite multiplet structure of highly ionized neon.

configuration was populated statistically. The top spectrum is a composite of all the predicted multiplet lines whereas the three bottom spectra show separately the transitions resulting from the various possible 1s 2s 2p initial vacancy states. Spectra for third row elements are further complicated by the inclusion of the effect of M-shell vacancies. In the composite spectrum the various transitions are grouped into a set of KL^n peaks. The arrows in the composite spectrum display the position of the experimentally resolved KL^n peaks from Ref. 17.

Typically, the energy resolution of heavy-ion induced Kα x-ray spectra has not been good enough to resolve the multiplet structure. Instead, a series of Kα satellite peaks are observed each of which is composed of overlapping lines arising from configurations having the same number of L-shell vacancies. Examples of Kα satellite spectra produced by heavy ions of 2 MeV/amu are shown in Fig. 4. In these spectra the first peak contains the $K\alpha_{1,2}$ lines, the second contains the KL^1 satellite lines, the third contains the KL^2 satellite lines, etc.

Chemical shifts in the Kα and Kβ satellite energies of aluminum compounds excited by hydrogen, helium, and neon ions were observed by Richard et al.,[18] and by Burkhalter et al.[19] in 1972. In 1974, McWherter et al.[20] observed chemical shifts of 1 eV or less for Kα satellite energies of Si and SiO_2 produced by hydrogen, helium, and oxygen ions and shifts of up to 8 eV for Kβ satellite energies of the same compounds.

The first evidence of a chemical effect on the relative intensities of satellite peaks resulting from heavy ion bombardment was reported by Watson et al.[21] in 1975. In this study, variations in the degree of L-shell ionization for sulfur atoms excited by oxygen and neon ions in

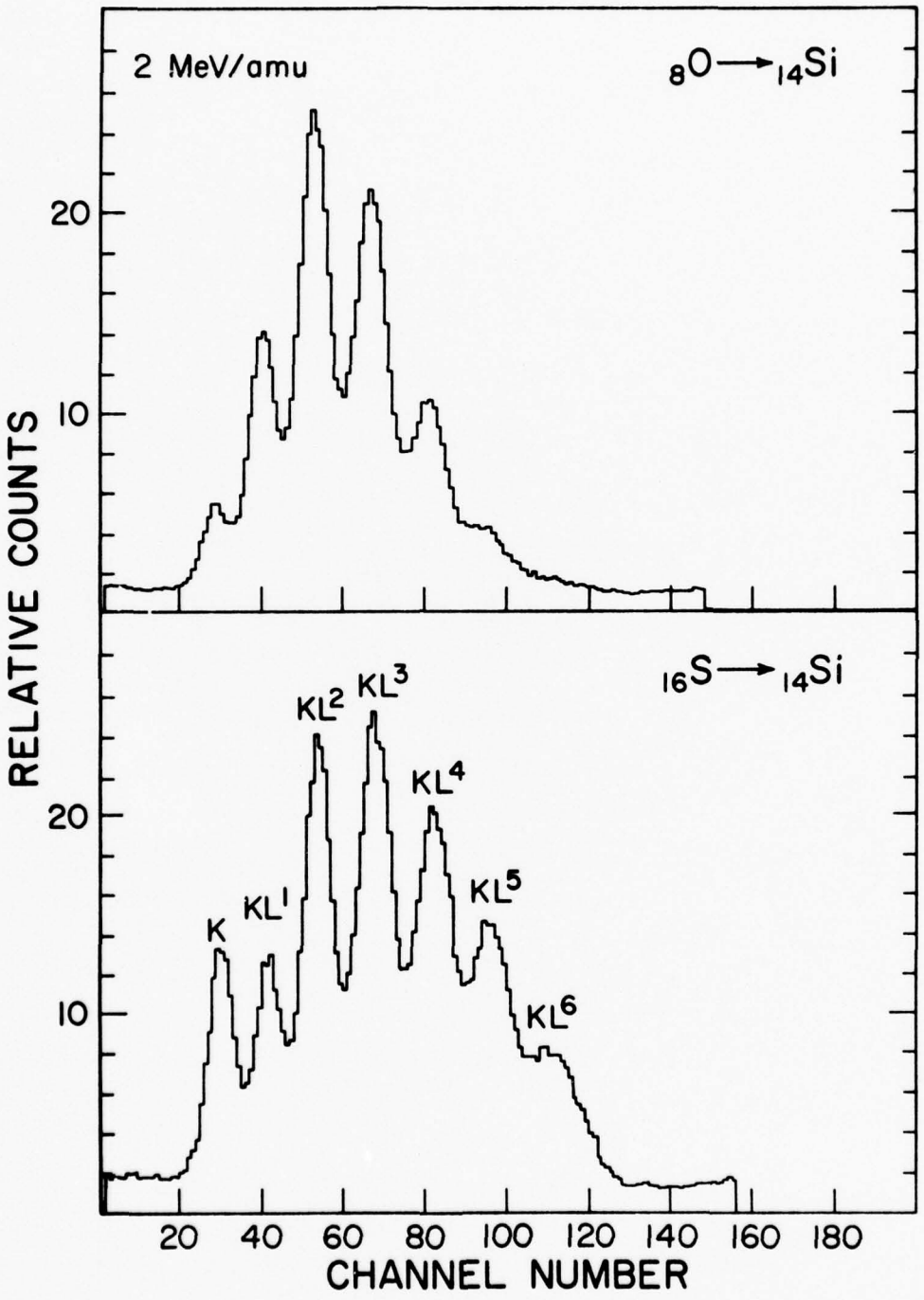

FIG. 4. Kα satellite spectra of Si produced by 2 MeV/amu oxygen and sulfur ions.

the compounds Na_2SO_4, S_8, ZnS, and Na_2S were observed. The changes in the relative satellite intensities were interpreted as evidence of interatomic L-vacancy filling processes, where valence electrons that on the average reside near the ligand atoms fill K- and L-vacancies in the host atom and effectively compete with Kα x-ray emission. Other measurements performed on several gaseous compounds of Si[22,23] and S[23] have shown that the hydrides (SiH_4 and H_2S) display much higher average L-shell ionization states than do SiF_4, SF_6 and solid Si and S_8.

The current work reported in this thesis was carried out for the purpose of further delineating the role of interatomic transitions in the fast electron rearrangement that precedes Kα x-ray emission in highly ionized gases, liquids and solids of third row compounds. The experimental procedures employed are discussed in Chapter II. In Chapter III the Kα satellite spectra of third row solids are discussed. Presented in Chapter IV are the features of Kα satellite spectra of third row gases and liquid CCl_4, and a comparison with corresponding solids. In addition, the measured Kα satellite distributions are compared with theoretical predictions. The results of Hartree-Fock satellite energy calculations are presented in Chapter V where they are applied to the problem of estimating the degree of M-shell ionization from measured Kα satellite energy shifts.

CHAPTER II

EXPERIMENTAL METHODS

A. Curved-Crystal Spectrometer System

The measurement of heavy-ion induced Kα satellite intensity distributions requires a compact detection system that can be operated within the cyclotron beam line vacuum with sufficient resolution to separate the various Kα satellite peaks. A Si(Li) detector with a resolution capability typically of 180 eV full width half maximum (FWHM) is not suitable for this purpose. However, with proper selection of reflecting crystals, adequate resolution can be obtained by the use of a crystal spectrometer. The spectrometer used in the present work was a recently acquired 12.7 cm curved-crystal spectrometer designed by Applied Research Laboratories (ARL).

The ARL spectrometer employs a Johansson curved-crystal arrangement as shown in Fig. 5. To obtain ideal focusing conditions with this arrangement, the target, crystal, and detection element must all lie on the circumference of a focal circle (Rowland circle) of radius R/2 while the crystal must have radius R.[24] In addition, the crystal must be everywhere tangent to the focal circle (i.e. the crystal surface must have a radius of R/2).

At first appearance these two conditions seem to be mutually exclusive. However, the Johansson arrangement satisfies both radii criteria by utilizing a crystal bent to radius R with a face ground to radius R/2. The target-crystal and crystal-detector distances, D, are equal and

$$D = n\lambda R/2d = R \sin \theta \qquad (2.1)$$

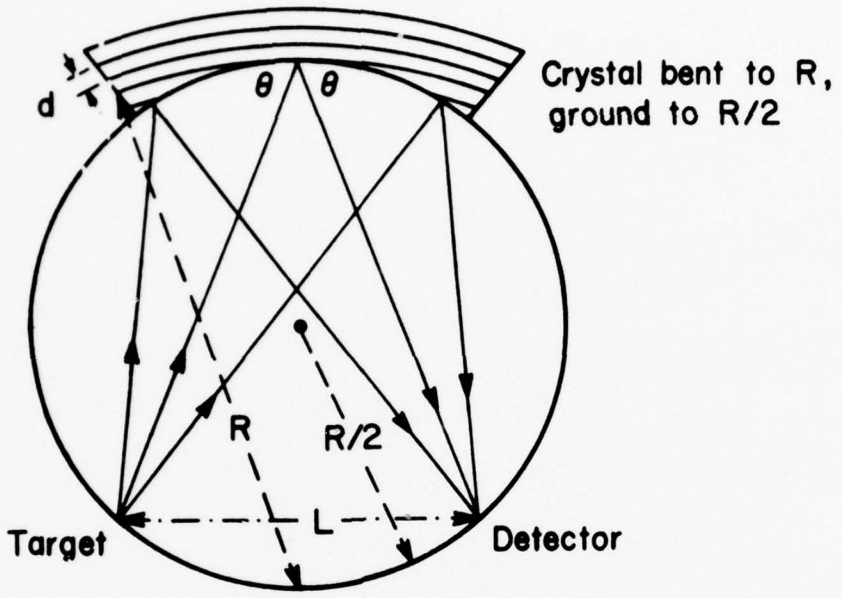

FIG. 5. Johansson curved-crystal arrangement.

where n, λ , d, and θ are the diffraction order, wavelength, crystal interplanar spacing, and Bragg angle, respectively.[25]

The ARL design provides for crystal movement in a straight line away from the target thereby increasing D in Eq. (2.1). For the detector to remain on the focal circle, it must move on an epicycloid path having the equation

$$L = R \sin \theta \qquad (2.2)$$

where L is the direct distance between the target and the detector aperature.

The ARL spectrometer design also provides a remotely driven linear wavelength range that corresponds to a Bragg angle range of 14.4°-71.8°. Other features of the spectrometer include fine adjustments to the crystal and focal circle. Modifications were made to the spectrometer system so that these adjustments could be operated by remote control. A rotating crystal mount allows for the selection of one of two different crystals without having to disturb the spectrometer chamber vacuum. The detection element is a gas flow proportional counter which contains a fixed slit width of 0.020" and holds a 1.5 cm^3 volume of P-10 gas (90% - Argon - 10% Methane) at atmospheric pressure separated from the vacuum by a 0.530 mg/cm^2 mylar window.

B. Experimental Configuration

The beam line geometry employed in the present measurements is indicated in Fig. 6. The target, crystal, detector, and cyclotron ion beam all lie in a horizontal plane. X-rays are observed at 142.5° with respect to the beam direction. Two sets of quadrupole magnets and a series of collimators were used to optically focus the ion beam onto a fluorescent

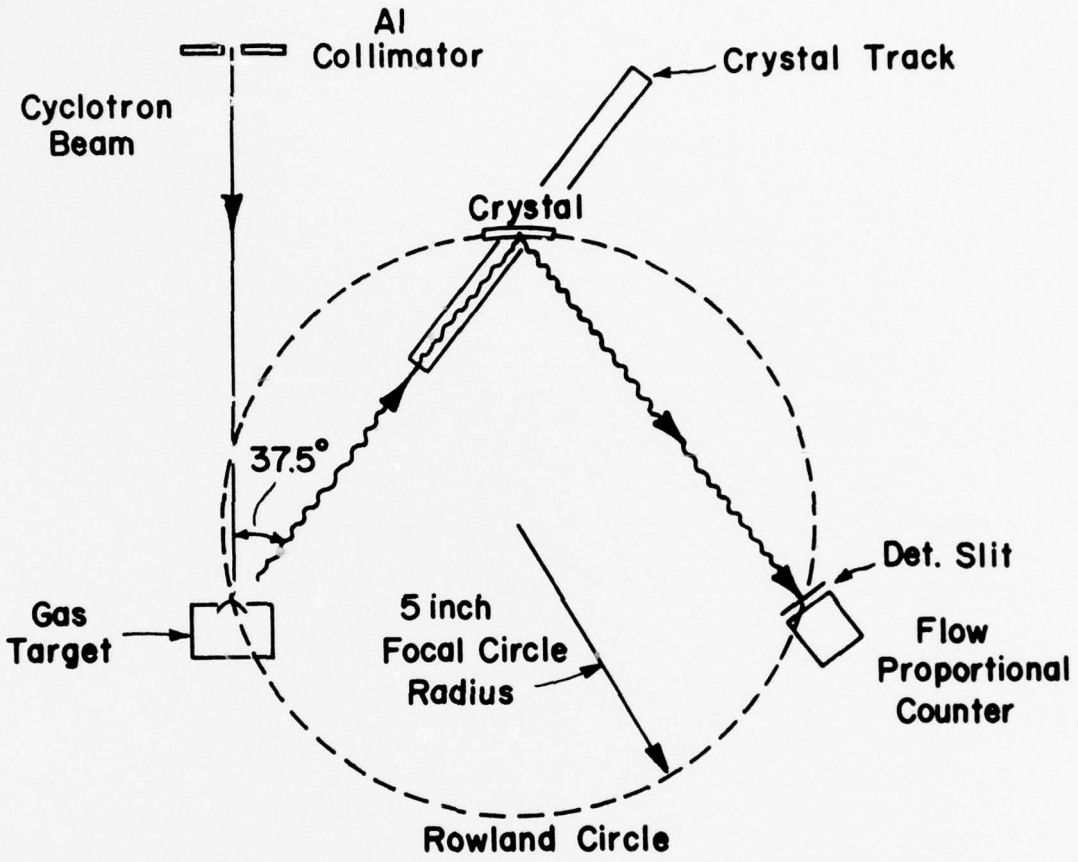

FIG. 6. Diagram of experimental configuration.

ZnS target that could be viewed by closed circuit television through a glass flange mounted on the side of the target chamber. The diameter of the beam spot was typically 0.3 cm.

The targets were mounted perpendicular to the beam on a four position remotely driven target wheel that allowed for adjustment of target movement along the direction of the beam. The photograph in Fig. 7 shows the physical setup of the ARL spectrometer mounted onto the target chamber with the target wheel in place.

The target compounds were contained in a small closed cell having a volume of 1.5 cm^3 and equipped with a 1.05 mg/cm^2 aluminized Kapton window through which the beam entered. Kapton foil was selected as a target window due to its strength, heat resistance, and x-ray transmission efficiency. The transmission efficiency, T, of a substance is given by

$$T = I/I_o = e^{-\mu x} \qquad (2.3)$$

where μ is the mass absorption coefficent measured in cm^2/g, x is the sample thickness in g/cm^2, I is the transmitted intensity, and I_o is the incident intensity. The mass absorption coefficent for Kapton ($C_{22}H_{10}N_2O_4$) as a function of x-ray energy is (as was determined using the tabulation of Storm and Israel[26]) given by the formula

$$\ln\mu = 2.830 \ln E(MeV) - 11.729 \qquad (2.4)$$

where E is the photon energy of interest. Table 1 lists the results of Eq. (2.4) applied to the transmission of x-rays of Si, S, Cl and Ar through 1.05 mg/cm^2 Kapton and 65 $\mu g/cm^2$ aluminum.

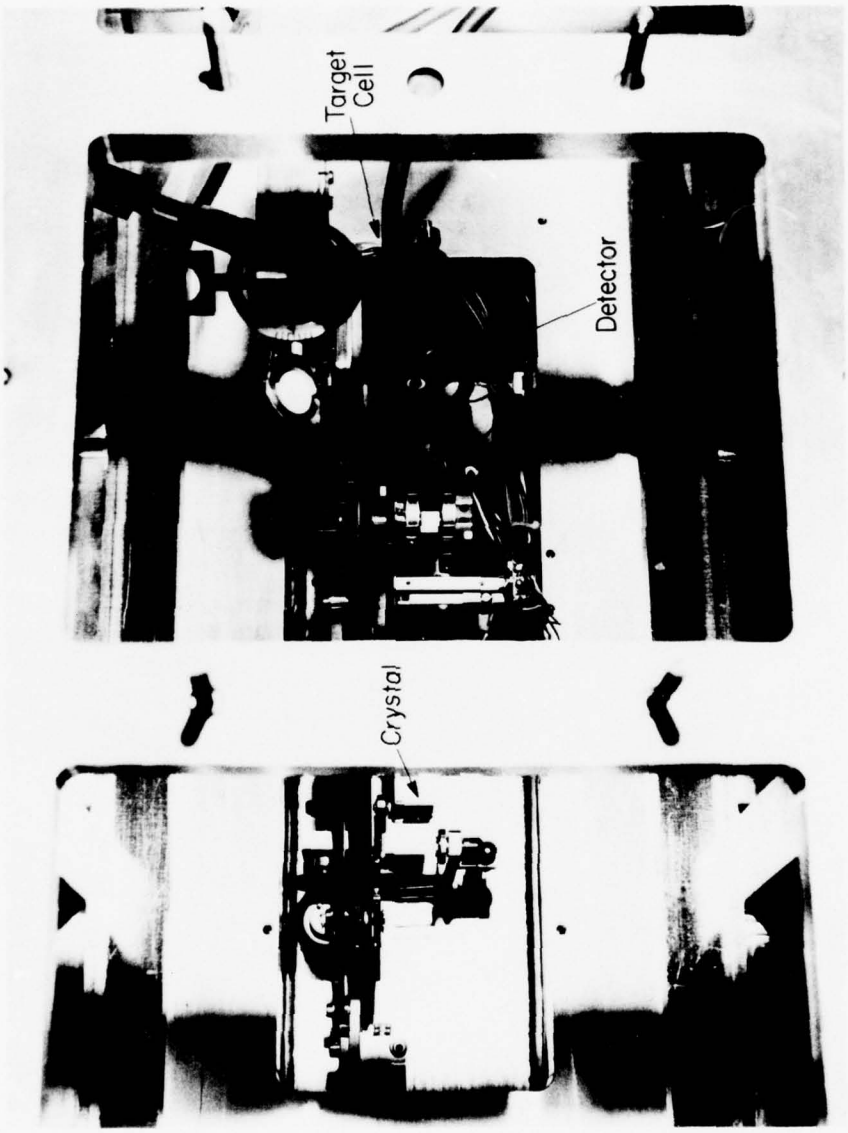

FIG. 7. Photograph of ARL curved-crystal spectrometer mounted in target chamber.

TABLE 1. Transmission efficency for x-rays through aluminized Kapton foil.

	Kapton	Aluminum	Total
Si	55%	79%	44%
S	77%	90%	69%
Cl	84%	93%	78%
Ar	88%	95%	84%

The spectrometer was mounted in the horizontal plane at the backward angle of 142.5° with respect to the beam direction in order to minimize a loss in transmission efficiency and to minimize the energy loss of the incident beam (i.e. 8.9 MeV for 32.4 MeV O and 0.9 MeV for 6.7 MeV He). Maximum transmission efficiency became an important factor in obtaining spectra of the light hydrated gases since these gases tended to decompose with beam exposures of greater than 20 minutes at beam currents of 25 nanoamperes on target. An illustration of the effects of decomposition on the Kα satellite spectra of H_2S gas are shown in Fig. 8 where the heavy line spectrum was succeeded by two spectra shown by the lighter lines. Decomposition was therefore easy to recognize since the spectra showed an intensification of the lower order satellite peaks and a downward shift in the satellite peak energies. In addition, the Kapton window would show evidence of decomposition products that condensed on the inside of the window surface. In an effort to prevent an overlap of a spectrum produced by condensed products with a gas spectrum, the gas cell windows were replaced after every second spectrum.

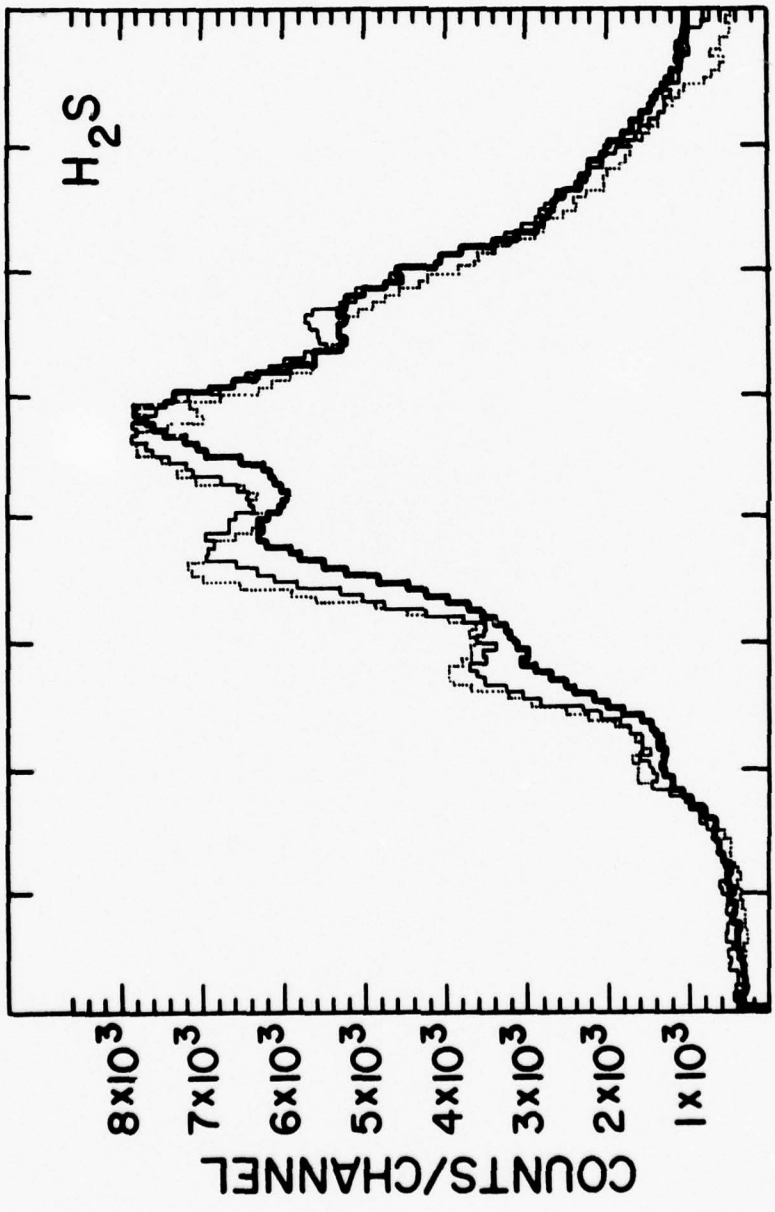

FIG. 8. Evidence of decomposition of H_2S gas shown by three time sequenced Kα satellite spectra.

The filling of the gas cell was accomplished by means of a gas manifold system designed to allow for evacuation of the gas cell through the beam line vacuum system. The gas manifold system is schematically displayed in Fig. 9. The higher pressures in the gas manifold system were measured by a mercury manometer while the lower pressures of the target chamber vacuum were measured by a Hastings thermocouple gauge. Due to the corrosive nature of the gases studied, only valves and lines of stainless steel and tygon tubing were utilized. The normal sequence of valve manipulation was as follows:

1. The ambient air initially in the system was evacuated by slowly opening all valves, save the gas bottle valve, to the target chamber vacuum.

2. Following gas line evacuation, the valve to the vacuum chamber was closed and the shut off valve opposite the fine metering valve was closed.

3. The gas bottle valve was opened and gas was allowed to flow into the system at the desired rate by manipulating the noncorrosive pressure regulator and the fine metering valve.

4. Once the mercury manometer indicated atomospheric pressure, all valves were closed and the vacuum chamber valve was opened to purge the target cell at least once with the target gas prior to taking measurements.

5. The vacuum chamber valve was then closed and the other valves opened to allow gas to return to atmospheric pressure in the manifold system.

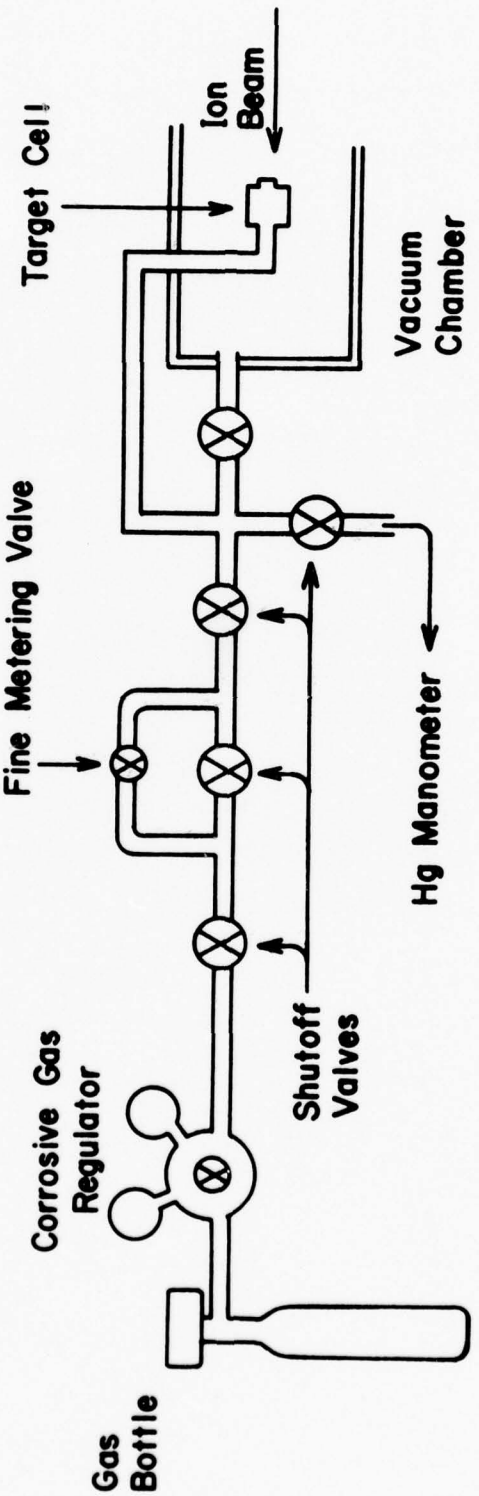

FIG. 9. Target gas manifold system.

C. Data Acquisition

The electronic configuration for data acquisition will be described only briefly since it has been reported previously.[27] A schematic diagram of the electronic configuration is shown in Fig. 10. X-ray signals from the proportional counter (x-ray detector) were sent to a single channel analyzer where an energy window was set around the x-rays of interest. The output of the single channel analyzer was directed to a spectrometer control system where counting signals were sent simultaneously to a Northern Scientific multichannel pulse height analyzer operating in an external-multiscale mode and to a PDP-15 computer. Beam monitor signals were sent to the monitor portion of the spectrometer control system. When the manually preset number of monitor counts were collected at the directed spectrometer wavelength, the spectrometer was automatically advanced to the next counting position and the analyzer and PDP-15 multiscalers were also automatically advanced. The PDP-15 computer allowed for on-line data analysis of a previous spectrum while a new spectrum was being acquired.

D. Data Analysis

The Kα satellite spectra were recorded onto magnetic tapes and a program called DIABOLICAL PLOT was used to transfer the data onto IBM cards, list and sum the raw data, and provide a Cal-Comp and printer plot of each spectrum. The spectra were then analyzed by a least squares fitting procedure that employed a Gaussian-plus-exponential-tail peak fitting function to extract the relative satellite intensities and

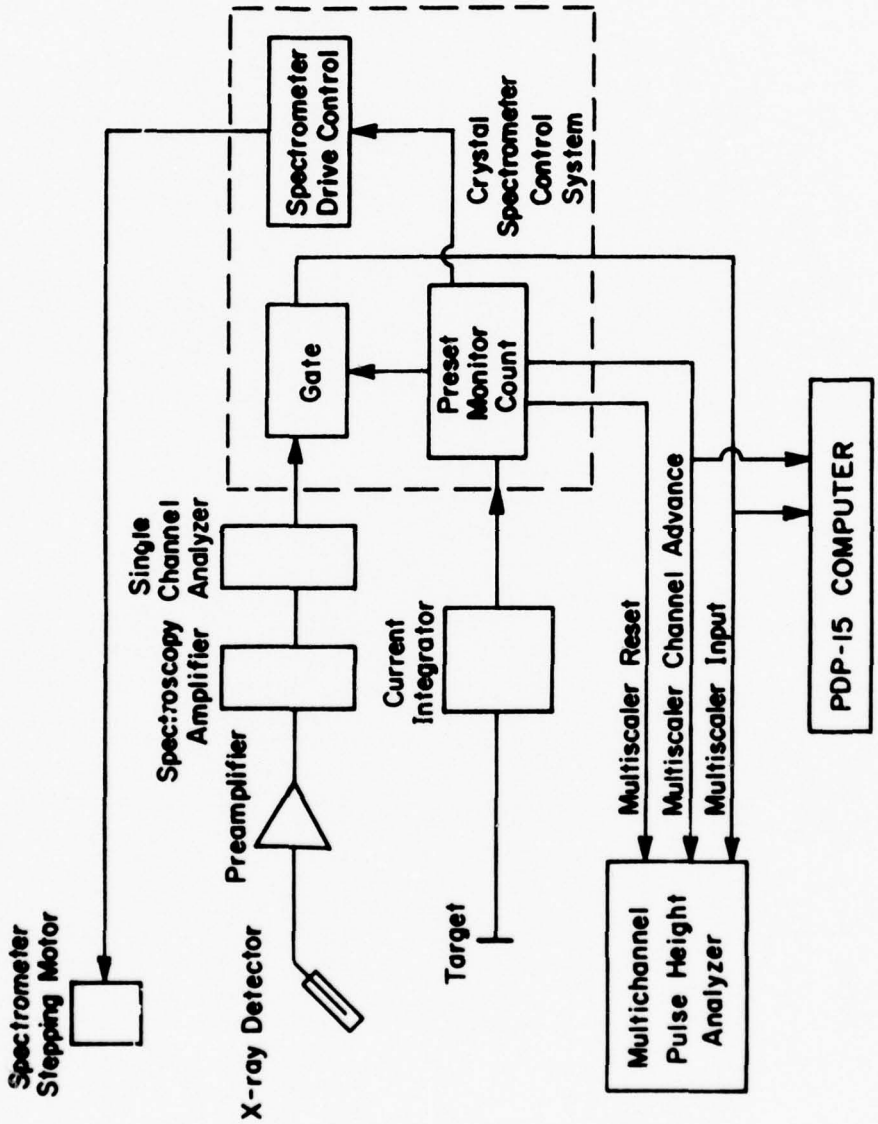

FIG. 10. Schematic diagram of the electronic configuration.

determine the peak centroids. An example of the fit of a typical spectrum is given in Ref. 27 and a description of the program is found in Ref. 28. The satellite intensities were then corrected for absorption in the target, absorption in the proportional counter window, and for detection efficiency. The details of this analysis are given in Ref. 29.

In order to make detailed comparisons of the satellite intensity distributions, it is useful to define a parameter p_L which represents the apparent average fraction of L-shell vacancies present at the time of Kα x-ray emission.[29] p_L is calculated by means of the formula

$$p_L = \frac{1}{N_L} \sum_{n=1}^{7} n\, fn \qquad (2.5)$$

where N_L is the number of L-shell electrons in the ground state and fn is the relative intensity of the n^{th} satellite peak. For example, a p_L value of 0.250 would indicate that on the average approximately 25% of the L-shell electrons are missing at the time of x-ray emission. The term "apparent" is applied to p_L since an exact determination of the number of L-shell vacancies must take into account the fact that the fluorescence yield depends upon the state of ionization. Theoretical calculations of fluorescence yields for free atom cases of neon, aluminum, and argon have been reported in Refs. 30, 31 and 32 and are shown in Fig. 11 where the values for ω_n are the statistically averaged fluorescence yields for the various KL^n vacancy configurations. Fluorescence yields interpolated from the theoretical values given in Fig. 11 are used in the calculations reported in Chapter IV. The calculation of the actual L-vacancy fraction, p_L^*, must incorporate the fluorescence yield

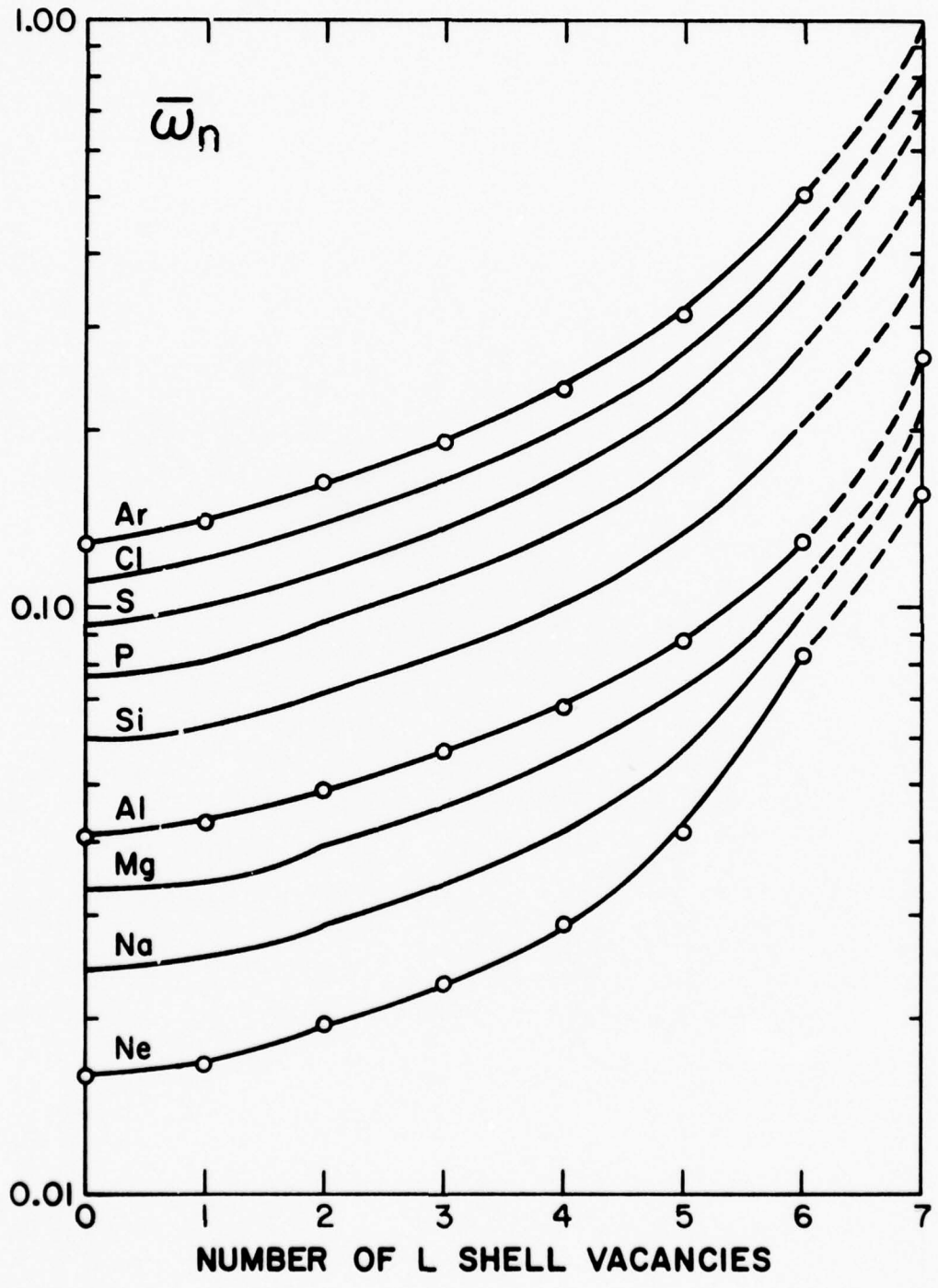

FIG. 11. Theoretical fluorescence yields for KL^n states.

for each KL^n state according to the expression

$$p_L^* = \frac{1}{N_L} \frac{\sum_{n=1}^{7} \omega_n \, n \, fn}{\sum_{n=0}^{7} \omega_n \, fn} \qquad (2.6)$$

Unfortunately, theoretical fluorescence yields cannot usually be used because the situation is further complicated by the fact that values for ω_n cannot be readily calculated for solids and molecular compounds since a detailed understanding of fast electron rearrangement which immediately follows a collision has not yet been reached.

After the p_L values were calculated from Eq. (2.5), they were further corrected for projectile energy loss in the target cell window and and in the target. These energy loss corrections, $\Delta p_L/\Delta E$, were determined experimentally by recording satellite spectra for solid targets placed in cells with and without Kapton windows and are listed in Table 2 for each of the elements studied. The average beam energies for the detection of Kα x-rays for each compound studied are tabulated in Chapter III and Chapter IV.

TABLE 2. Energy loss and flat crystal normalization corrections to p_L.

Projectile	Target	$\Delta p_L/\Delta E$ (MeV^{-1})	$N_{(FC/CC)}$
32.4 MeV O	Si	-3.15×10^{-3}	1.034
32.4 MeV O	P	-2.70×10^{-3}	0.997
32.4 MeV O	S	-2.22×10^{-3}	0.961
32.4 MeV O	Cl	-1.71×10^{-3}	0.935
32.4 MeV O	Ar	-1.67×10^{-3}	0.946
32.4 MeV O	K	-1.62×10^{-3}	0.956
6.7 MeV He	Si	-5.75×10^{-3}	---

In order to compare the present data with previous extensive measurements of solid compounds[29] obtained by use of a flat crystal spectrometer oriented at 90° with respect to the beam, it was necessary to apply a multiplicative correction, $N_{FC/CC}$, (also listed in Table 2) to p_L in order to account for differences in crystal reflectivity and spectrometer geometry and alignment. This correction was determined by comparison of measurements of a number of identical solid targets in each spectrometer system.

E. Energy Calibration Procedure

Aside from extracting the relative satellite intensities from the data, great care was taken to obtain the absolute energies of the measured x-rays. As previously mentioned, the automatically stepped movement of the curved crystal is a linear function of the reflected x-ray wavelength. The spectrometer is calibrated in terms of the wavelength for a LiF crystal which has a 2d crystal spacing of 4.0267 Å. When using reflecting crystals other than LiF it is necessary to compute a spectrometer setting using the relation

$$\lambda_{spec.} = \lambda_{True} \times \frac{2d\ LiF}{2d\ crystal} \times 10^3 \qquad (2.6)$$

where λ_{True} is the desired wavelength in Ångstroms. Table 3 shows the crystals and spectrometer settings used to obtain the Kα satellite spectra within 145 channels. The steps/channel setting represents the number of control counts advanced by the spectrometer control unit for each counting position. An advance of 20 control counts represents a spectrometer odometer movement of 1.0 units.

Equation (2.6) is only an approximation, however, since the slope

of the wavelength calibration equation varies as a function of target position. Therefore it was necessary to conduct a detailed energy calibration to obtain accurate absolute energies of the Kα satellite peaks for those elements not previously reported.

TABLE 3. Crystals and spectrometer settings used for curved-crystal Kα satellite measurements.

Target	Crystal	Starting Odometer Setting (yo)	Steps/Channel (S)
Si	EDDT	3280	30
P	EDDT	2780	24
S	NaCl	3835	35
Cl	NaCl	3400	30
Ar	NaCl	2950	24
K	NaCl	2647	22

A flat crystal spectrometer was used for the energy calibration since it was found previously that this system is relatively insensitive to small variations in target position.

To obtain accurate sulfur Kα satellite energies, solid targets of S_8 and KCl were bombarded by 2.75 MeV protons and $K\alpha_{1,2}$ measurements were acquired by use of an NaCl crystal. Proton bombardment was utilized to prevent energy shifts of the $K\alpha_{1,2}$ peaks due to M-shell ionization. The spectrometer was aligned on sulfur $K\alpha_{1,2}$ x-rays and then spectra were acquired for sulfur, chlorine, and potassium. The centroids of the $K\alpha_{1,2}$ peaks were used to determine the spectrometer position, C_i, by

$$C_i = C_o - S X_i \qquad (2.7)$$

where C_o is the initial spectrometer position, S is the number of steps per channel (S = 5 for these measurements), and X_i is the channel number for the peak centroid.

Next, the Bragg angles, θ, were calculated from wavelengths in Ref. 33 by the Bragg equation

$$\theta = \sin^{-1}\left(\frac{\lambda}{2d}\right) \qquad (2.8)$$

where λ is the wavelength in Å and 2d is the crystal spacing in Å. Results of the flat crystal spectrometer calibration measurements are shown in Table 4.

TABLE 4. Flat crystal spectrometer energy calibration measurements.

Target	$K\alpha_{1,2}$ Ch. #	Spect. Position	Energy (eV)[33]	θ (rad)
S_8	25.2	7934.0	2307.44	1.26137
Cl	20.5	6247.5	2621.85	0.99413
K	30.5	4547.5	3312.87	0.72539

In the case of a flat crystal spectrometer, x-ray intensity is measured as a function of Bragg angle with a linear equation of

$$\theta_i = \frac{d\theta}{ds} C_i + b \qquad (2.9)$$

where $d\theta/ds$ and b are the slope and intercept of a least squares fit of values for spectrometer position and Bragg angle. The results listed in Table 4 give a $d\theta/ds$ value of 1.5827×10^{-4} radians/step and an intercept of 5.5538×10^{-3} radians. A subsequent spectrometer calibration procedure gave values for $d\theta/ds$ and b of 1.5804×10^{-4} radians/step and 8.0895×10^{-3} radians, respectively.

Once the spectrometer was aligned and calibrated a spectrum of 32.4 MeV oxygen on S_8 was acquired. The Kα satellite energies were then obtained from the extracted peak centroids by applying equations (2.7), (2.9) and the Bragg equation. The resultant energies (eV) for the S_8 satellites for peaks KL^0-KL^5 are 2308.7±0.5, 2323.5±0.4, 2340.1±0.3, 2357.5±0.8, 2376.4±0.8, and 2395.4±0.8.

These energies served as an energy reference for spectra of S_8 measured on the curved crystal spectrometer. The reference energies, E_i, were converted to wavelength, λ_i, in Å by

$$\lambda_i = \frac{12398.1}{E_i(eV)} \qquad (2.10)$$

The channel numbers for the Kα satellite peak centroids, X_i, were converted to the spectrometer odometer setting, y_i, by

$$y_i = y_o - \frac{X_i}{20} S \qquad (2.11)$$

where y_o and S are listed in Table 3 (p. 27). A linear least squares fit of λ_i and y_i yielded a slope, $d\lambda/dy$, and an intercept, λ'. Si λ_i values were obtained from Ref. 34; Cl and K λ_i values were obtained from Ref. 27. Table 5 lists the values of $d\lambda/dy$ and λ' for the reference elements Z = 14 through Z = 19 and these values were used to calculate the Kα satellite peak wavelengths for other compounds of the same element.

F. Experimental Broadening Effect

Once the curved crystal spectrometer was aligned on the x-rays of a solid target it was found that the target could be moved several mm along the direction of the beam and x-rays would still be detected. Unfortunately, the target displacement causes an apparent shift in the wavelength of the measured x-rays.

TABLE 5. Curved crystal calibrated wavelength equation values.

Target	$d\lambda/dy$	λ'
Si	2.1656×10^{-3}	7.9386×10^{-2}
P_4	2.1656×10^{-3}	1.9828×10^{-1}
S_8	1.2769×10^{-3}	5.0836×10^{-1}
NaCl	1.3734×10^{-3}	1.3022×10^{-1}
KCl (Cl)	1.3693×10^{-3}	1.6875×10^{-1}
Ar	1.3693×10^{-3}	1.8533×10^{-1}
KCl (K)	1.3545×10^{-3}	1.9754×10^{-1}

This point is illustrated in Fig. 12 where spectra of Si and K are shown with the target shifted fore and aft. The results of an analysis of the spectra in Fig. 12 are shown in Table 6.

TABLE 6. Effects of target displacement along the beam axis.

Target	$\Delta E/\Delta X$ (eV/mm)	$\Delta p_L/\Delta X$ (mm^{-1})	$dE/d\theta$ (eV/deg)
Si	0.60	0.0011	22.0
S_8	1.23	0.0004	12.9
K	6.07	0.0026	65.2

Not only is there a shift in energy with target displacement, $\Delta E/\Delta X$, but a slight change in p_L is also observed. These effects are also directly related to the crystal dispersion, $dE/d\theta$, which can be

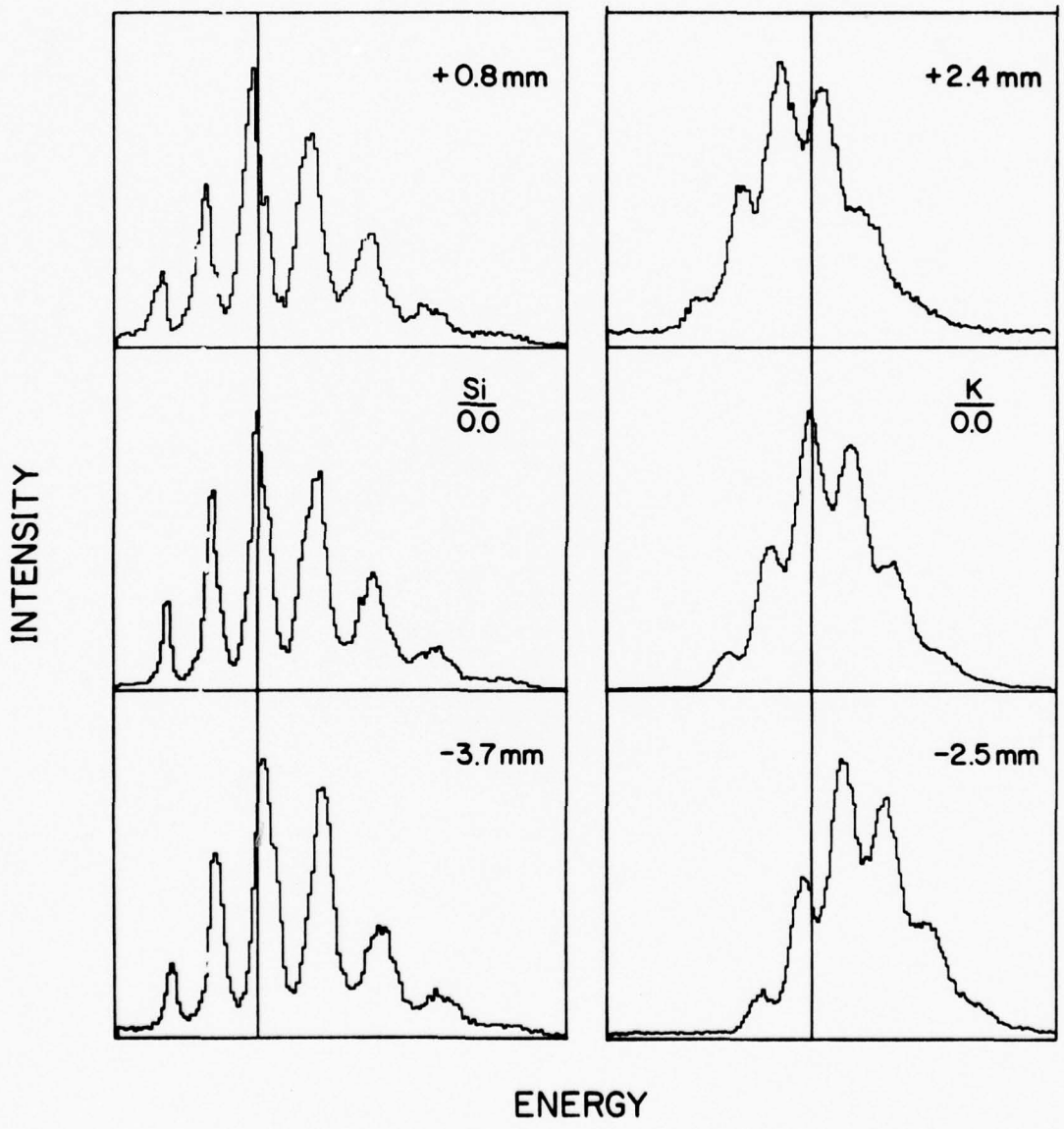

FIG. 12. Apparent Kα satellite energy shift due to target displacement.

calculated from

$$\frac{dE}{d\theta} = E \cot \theta \qquad (2.13)$$

However, the $\Delta E/\Delta X$ value for Si is much lower than that expected based on a correlation of $\Delta E/\Delta X$ with $dE/d\theta$.

The next point to consider is the determination of an average target thickness for x-ray detection, x_L, to see if this thickness is so great that an overlap of spectra like that shown in Fig. 12 will occur, thereby resulting in a peak broadening effect. Program ORION[35] allows for the calculation of an average limiting depth for detection of x-rays, t_L (mg/cm^2). Then x_L can be obtained by dividing t_L by the target density, ρ, in mg/cm^3. For solid targets, x_L is calculated to be on the order of 10^{-3} cm.

Gases, however, are three orders of magnitude less dense and x_L values of nearly 0.5 cm were calculated for the very light gases studied. Hence a considerable amount of spectral overlap is expected and should be observed as peak broadening. This effect is exactly what is observed.

Shown in Fig. 13 is the correlation of the measured peak broadening, $\Delta\bar{\Gamma}$, with x_L and ρ. The peak broadening was determined by

$$\Delta\Gamma_n = [\Gamma_{total}^2 - \Gamma_{solid}^2]^{1/2} \qquad (2.14)$$

and

$$\Delta\bar{\Gamma} = \Sigma \text{ fn } \Delta\Gamma_n \qquad (2.15)$$

where $\Delta\Gamma_n$ is the broadening of an individual KL^n peak, Γ_{total} is the total measured peak width, Γ_{solid} is the corresponding KL^n peak width for the reference solid, and fn is the relative satellite intensity.

Reasonable agreement of $\Delta\bar{\Gamma}$ with x_L and ρ is found in Fig. 13. Therefore it is concluded that the observed peak broadening in the

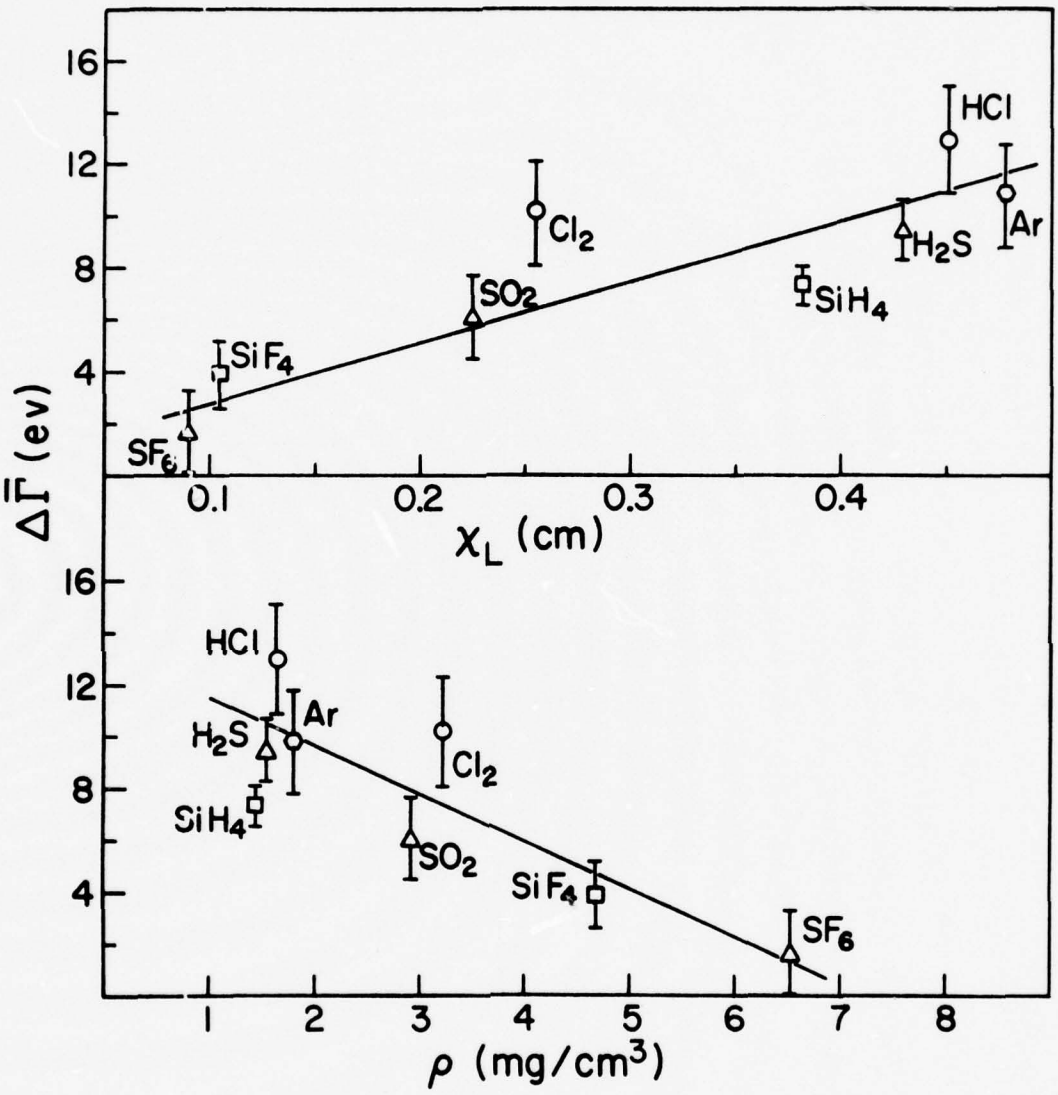

FIG. 13. Comparison of Kα satellite peak broadening of gases with target density and average target thickness for x-ray detection.

spectra of light gases is due primarily to the finite path length for x-ray emission in these gases caused by their low densities. Contributions from other broadening mechanisms will be considered in Chapter IV.

CHAPTER III

Kα SATELLITE SPECTRA OF SOLIDS

A. Presentation of Data

Sample Kα satellite spectra of Si, P, S, Cl, Ar, and K produced by 32.4 MeV oxygen ion bombardment are shown in Figs. 14 and 15. The solid targets were used as references for measurements of the gaseous compounds of the same elements. In addition, measurements of solid Si, S_8, and KCl allowed for comparison of the present data with previous extensive measurements of Kα satellite spectra of third row solids.[29]

The relative Kα satellite intensities (fn) for spectra of the reference solids are summarized in Table 7. Each fn is the ratio

TABLE 7. Relative Kα x-ray satellite intensities of third row reference solids excited by 32.4 MeV oxygen ions.

	fn[a]						
Compound	n=0	n=1	n=2	n=3	n=4	n=5	n=6
Si	0.032	0.113	0.259	0.275	0.192	0.090	0.038
P_4	0.051	0.158	0.256	0.272	0.174	0.089	
S_8	0.044	0.137	0.282	0.268	0.173	0.097	
NaCl	0.021	0.098	0.252	0.338	0.203	0.088	
KCl(Cl)	0.044	0.093	0.244	0.334	0.208	0.076	
KCl(K)	0.024	0.122	0.315	0.302	0.168	0.070	

[a] Ratio of the n^{th} satellite peak intensity to the sum of the intensities of all the Kα peaks - corrected for absorption in the target and detector window, and for detection efficiency.

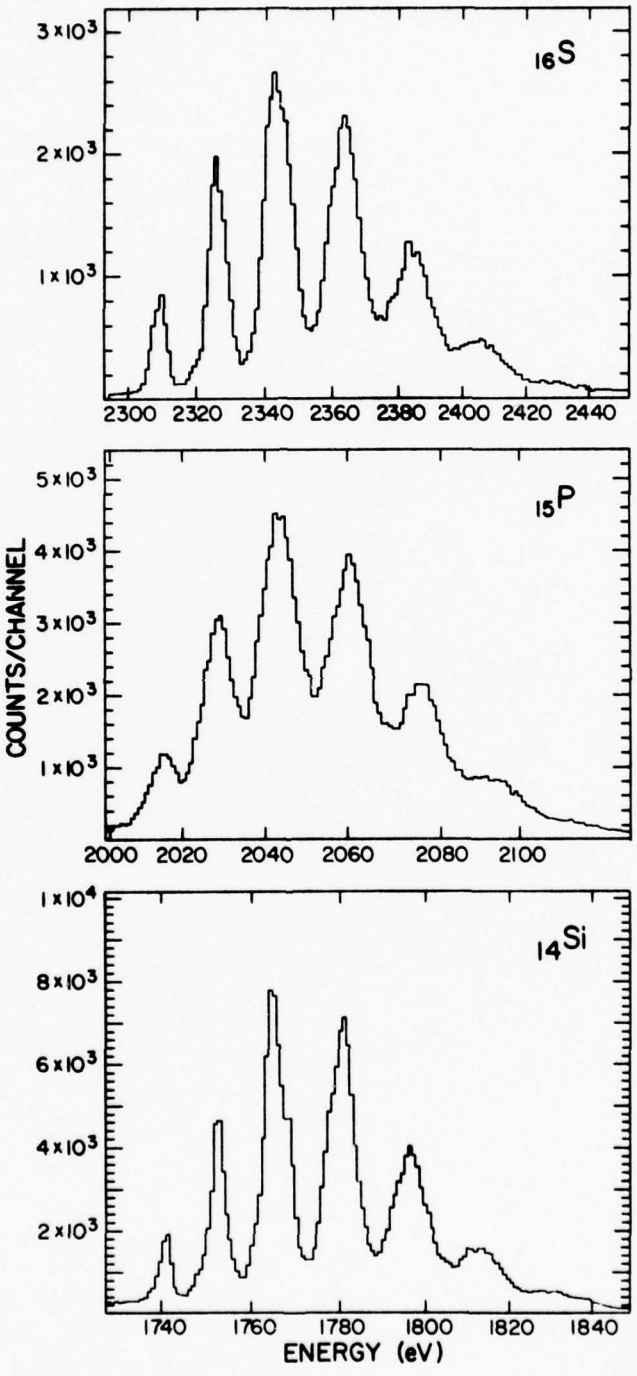

FIG. 14. Representative Kα satellite spectra of solid Si, P_4, and S_8 produced by 32.4 MeV oxygen ions.

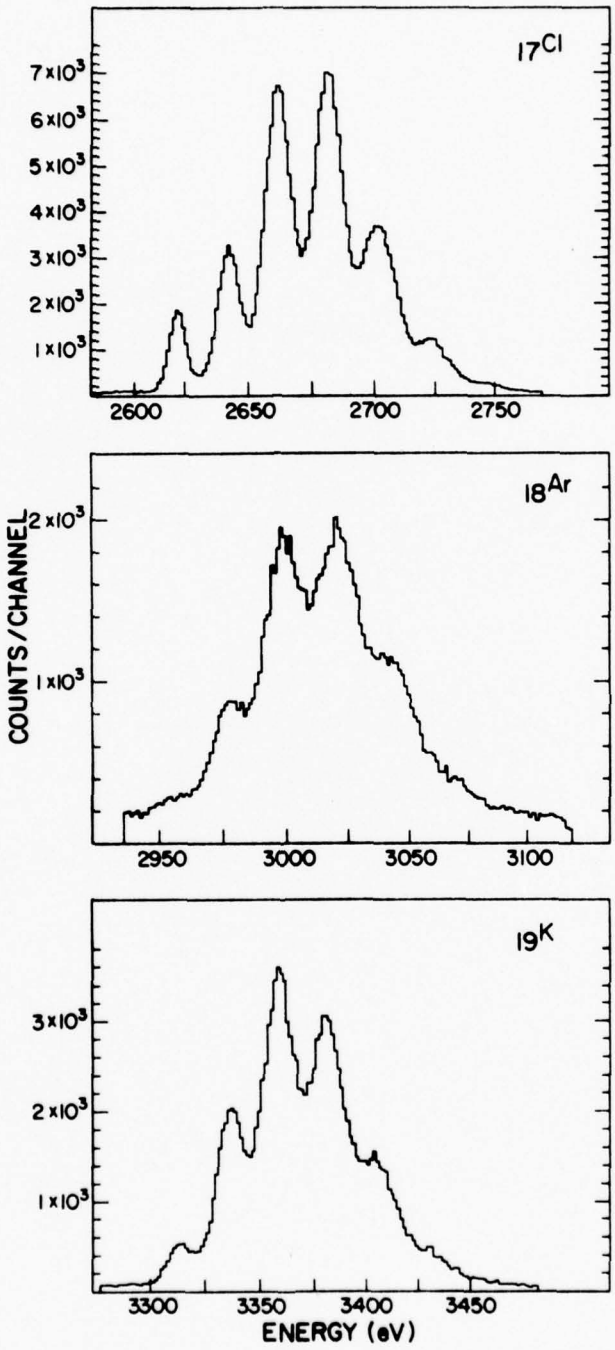

FIG. 15. Representative Kα satellite spectra of solid Cl(KCl), gaseous Ar, and solid K(KCl) produced by 32.4 MeV oxygen ions.

of the n^{th} satellite peak intensity to the sum of the intensities of all the Kα peaks - corrected for absorption in the target and detector window, and for detection efficiency. Table 8 lists the calculated average beam energies for the detection of Kα x-rays and the p_L values before and after the corrections for energy loss and flat crystal spectrometer normalization. For the sake of consistency the energy loss corrections were made to yield p_L values representative of the incident beam energy. The Kα x-ray satellite energies and peak widths (FWHM) are given in Table 9 for the reference solids. The errors indicated are experimental root-mean-square deviations.

TABLE 8 Calculated average beam energies for the detection of Kα x-rays and p_L values for third row reference solids excited by 32.4 MeV oxygen ions.

Compound	E (MeV)	p_L [a]	p_L (corr) [b]
Si	18.4	0.363	0.330±0.002
P_4 [c]	25.6	0.329	0.311±0.002
S_8	18.6	0.335	0.292±0.002
NaCl	19.1	0.358	0.313±0.003
KCl(Cl) [d]	18.7	0.355	0.310±0.003
KCl(K)	19.9	0.335	0.301±0.005

[a] p_L value determined directly from fn values.

[b] p_L value corrected for projectile energy loss and flat crystal normalization. The indicated errors are root-mean-square deviations.

[c] P_4 measurement was taken without a Kapton absorber, measurements of all other compounds were taken with a Kapton absorber for consistency with corresponding gases of the same element.

[d] The p_L value for Cl in KCl has been corrected for $K\alpha_{1,2}$ photoionization by K K x-rays (see Ref. 29).

TABLE 9. Kα x-ray satellite energies and FWHM peak widths for third period reference solids excited by 32.4 MeV oxygen ions.

Compound	Peak	Energy (eV)	FWHM (eV)	Compound	Peak	Energy (eV)	FWHM (eV)
Si	KL^0	1739.8±0.1	3.4±0.4	P_4	KL^0	2013.4±0.3	7.6±0.5
	KL^1	1751.2±0.5	4.2±0.4		KL^1	2026.0±0.3	8.5±0.5
	KL^2	1763.9±0.3	5.9±0.4		KL^2	2040.2±0.3	9.2±0.5
	KL^3	1778.7±0.6	6.8±0.4		KL^3	2056.7±0.3	11.1±0.5
	KL^4	1794.0±0.3	8.5±0.4		KL^4	2074.2±0.4	12.7±0.8
	KL^5	1809.3±0.5	12.5±0.8		KL^5	2092.1±0.4	15.1±1.0
	KL^6	1826.8±0.7	14.4±1.0				
S_8	KL^0	2308.6±0.5	4.5±0.5	NaCl(Cl)	KL^0	2621.7±0.5	5.5±0.7
	KL^1	2323.7±0.4	5.2±0.5		KL^1	2640.2±0.4	8.3±0.7
	KL^2	2339.8±0.2	8.1±0.5		KL^2	2659.0±0.5	10.2±0.7
	KL^3	2357.9±0.5	10.6±0.6		KL^3	2678.8±0.4	12.3±0.7
	KL^4	2376.2±0.7	12.0±0.8		KL^4	2698.9±0.7	15.1±1.0
	KL^5	2395.4±0.7	14.6±1.0		KL^5	2720.2±0.8	19.2±1.2
KCl(Cl)	KL^0	2621.4±0.5	6.1±0.7	KCl(K)	KL^0	3314.1±1.0	11.8±0.9
	KL^1	2640.4±0.5	8.4±0.7		KL^1	3335.1±0.9	14.2±0.9
	KL^2	2659.0±0.4	10.5±0.7		KL^2	3356.4±1.0	17.5±0.9
	KL^3	2679.1±0.4	12.0±0.7		KL^3	3378.7±1.1	20.0±1.0
	KL^4	2699.0±0.7	14.8±1.0		KL^4	3402.4±1.1	21.3±1.2
	KL^5	2719.9±0.7	21.6±1.2		KL^5	3428.1±0.9	23.2±1.4

An example of the influence of the chemical environment on Kα x-ray spectra is illustrated in Fig. 16 taken from Ref. 29. In this figure a distinct change of the intensity distribution from one compound to another is evident. The spectra at the top of the figure show greater intensity in the lower order satellites whereas the bottom spectra display greater intensity in the higher order satellites. The dashed lines in the figure accentuate this variation of the intensity distributions. In this study the p_L values for Si compounds ranged from 0.303 to 0.336, S compounds ranged from 0.263 to 0.315 and Cl compounds ranged from 0.296 to 0.314.

In determining the reason for the changes in the intensity distribution one has to consider whether the cause is associated with the vacancy production mechanism or the de-excitation process following vacancy production. Several reasons can be given which demonstrate that the vacancy production mechanism is not responsible for the observed effect. First of all, in a collision system with a relatively low Z projectile with an energy of 2 MeV/amu, the vacancy production mechanism is direct Coulomb-ionization and the complexities of molecular orbital excitation via electron promotion to bound molecular orbital levels are avoided. With Coulomb-ionization the probabilities for L-shell ionization depend upon the L-shell binding energies. Therefore a change in L-shell binding energies due to the chemical environment may result in a difference in the observed p_L value. A change in p_L versus a change in L-shell binding energy, $\Delta p_L/\Delta u_L$, can be estimated from the p_L values measured for SiH_4 and H_2S (reported in Chapter IV) versus their L-shell binding energies. SiH_4 and H_2S were chosen for this argument

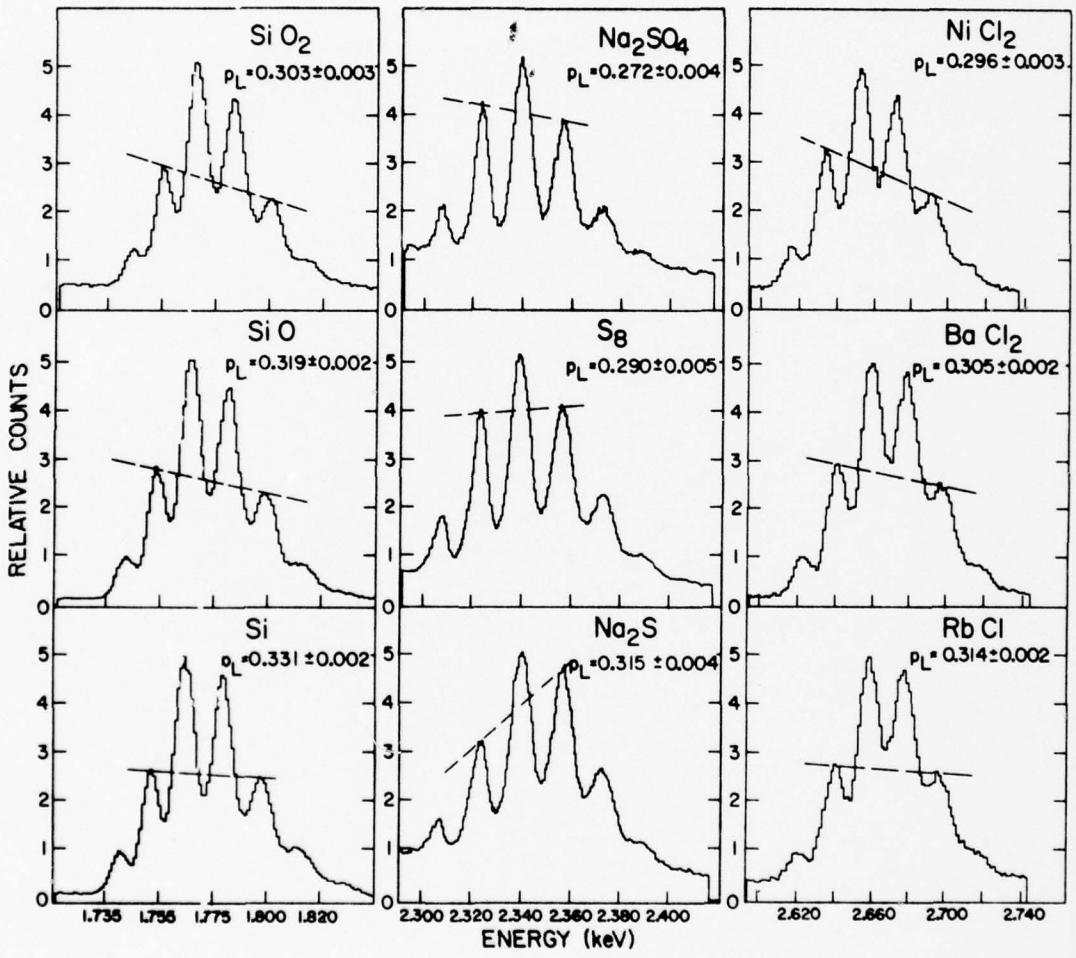

FIG. 16. Sample Kα x-ray spectra of compounds of Si, S, and Cl produced by 32.4 MeV oxygen ions showing the variation of the relative satellite intensities with chemical environment. Taken from Ref. 29.

since the p_L values for these gases would nearly represent the original vacancy configuration produced in the ion-atom collision. The resultant $\Delta p_L/\Delta u_L$ value of 5.7×10^{-4} eV^{-1} would mean that the predicted p_L difference in Na_2S and Na_2SO_4 would be 0.004 versus the observed difference of 0.043 (an order of magnitude in error).

Recoil effects are also expected to be negligible at the projectile energies employed. (This point will be considered in more detail in Chapter 4).

Finally, the most convincing justification for concluding the observed effect is connected to the de-excitation mechanism and not the vacancy production mechanism is supported by the observation that a similar effect in the variation of intensity distributions occurs with a variety of projectiles ranging from carbon to argon.[29]

B. Discussion

Once formed, a particular KL^n state can decay either by the filling of the K-vacancy or one of the L-vacancies. K-vacancy transfer processes include radiative (Kα and Kβ x-rays) and non-radiative Auger electron decay (KLL, KLM, KMM). L-vacancy transfer processes include L x-ray and L Auger transitions. These decay schemes are illustrated in Fig. 17. Not considered are transitions that require multielectron transfer where two or more holes are filled simulataneously since these transitions are relatively improbable.[36] The probabilities of decay of a KL^n state via Kα x-ray, Kβ x-ray, K Auger, and L-vacancy transfer are denoted by f_α, f_β, f_A, and f_L, respectively as shown in Fig. 17. Since these transitions represent the total number of ways a KL^n vacancy state may decay,

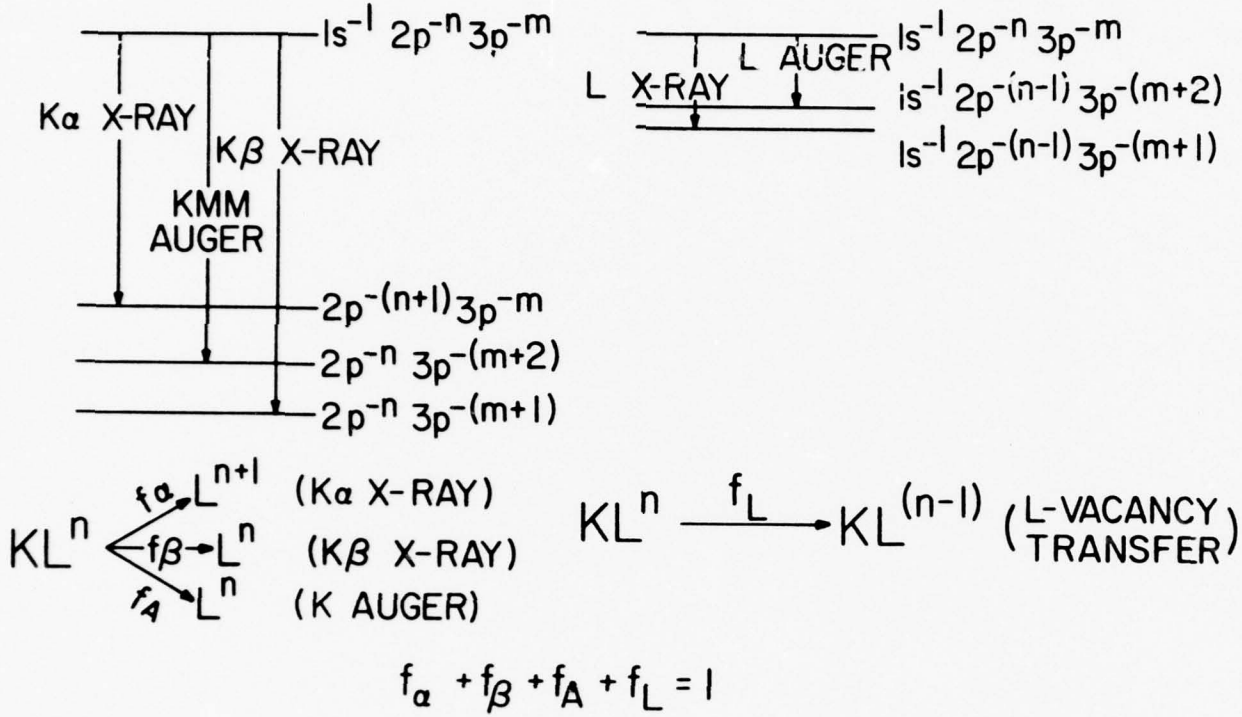

FIG. 17 The decay of a KL^n state illustrating the various K- and L-vacancy transfer processes for a third row atom having an initial state with one - 1s vacancy, n - 2p vacancies and m - 3p vacancies.

the probabilities of these processes must add up to one. In order to interpret a Kα satellite spectrum, it is necessary to understand how these probabilities are affected by the chemical environment.

All elements of interest in this study are third row elements where the L-vacancy transfer processes must involve the valence (M-shell) electrons. Valence electrons also participate in K-vacancy transfer via KLM and KMM Auger decay and Kβ x-ray emission. The influence of chemical bonding upon the rates of KLM, KMM and LMM vacancy transfer can affect the apparent degree of L-shell ionization in two ways. In the first case where the electron population of the M-shell is high, it is expected that the p_L will be decreased due to the increase in the rates of LMM Auger transitions which reduce the average number of L-shell vacancies prior to Kα x-ray emission. The second effect (which is more subtle) results from an increase in the rates of KLM and KMM Auger transitions which in turn causes a decrease in the fluorescence yields for the higher order satellite states (for which these transitions are more important due to the large number of L-shell vacancies).

If oxidation number is taken as a measure of the relative local valence electron density, a high positive oxidation number such as 6^+ in Na_2SO_4 signifies that a large fraction of the sulfur atom valence electron density has been transferred to the surrounding oxygen ligands. Similarly, a negative oxidation number such as 2^- in Na_2S signifies that the valence electron density of the sulfur atom has been increased by the electron density transferred from the two neighboring sodium atoms.[21] Based on the arguments given above, the p_L value for Na_2S is expected to be lower than for Na_2SO_4. The experimental p_L values contradict this

prediction. What has been ignored is the total valence electron density surrounding the sulfur atom which includes the valence electron density contributed by the neighboring atoms. Therefore it is suggested that merely accounting for intra-atomic transitions in terms of local valence electron density is not sufficient but interatomic crossover transitions from ligand valence levels to the K, L, and M shells of the target atom need to be considered. In fact, interatomic transitions may play a dominant role in the rearrangement processes occuring prior to $K\alpha$ x-ray emission.

As pointed out in Ref. 29, the idea of interatomic transitions is not new but was first suggested by Valasek[37] in 1938. Further consideration of interatomic transitions in the form of interatomic x-ray and Auger decay of ionized systems by photoabsorption or electron bombardment were presented by Åberg,[15] Best,[38] and Citrin.[39,40] These studies are concerned with interatomic transitions in the presence of a single or at most a double vacancy state in the host atom. Since the present work deals with states having single K-plus multiple L- and M-shell vacancies in the target atom, it is reasonable to expect a much greater amplification of this effect.

Citrin[41] suggested that the magnitude of the interatomic transition rate should depend on the spatial overlap of the bonded valence states and the electron density contributing to this overlap. Thus, in order to test further the hypothesis of interatomic transitions in L-vacancy transfer of highly ionized compounds, it is of interest to see if the p_L values correlate with the average valence electron density of the solid. Such a comparison can be accomplished by use of a parameter, Dv,

which is calculated from the mass densities of the compounds and is given by

$$D_v = 0.602 \frac{n_v \rho}{W_{mol.}} \text{ electrons/Å}^3 \qquad (3.1)$$

where n_v is the total number of valence electrons from the target atom and its ligands, $W_{mol.}$ is the molecular weight, and ρ is the mass density.

Shown in Fig. 18 (taken from Ref. 29) are p_L values for compounds of Al, Si, S, and Cl plotted versus D_v. A definite correlation of p_L with the total average valence electron density is apparent in Fig. 18. Also, the correlation of p_L with D_v is in the expected direction - as D_v increases, rearrangement rates increase thereby causing p_L to decrease.

The discussion and data presented to this point have indicated that electron rearrangement rates of highly ionized systems involve both interatomic as well as intra-atomic transitions, and that sizable chemical effects are observed primarily as a result of the interatomic contribution. To judge the relative contribution interatomic rearrangement processes make in the de-excitation of targets following heavy ion collisions it is advantageous to study free atoms where only intra-atomic rearrangement processes can occur. It was this line of reasoning which motivated the work reported in Chapter IV.

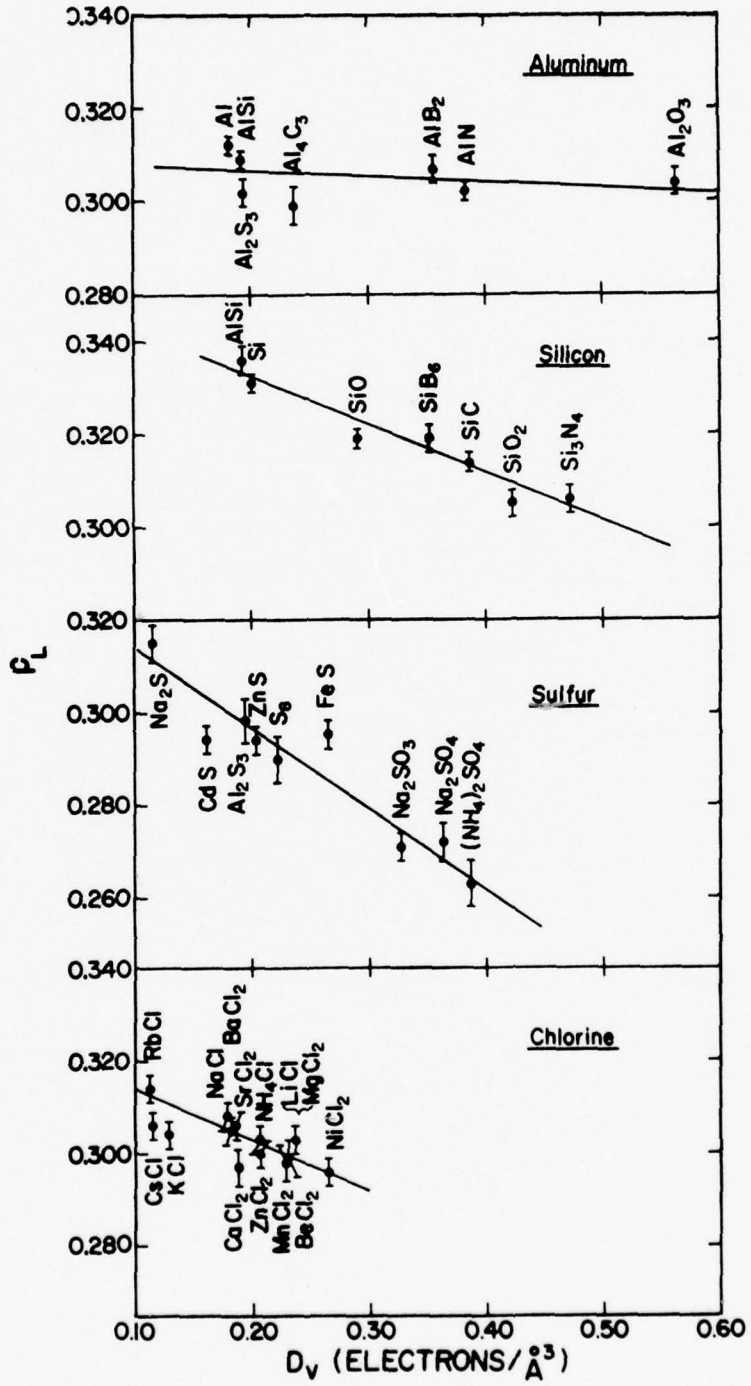

FIG. 18. The variation of p_L with average valence electron density for solid compounds excited by 32.4 MeV O ions.

CHAPTER IV

Kα SATELLITE SPECTRA OF GASES AND LIQUIDS

A. Presentation of Data

The previously mentioned study[29] of solid compounds of third row elements has been extended by the current work to include Kα satellite spectra for the gaseous compounds SiH_4, SiF_4, H_2S, SO_2, SF_6, HCl, Cl_2, and Ar, and the liquid CCl_4. The advantage of studying the light hydrated gases is that they represent nearly free atoms and hence the only electron rearrangement processes contributing to inner shell vacancy transfer are solely intra-atomic processes. On the other hand, the heavier gases represent free molecules and it is expected that changing ligands should result in Kα satellite spectra that show a chemical effect via interatomic rearrangement processes, similar to the effect observed in solids. Thus a comparison of spectra obtained from these gaseous systems will provide a clear assessment of the role of interatomic vacancy transfer on a time scale of 10^{-14} sec.

Three important features of x-ray spectra which display the effects of chemical environment are:

1. Changes in integrated peak intensities.
2. Energy shifts in the resolved peaks.
3. Changes in the shapes of the peaks.

All of these features contribute to the interpretation of the data to be presented.

Fig. 19 shows a comparison of spectra obtained for SiH_4, SiF_4 and solid Si. The most noticeable feature in this comparison is the enhancement of the higher order satellite intensities for SiH_4 over those for

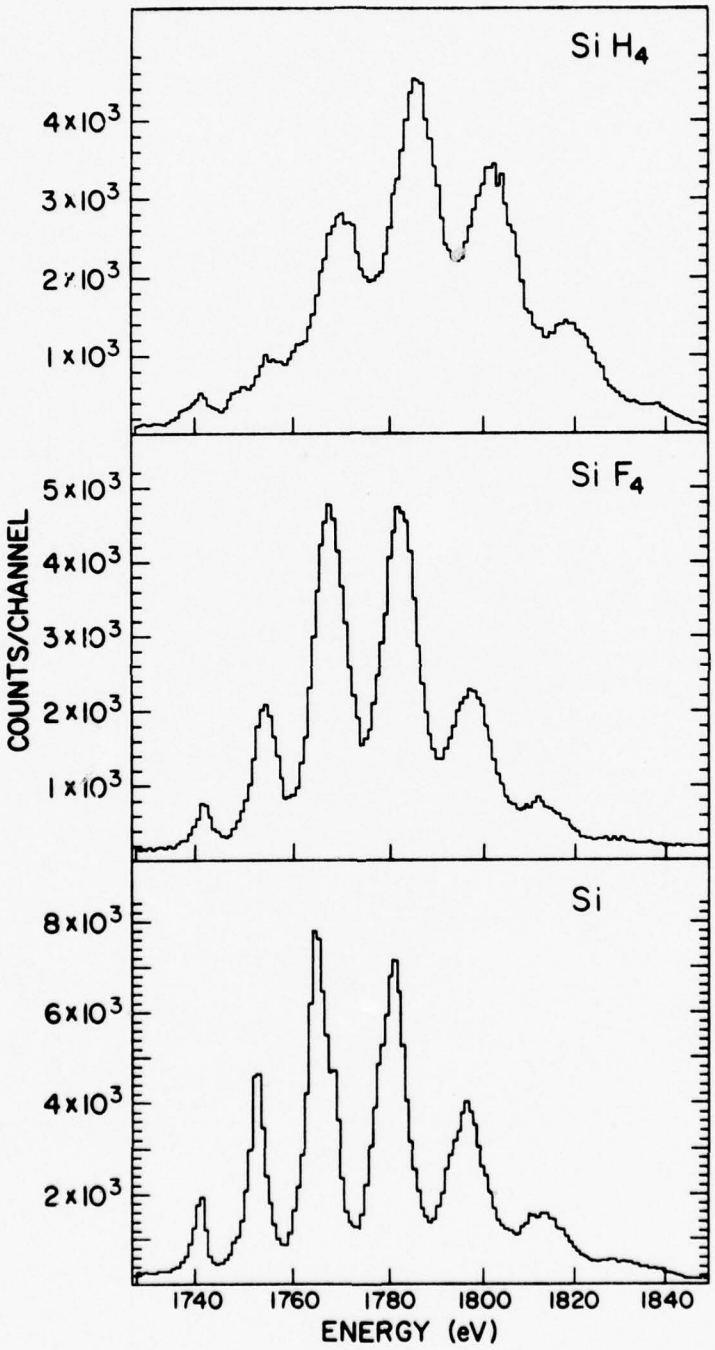

FIG. 19. Kα satellite spectra of the gases SiH_4, SiF_4 and solid Si produced by 32.4 MeV O ions, showing the variation of the relative satellite intensities with molecular environment.

SiF_4 and Si. This feature in itself is not new since it has been described several times before (Ref. 22 and Ref. 23). However, a more detailed and systematic examination of the larger body of data provided by this present work leads to several new and interesting conclusions that will be revealed in the sections that follow.

Inspection of Fig. 19 also indicates that the spectrum of SiF_4 displays nearly the same degree of L-shell ionization as that for solid Si. This fact proves that the high degree of L-shell ionization observed in SiH_4 is not merely a characteristic of the gaseous physical state but rather is associated with the fact that SiH_4 has few extra-atomic electrons.

Apart from the shifts in the relative satellite distributions of these silicon compounds, a definite narrowing of the distribution width is also observed in the gases as opposed to the distribution in the solid. This observation was reported by Hopkins et al.[23] and is especially noticeable with Cl ions. A means of quantitatively evaluating the widths of the relative satellite distributions is given by the root-mean-square deviation, σ_n, and can be calculated by

$$\sigma_n = [\Sigma\, fn\, (n - \bar{n})^2]^{1/2} \qquad (4.1)$$

where fn is the relative satellite intensity, $\bar{n}$ is the average number of L-shell vacancies obtained from $8 \times p_L$, and n is the number of L-shell vacancies. Values for $\bar{n}$ and σ_n are presented in Table 10. The values of σ_n for the gases of silicon and sulfur are consistently smaller than for the reference solids. However, as the ground state population of the M-shell increases (i.e. as the atomic number increases) the difference in distribution width decreases.

TABLE 10. The average number of L-shell vacancies, the relative intensity distribution root-mean-square deviation, and the mean x-ray energy for the satellite distribution.

	$\bar{n}$	σ_n	$\bar{E}_x$ (eV)
Si	2.640	1.373	1776.3
SiF_4	2.600	1.146	1780.0
SiH_4	3.096	1.237	1787.0
P_4	2.488	1.318	2051.6
S_8	2.336	1.296	2355.1
SF_6	2.152	1.181	2351.7
SO_2	2.256	1.177	2350.1
H_2S	2.808	1.119	2362.6
KCl(Cl)	2.480	1.219	2672.6
NaCl	2.504	1.171	2676.6
CCl_4	2.424	1.206	2674.9
Cl_2	2.448	1.188	2676.8
HCl	2.568	1.156	2679.1
Ar	2.472	1.061	3014.3
KCl(K)	2.408	1.167	3375.6

The second feature of interest in Fig. 19 (p. 49) is the satellite energy shifts. The peak centroids of SiH_4 are shifted higher in energy than those for solid Si or SiF_4 and hence the mean energy of the satellite distribution is also higher. The mean energy of the satellite distribution is determined by

$$\bar{E}_x = \frac{\Sigma\ fn\ En}{\Sigma\ fn} \qquad (4.2)$$

Values for $\bar{E}_x$ for the compounds studied are also given in Table 10.

The third feature of interest is the apparent broadening of the peak widths in the SiH_4 spectrum. The broadening can be confirmed by noting that the valleys between the peaks in Si and SiF_4 are quite deep, whereas in SiH_4 they are much shallower. This broadening feature is very obvious in all of the light gas spectra and is due to an instrumental effect associated with the relatively long path lengths for x-ray emission in the low density gases, as was discussed in Chapter II.

A comparison of Kα satellite spectra for the gases H_2S, SO_2 and SF_6 with solid S_8 is shown in Fig. 20. Here again it is clearly recognizable that the higher order satellites of H_2S (where sulfur is in a nearly free atom environment) are enhanced over those for the heavier gases and the solid. Satellite energy shifts and peak broadening are also notable features of the light gas in this comparison.

A study of chlorine gases, HCl and Cl_2, compared to solid NaCl provide the spectra for Fig. 21. Only a small change in the Kα satellite distributions is detectable in these spectra. In addition, the energy shifts in the satellite lines for the light gas HCl are much smaller in comparison to the energy shifts measured for the lower Z light gases. The peak broadening of the light gases, however, is still very evident.

Fig. 22 shows a comparison of the Kα satellite spectra of liquid CCl_4 and solid NaCl. This figure in itself is noteworthy since it is the first Kα satellite spectrum reported for a compound in the liquid state. This was made possible by the success of the closed target cell system. In this figure it is evident that the p_L value for CCl_4 is lower than NaCl since the second satellite peak of CCl_4 appears to be the most intense peak, whereas it is the third satellite peak that is the most

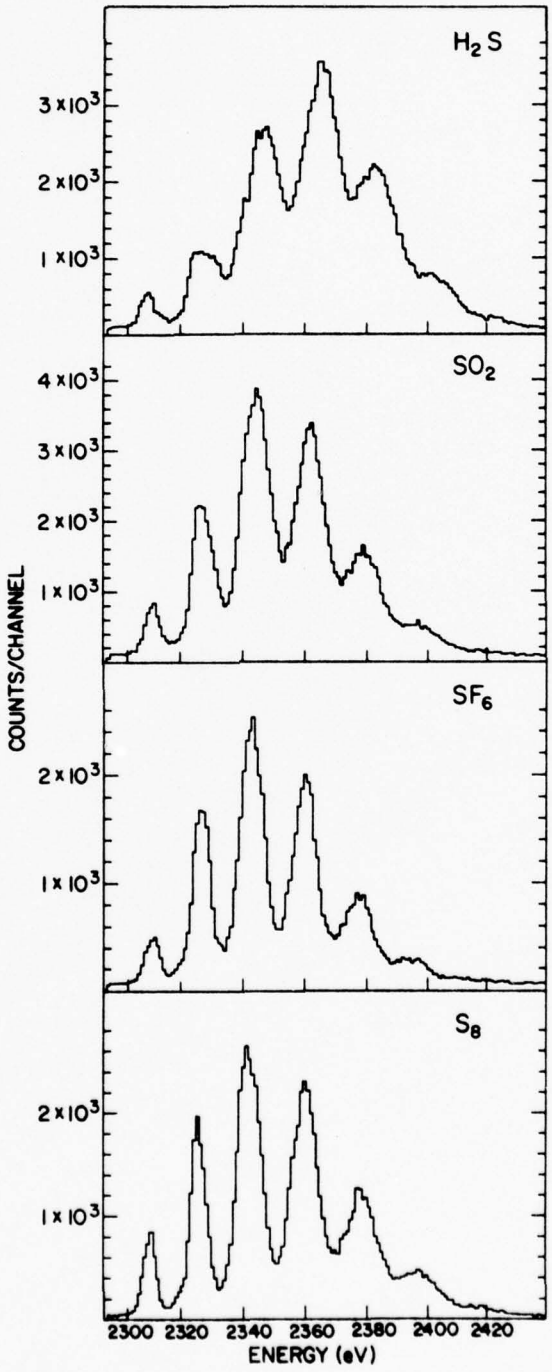

FIG. 20. Kα satellite spectra for the gases H_2S, SO_2, SF_6 and solid S_8 produced by 32.4 MeV O ions.

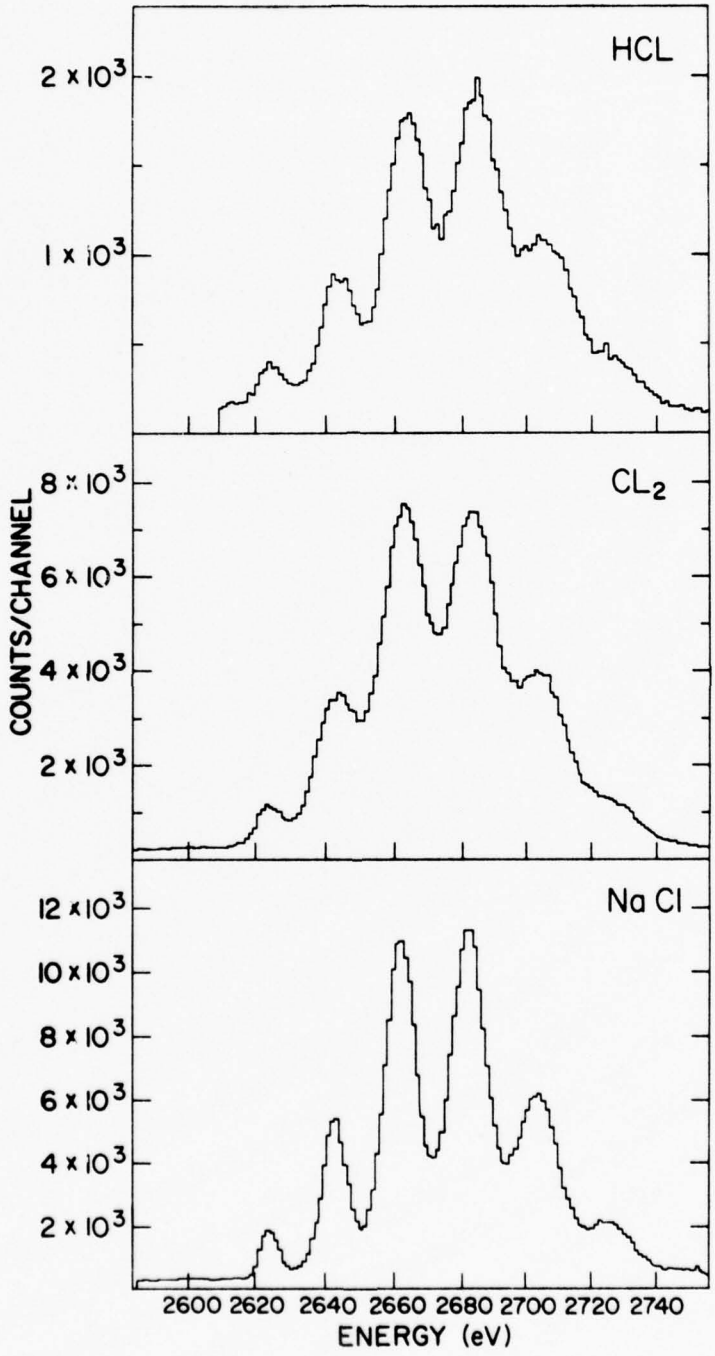

FIG. 21. Kα satellite spectra for the gases HCl, Cl_2 and solid NaCl produced by 32.4 MeV O ions.

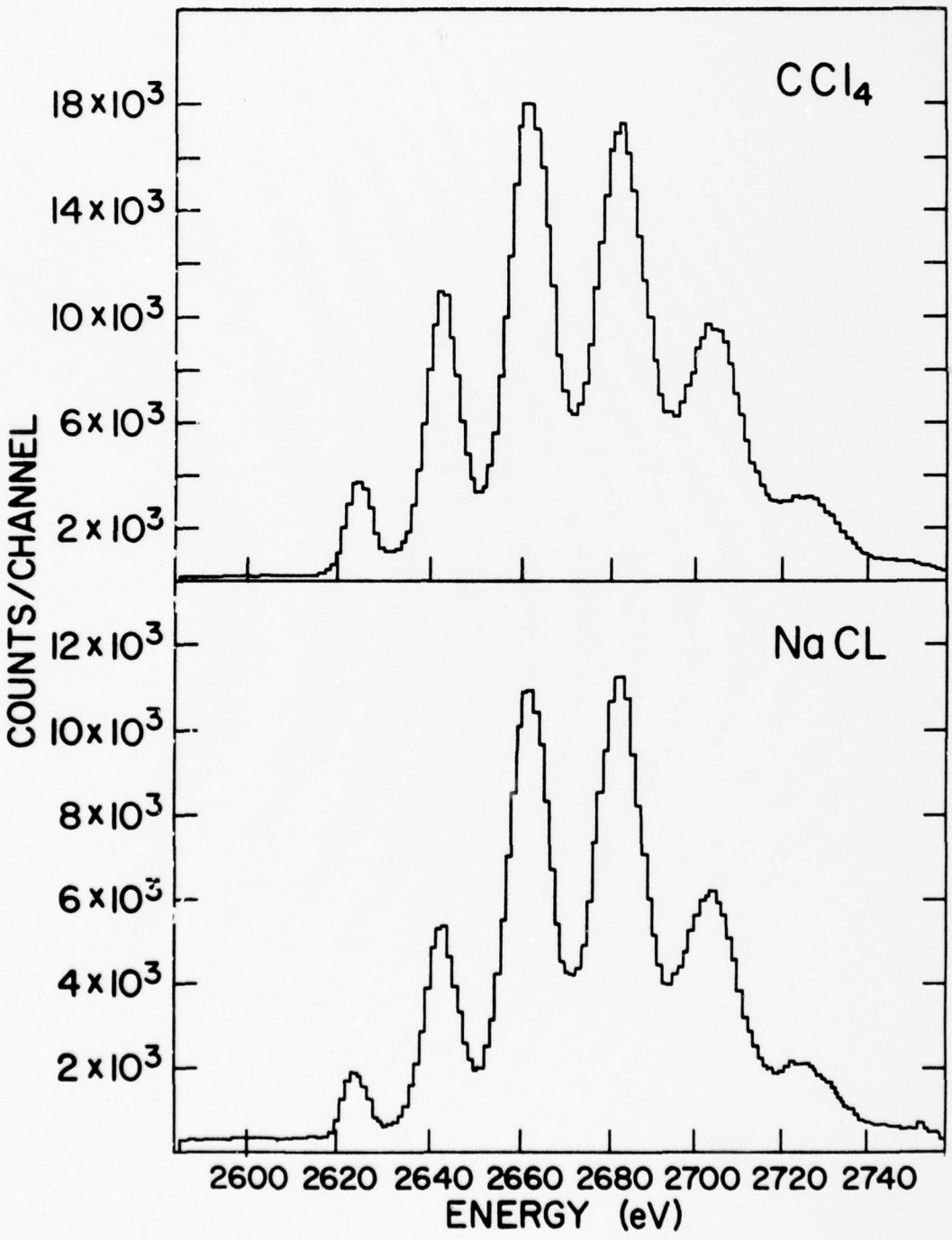

FIG. 22. Kα satellite spectra of liquid CCl_4 and solid NaCl produced by 32.4 MeV O ions.

intense in solid NaCl.

Gaseous argon is compared with solid KCl in Fig. 15 (p. 37). The relative Kα satellite distribution of Cl in KCl and Ar appear to be very similar. An attempt to measure the Kα satellite distribution of solid argon by freezing gaseous argon onto a liquid nitrogen cooled copper cold finger failed. It was determined that a colder coolant than liquid nitrogen would be required to freeze measureable amounts of argon onto the cold finger in the present experimental configuration.

Table 11 lists the relative Kα x-ray satellite intensities (fn) for the gaseous compounds of Si, S, Cl and Ar and the liquid CCl_4 obtained using 32.4 MeV oxygen ions. Also for these compounds, Table 12 lists the calculated average beam energies (MeV) for the detection of Kα x-rays, the p_L values determined directly from the fn values according to Eq. (2.5), and the p_L value corrected for projectile energy loss and flat crystal normalization.

The measured Kα x-ray satellite energies (eV) for these compounds are listed in Table 13 along with the measured individual satellite peak widths (FWHM). The errors are root-mean-square deviations. Energy shifts of the satellite peaks are significant in comparisons of spectra of the gases with the reference solid. These energy shifts provide a measure of the number of valence electrons present in the M-shell at the time of Kα x-ray emission. This point will be discussed in detail in Chapter V. The variations of the peak widths are for the most part due to the experimental effect described in Chapter II, however a more detailed treatment of Kα x-ray satellite peak width broadening to be presented in the next section will reinforce this conclusion and will demonstrate the significance of other broadening mechanisms.

TABLE 11. Relative Kα x-ray satellite intensities of the gaseous compounds of Si, S, Cl and Ar and liquid CCl_4 using 32.4 MeV oxygen ions.

	fn^a						
Compound	n=0	n=1	n=2	n=3	n=4	n=5	n=6
SiF_4	0.020	0.090	0.281	0.338	0.207	0.053	0.012
SiH_4	0.011	0.055	0.170	0.318	0.295	0.121	0.029
SF_6	0.038	0.162	0.328	0.277	0.146	0.050	
SO_2	0.031	0.133	0.324	0.301	0.142	0.068	
H_2S	0.011	0.058	0.199	0.336	0.273	0.122	
CCl_4	0.029	0.123	0.255	0.311	0.192	0.090	
Cl_2	0.016	0.112	0.274	0.314	0.212	0.072	
HCl	0.023	0.090	0.210	0.366	0.227	0.084	
Ar	0.013	0.093	0.267	0.396	0.171	0.060	

[a] Ratio of the n^{th} satellite peak intensity to the sum of the intensities of all the Kα peaks - *corrected for* absorption in the target and detector window, and for detector efficiency.

TABLE 12. Calculated average beam energies for the detection of Kα x-rays and p_L values for gaseous and liquid compounds excited by 32.4 MeV oxygen ions.

Compound	$\bar{E}$(MeV)	p_L [a]	$p_{L(corr)}$ [b]
SiF_4	19.8	0.354	0.325±0.002
SiH_4	18.1	0.414	0.387±0.006
SF_6	19.1	0.310	0.269±0.006
SO_2	18.8	0.324	0.282±0.010
H_2S	18.5	0.396	0.351±0.006
CCl_4	18.5	0.348	0.303±0.003
Cl_2	18.5	0.351	0.306±0.008
HCl	18.4	0.367	0.321±0.006
Ar	18.7	0.350	0.309±0.006

[a] p_L value determined directly from the fn values.

[b] p_L values corrected for projectile energy loss and flat crystal normalization. The indicated errors are root-mean-square deviations.

TABLE 13. Kα x-ray satellite energies and FWHM peak widths of gaseous and liquid compounds of Si, S, Cl and Ar excited by 32.4 MeV oxygen ions.

Compound	Peak	EKL^n(eV)	FWHM(eV)
SiF_4	KL^0	1740.6±0.6	3.7±0.4
	KL^1	1752.8±0.5	5.3±0.4
	KL^2	1766.0±0.3	6.7±0.4
	KL^3	1780.4±0.6	8.2±0.4
	KL^4	1795.3±0.3	9.9±0.4
	KL^5	1809.6±0.5	12.1±0.8
	KL^6	1826.0±0.7	15.4±1.0
SF_6	KL^0	2309.3±0.5	5.6±0.6
	KL^1	2324.8±0.4	6.2±0.6
	KL^2	2340.7±0.4	8.6±0.6
	KL^3	2357.9±0.5	9.7±0.6
	KL^4	2375.3±0.7	12.0±0.8
	KL^5	2393.4±0.7	14.6±1.0
H_2S	KL^0	2308.7±0.9	6.8(6.8)[a]±0.6
	KL^1	2325.8±0.6	9.1(8.1)±0.6
	KL^2	2343.7±0.3	12.3(9.9)±0.6
	KL^3	2361.8±0.7	13.5(12.4)±0.6
	KL^4	2380.0±0.7	14.4(14.4)±0.8
	KL^5	2398.5±0.7	18.3(17.3)±1.0
Cl_2	KL^0	2621.5±0.8	6.7±0.8
	KL^1	2640.7±0.7	12.8±0.8
	KL^2	2660.1±0.7	15.0±0.8
	KL^3	2680.5±0.6	15.4±0.8
	KL^4	2700.7±0.7	17.9±1.2
	KL^5	2721.7±0.8	20.3±1.5
Ar	KL^0	2957.0±0.9	12.3±1.0
	KL^1	2975.8±1.1	14.3±1.0
	KL^2	2996.5±0.8	16.8±1.0
	KL^3	3018.3±0.8	21.3±1.0

TABLE 13. Continued

Compound	Peak	EKL^n(eV)	FWHM(eV)
Ar (continued)	KL^4	3041.2±0.8	18.7±1.3
	KL^5	3061.9±0.9	21.9±1.6
SiH_4	KL^0	1739.6±0.6	5.6±0.6
	KL^1	1754.3±1.0	9.5±1.5
	KL^2	1768.0±0.7	8.9±0.6
	KL^3	1783.6±0.8	9.8±0.6
	KL^4	1799.4±0.8	11.6±0.6
	KL^5	1815.4±0.7	14.2±0.8
	KL^6	1831.2±0.7	15.5±1.0
SO_2	KL^0	2309.4±0.5	5.2±0.6
	KL^1	2325.0±0.7	7.3±0.6
	KL^2	2341.9±0.4	10.5±0.6
	KL^3	2359.4±0.5	11.8±0.6
	KL^4	2377.0±0.7	12.4±0.8
	KL^5	2394.2±0.7	17.0±1.0
CCl_4	KL^0	2622.3±0.5	5.5±0.7
	KL^1	2640.1±0.4	8.3±0.7
	KL^2	2658.8±0.5	10.2±0.7
	KL^3	2679.0±0.4	12.3±0.7
	KL^4	2699.0±0.7	15.1±1.0
	KL^5	2719.9±0.8	19.2±1.2
HCl	KL^0	2619.2±0.7	9.4(8.0)[a]±0.8
	KL^1	2640.1±1.6	17.7(10.6)±1.0
	KL^2	2659.3±1.9	17.7(12.7)±1.0
	KL^3	2680.3±1.8	16.8(16.8)±1.0
	KL^4	2701.0±1.2	19.4(17.9)±1.2
	KL^5	2721.7±1.5	20.3(18.7)±1.5

[a]Thin target measurement where $x_L \approx 0.16$ cm.

B. Consideration of Peak-Broadening Mechanisms

1. Molecular dissociation Doppler shift broadening

In ionizing collisions of third row molecular gas targets at MeV/amu energies where a single K-shell vacancy and multiple L-and M-shell vacancies are created, it is expected that a Coulomb explosion will occur between the highly charged fragments that were formerly bound together. Such a kinematic broadening effect has been observed in K-Auger transitions of carbon and nitrogen containing molecules upon bomardment by 56 MeV Ar ions.[42] The line broadening component of the 318 eV KL_1L_2 Auger peaks resulting from the molecular dissociation of N_2 was found to be 6.85 eV - in good agreement with calculations.

A similar kinematic broadening is in principle possible for the Kα x-rays emitted by the fragments of a dissociated molecule. It is here assumed that the path directions of the dissociated fragments will be isotropically distributed and will lead to a Doppler broadening of the photon representative of the kinetic energy increase imparted to the photon by the moving fragments.

The following equations lead to the Doppler shift broadening observed in the dissociation of two fragments of masses m_1 and m_2.

Conservation of momentum requires the

$$m_1 v_1 = m_2 v_2 \tag{4.3}$$

Solving for v_2 yields

$$v_2 = m_1/m_2 \, v_1 \quad . \tag{4.4}$$

Total energy is conserved

$$E_T = 1/2\ m_1 v_1^2 + 1/2\ m_2 v_2^2 \ . \qquad (4.5)$$

Substitution for v_2^2 leads to

$$E_T = 1/2\ m_1 v_1^2 + 1/2\ m_2 \left(\frac{m_1}{m_2}\right)^2 v_1^2 \qquad (4.6)$$

or

$$E_T = 1/2\ \left[\frac{m_1 (m_2+m_1)}{m_2}\right] v_1^2 \ . \qquad (4.7)$$

Solving for v_1 one obtains

$$v_1 = \left[\frac{2\ E_T\ m_2}{m_1 (m_2+m_1)}\right]^{1/2} \ , \qquad (4.8)$$

but E_T is also equal to the Coulomb potential,

$$E_T = \frac{q_1 q_2\ e^2}{R} \qquad (4.9)$$

where q_1 and q_2 are the respective charges of the fragments and R is the molecular bond length prior to dissociation.

Then the ratio of v_1 to the speed of light, c, is expressed by β or

$$\beta = \frac{v_1}{c} = \left[2\ \frac{q_1 q_2\ e^2}{R}\ \frac{m_2}{m_1 (m_2+m_1) c^2}\right]^{1/2} \ . \qquad (4.10)$$

The Doppler shift, ΔE, is given by

$$\Delta E = E_0\, \beta \cos\theta \simeq E_0\, \beta \qquad \text{for } \beta << 1,\ \theta = 0 \qquad (4.11)$$

where E_0 is the emitted photon energy. The maximum Doppler shift is therefore

$$\Delta E_{max} = E_0 \left[\frac{2\ q_1 q_2\ e^2}{R}\ \frac{m_2}{m_1 (m_2+m_1) c^2}\right]^{1/2} \ . \qquad (4.12)$$

The molecular breakup of H_2S into H and HS will serve as an example of this form of broadening. The most probable charge state of the HS fragment is 8^+, representing one K-, three L-, and four M-shell vacancies.

The L-shell ionization is obtained from the measured p_L value and the M-shell ionization is estimated from the satellite energy shifts (see Chapter V). The H fragment is assumed to be singly ionized. The maximum Doppler broadening is $\sim 2\Delta E_{max}$ and use of Eq. (4.12) results in a value of 0.06 eV. The average Doppler broadening will be less than this value for two reasons: (a) the fragments are isotropically distributed so that θ in Eq. (4.11) will not always be 0° or 180°, (b) the lifetime of the emitted Kα x-ray is so short that only metastable transitions will be Doppler-broadened by the full dissociation velocity.[42] The observed broadening for H_2S is 9.8 eV, thus it is concluded that kinematic broadening by molecular dissociation cannot account for the experimental observations.

2. Recoil Doppler shift broadening

Another source of kinematic Doppler broadening is due to the momentum transfer from the projectile to the target nucleus during the ionizing collision.

The following considerations provide a means of calculating the maximum and minimum Doppler shift due to target atom recoil.

In collisions that ionize the K-shell, it is assumed that the most probable distance of closest approach, ρ_{min}, of the projectile to the target atom is given by the radius of the K-shell at maximum electron density, r_K.

ρ_{min} is related to the collision diameter, b, by

$$\rho_{min} = \frac{b}{2}\left(\csc\frac{\Theta}{2} + 1\right) \qquad (4.13)^{43}$$

where Θ is the deflection angle of the target atom in the center of mass system.

Solving for $\csc \frac{\Theta}{2}$ yields

$$\csc \frac{\Theta}{2} = \frac{\rho_{min} - b/2}{b/2} \tag{4.14}$$

where b is given by

$$b = \frac{Z_1 Z_2 e^2}{E_{cm}} \quad . \tag{4.15}$$

The nuclear charges of the projectile and target are Z_1 and Z_2 and the energy of the center of mass, E_{cm}, is given by

$$E_{cm} = \frac{1}{2} \frac{m_1 m_2}{(m_1+m_2)} v^2 = \frac{m_2}{m_1+m_2} E_{lab} \tag{4.16}$$

where m_1 and m_2 are the masses of the projectile and E_{lab} is the incident beam energy.

The recoil energy of the target atom, Q, is then given by

$$Q = \frac{2}{m_2 c^2} \left(\frac{Z_1 Z_2 e^2}{v/c}\right) \frac{1}{x^2 + (b/2)^2} \tag{4.17}$$

where c is the velocity of light, v, the velocity of the projectile, and x, the impact parameter calculated by

$$x = \frac{b}{2} \cot \frac{\Theta}{2} \quad . \tag{4.18}$$

As an example, the recoil Doppler shift broadening of 23.5 MeV oxygen on sulfur will be calculated. In this case $r_{K\ max}$ is 3.35×10^{-10} cm.[44]

Equation (4.13) gives for Θ a value of 0.201 degrees which means that there is very little deflection of the projectile at this incident energy with the distance of closest approach equal to $r_{K\ max}$. Equation (4.17) gives a target recoil enorgy of 64.7 eV. The sulfur atom recoil

angle is 89.9° with respect to the ion beam so that the Doppler shift broadening found by use of Eq. (4.11) with $\theta = 57.6°$ is 0.18 eV. Therefore it is concluded that Doppler shift broadening caused by target atom recoil is not a significant broadening mechanism in these experiments.

3. Lifetime broadening

The mean lifetime of the transition of interest provides a natural linewidth that can be calculated by

$$\Delta E = \frac{\hbar}{\tau} = \frac{27.1}{\tau \text{ (atu)}} \qquad (4.19)^{45}$$

where ΔE is the natural linewidth in eV and τ is the mean lifetime in atomic time units (1 atu = 2.42×10^{-17} sec.). For sulfur, the mean lifetime of a single K vacancy has been determined by the transition rates reported by McGuire[46] to be 1.4×10^{-15} seconds. Equation (4.19) gives a natural linewidth of 0.472 eV for this transition. Calculations of higher order satellite lines show that these transitions have increased mean lifetimes over those for the single K-shell ionization state.[32] This increase is easily understood since the density of electrons that provide such transitions is greatly reduced.

A new experimental technique developed by Betz et al.[47] enables the determination of the lifetimes of highly ionized states and the lifetime of the KL^7 transition was determined to be 1.7×10^{-14} seconds which equates to a linewidth of 0.039 eV. Therefore lifetime broadening does not have a significant effect on the current measured widths since lifetime widths <u>decrease</u> with an increase in L-shell ionization whereas the experimental widths <u>increase</u> with an increase in L-shell ionization.

4. Broadening due to vibrational excitation

Recent studies of gaseous molecules of carbon, nitrogen, and sulfur[48] indicate that vibrational broadening is a significant effect in the photoionization process of core electrons. The linewidth of the sulfur 2p level is seen to increase by 0.1 eV from SF_6 to COS by this mechanism. This effect is still insignificant when compared to the present Kα x-ray broadening measurements.

5. Doppler broadening due to the thermal motion of the molecule or atom

The average kinetic energy of a molecule, $\bar{E}$, due to thermal agitation is given by

$$\bar{E} = \frac{3}{2} k T \qquad (4.20)^{49}$$

where T is the absolute temperature and k is the Boltzmann constant. For H_2S at room temperature $\bar{E}$ equals 2 meV and use of Eq. (4.11) results in a negligible maximum Doppler broadening of 0.002 eV for the KL^3 peak in the Kα satellite spectrum.

6. M-shell vacancy distribution broadening

The results of the Hartree-Fock calculations presented in Chapter V can be used to show how the distribution of M-shell vacancies leads to a significant spread in energy for each KL^n transition depending upon the number of M-shell electrons present at the time of Kα x-ray emission. In sulfur a particular KL^n peak can vary in energy from 7 eV for the KL^0 peak up to 25 eV for the KL^7 peak according to the M-shell configuration.

An apparent average M-shell vacancy fraction, p_M, can be determined by

$$p_M = \frac{\bar{n}}{N_m} \tag{4.21}$$

where N_m is the total number of M-shell electrons in a ground state atom and $\bar{n}$ equals the average number of M-shell vacancies. This latter quantity can be approximated by a comparison of experimental Kα-satellite energies with the results of Hartree-Fock calculations. The Hartree-Fock calculations and experimental energies will be compared in detail in Chapter V.

Since the distribution of M-shell vacancies for each KL^n transition was not determined experimentally, it is assumed that the distribution of M-shell vacancies is binomial in character. Then the relative probability of producing a particular M-shell configuration, P_n, can be calculated

$$P_n = \binom{N_N}{n} p_m \, (1 - p_M)^{N_M - n} \tag{4.22}$$

where $\binom{N_M}{n}$ is the binomial coefficient $N_M!/(N_M-n)!n!$ and n equals the number of M-shell vacancies.

The root-mean-square deviation, σ_M, of the M-shell vacancy distribution is given by

$$\sigma_M = [\Sigma \, P_n \, (n-\bar{n})^2]^{1/2} \tag{4.23}$$

and the FWHM, Γ_M, is approximately given by

$$\Gamma_M \approx 2.35 \, \sigma_M \tag{4.24}$$

[Eq. (4.24) is exact only for a Gaussian distribution]. Thence Γ_M can be used to determine ΔE_M, the energy broadening due to the spread in M-shell vacancies, from the Hartree-Fock calculated energy values for each Kα satellite peak. Fig. 23 shows the calculated M-shell vacancy

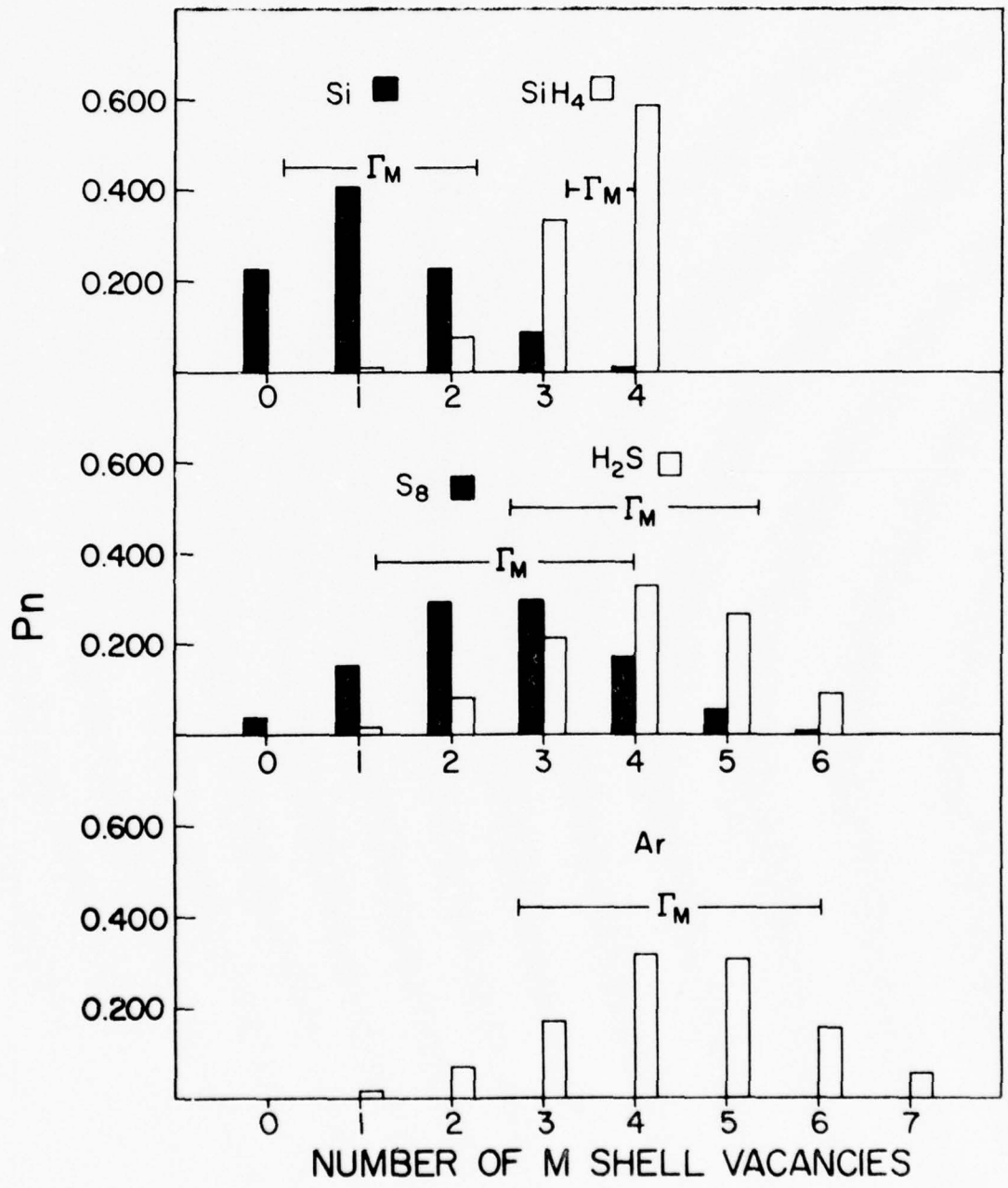

FIG. 23. Calculated M-shell vacancy distributions for Si, SiH_4, S_8, H_2S, and Ar.

distributions for Si, SiH_4, S_8, H_2S and Ar.

Table 14 presents the values for $\bar{n}$, p_M, Γ_M, and ΔE_M for Si, SiH_4, S_8, H_2S, and Ar. The values predicted for ΔE_M are much more significant than the contributions from any of the other broadening mechanisms considered up to this point. In fact, the ΔE_M broadening appears to account for a large fraction of the broadening observed in the higher order satellites.

The total width of a KL^n peak, ΔE_T, can be approximated by four components

$$\Delta E_T = [(\Delta E_{sp})^2 + (\Delta E_{X_L})^2 + (\Delta E_M)^2 + (\Delta E_{Res})^2]^{1/2} \qquad (4.25)$$

where ΔE_{sp} is the resolution of the spectrometer (FWHM), ΔE_{X_L} is the predicted broadening due to extended path length, ΔE_M is the broadening due to the distribution of M-shell vacancies, and ΔE_{Res} is a residual broadening factor.

TABLE 14. Calculated M-shell vacancy distribution values.

Target	$\bar{n}$	p_M	Γ_M	ΔE_M(eV)
Si	1.25	0.313	2.18	4.4
SiH_4	3.50	0.875	0.78[a]	1.8
S_8	2.60	0.433	2.86	7.4
H_2S	4.00	0.667	2.70	7.3
Ar	4.40	0.550	3.31	10.3

[a]The Γ_M for SiH_4 was taken to be 1/2(FWHM) since no more than four M-shell electrons can be ionized.

The resolution of the spectrometer can be determined from the FWHM of the KL^0 peak of the reference solid. The spin-orbit splitting of the KL^0 peak is only 0.65 eV[50] for silicon and 1.30 eV[51] for sulfur which is not significant compared to the instrumental resolution. The predicted broadening for the gases, ΔE_{X_L}, is calculated by

$$\Delta E_{X_L} = 2\ X_L\ \Delta E/\Delta X \qquad (4.26)$$

where X_L is the average target thickness in cm for x-ray detection and $\Delta E/\Delta X$ is the peak energy shift in eV per cm. These two paramters are given in Table 6 (p. 30) and Fig. 13 (p. 33) in Chapter II. The residual broadening factor, ΔE_{Res}, is associated with complex multiplet structure resulting from LS coupling of the initial and final hole states as illustrated in Fig. 3 (p. 7) of Chapter I. Also included in ΔE_{Res} is any other undetermined broadening effect. Unless much better resolution of K satellite spectra can be achieved, an accurate determination of ΔE_{Res} is not possible. However, to a first approximation, ΔE_{Res} can be determined from Eq. (4.25) for the reference solid when the experimental FWHM value for ΔE_T and values for ΔE_{sp} and ΔE_M are supplied. Then use of this value for ΔE_{Res} for the gas will enable a calculation of ΔE_T for the gas. Table 15 lists the results of applying the above procedure to the third satellite peak for a number of solids and gases studied. The third satellite peak was chosen for comparison since it was generally the most intense peak and would reduce statistical error. Reasonable agreement between the calculated total peak width ΔE_T(calc) and experimental total peak width, ΔE_T(exp), is obtained by use of Eq. (4.25) but until the uncertainties of ΔE_{Res} can be resolved the accuracy of the estimate for E_M remains in question. The main conclusion, however, is

that the peak widths are consistent with expectations based upon the various sources of broadening considered, and the widths observed for the gases, after correction for path length effects, are the same as those for solids.

TABLE 15. KL^3 satellite peak width components, experimental width and theoretical calculation of total width in eV.

Compound	ΔE_{sp}	ΔE_{X_L}	ΔE_M [a]	$\Delta E_{(Res)}$	$\Delta E_{T(calc)}$	$\Delta E_{T(exp)}$
Si	3.4	0	4.4	3.9		6.8±0.4
SiH_4	3.4	4.6	1.8	3.9	7.2	9.8±0.6
P_4	7.6	0	[5.7]	[5.0]	10.7	11.1±0.5
S_8	4.5	0	7.4	6.1		10.6±0.6
H_2S	4.5	10.6	7.3	6.1	14.9	13.5±0.6
KCl(Cl)	6.1	0	[8.8]	[7.2]	12.9	12.0±0.8
Ar	9.3	16.0	10.3	[8.3]	22.8	21.3±1.0
KCl(K)	11.8	0	[11.7]	[9.4]	19.1	20.0±1.2

[a]Values in brackets were interpolated or extrapolated.

C. Interpretation of Data

1. Dependence of p_L on target atomic number

The real significance of the degree of L-shell ionization of the various gases and liquid studied becomes apparent when compared to measurements for solid compounds of Al, Si, P, S, Cl and K. Such a comparison is shown in Fig. 24 where the p_L values for the gases and

liquid are indicated by data points or arrows and the ranges of values observed for solids are indicated by solid vertical bars.

Examination of Fig. 24 reveals several important observations:

a. The gases SiH_4, H_2S and HCl have much larger p_L values than do the corresponding gases having ligands containing large numbers of valence electrons (i.e. SiF_4, SO_2, SF_6, and Cl_2). In addition, the p_L values for the hydrated gases decrease monotonically with increasing target atomic number and converge with the solid compound values near $Z = 18$.

b. The gases SiF_4, SO_2, SF_6, and Cl_2 and the liquid CCl_4 have p_L values which fall within the ranges observed for the corresponding solids.

It is apparent from the trends established by the data in Fig. 24 that interatomic transitions must play an important role in the fast electron rearrangement which occurs in solid, liquid and heavy gas compounds of Si, S, and Cl within the lifetime of the K-vacancy state. The low p_L values for these compounds indicate electron transfer from either of two sources: (a) electron transfer from the target atom's own M-shell (intra-atomic transitions) or (b) electron transfer from neighboring atoms (interatomic transitions). The answer as to which is the more likely of the above two processes lies in the analysis of the M-shell electron population. For (a) to be the more likely case L-vacancy transfer would deplete the M-shell. This is not the case, however, as Table 14 indicates that solid silicon and sulfur have an average of only 31% and 43% of their M-shell electrons missing whereas SiH_4 and H_2S have an average of 88% and 67% of their M-shell electrons missing. This

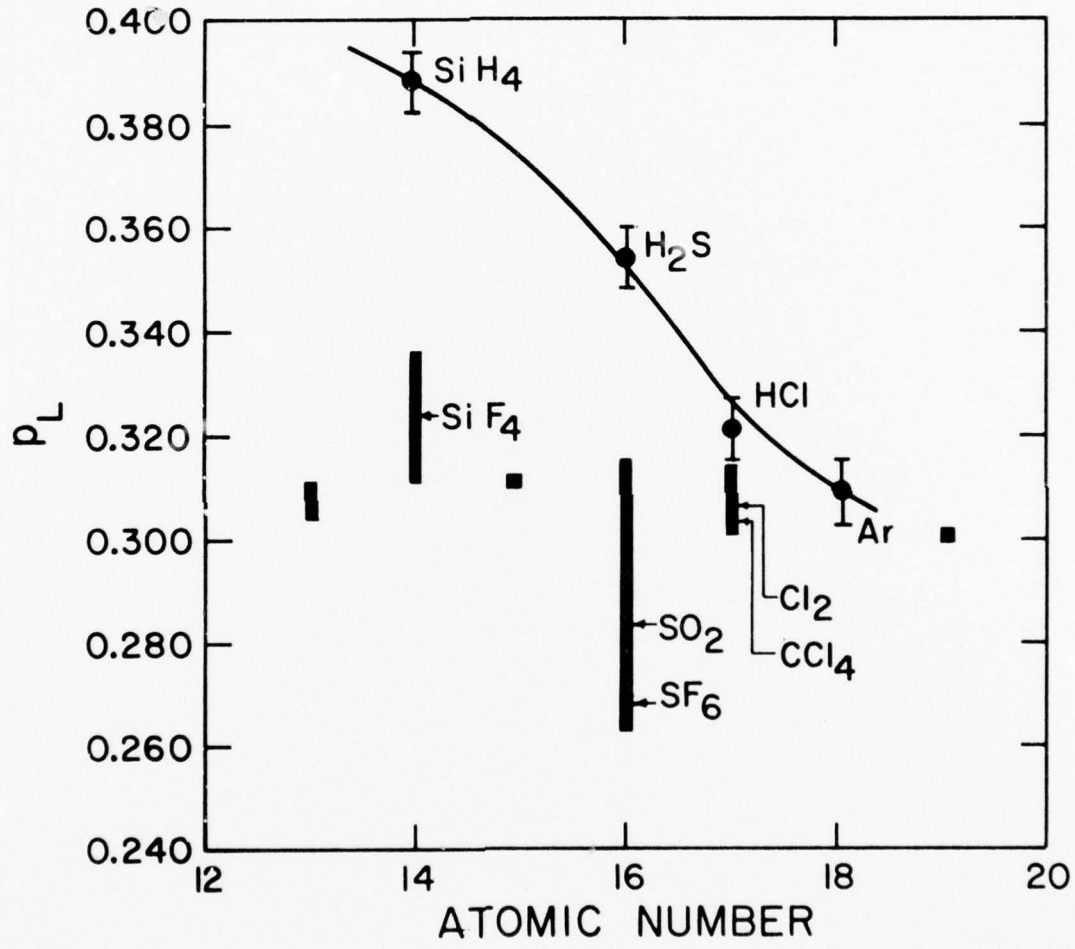

FIG. 24. A comparison of the p_L values for the gases and liquid studied in the present work (data points and arrows) with ranges of values observed (Ref. 29) for various solid compounds (vertical bars).

clearly indicates that process (b) above accounts for the refilling of the M-shell of the solids. The K- and L-shells can then be filled directly by interatomic transfer or by a cascade of electrons from the replenished M-shell. In addition, the differences between p_M and p_L values for the solids and light gases decrease with an increase in atomic number which indicates that the relative importance of fast interatomic transitions rapidly diminishes as the population of the M-shell increases. As a consequence, it can be inferred that for atomic numbers higher than Ar, a chemical effect on the Kα satellite intensity distributions will not be evident.

In order to reinforce these conclusions, it is desirable to examine the dependence of p_L on valence electron density to determine how the gases and liquid compare with the observed behavior of solids.

2. Correlation of p_L with effective charge

As pointed out in the last chapter, the effects of chemical environment on the Kα satellite intensity distributions of solids reveal that the apparent degree of L-shell ionization present at the time of Kα x-ray emission (a) decreases as the average <u>total</u> valence electron density of the compound increases and (b) increases as the <u>localized</u> valence electron density of the target atom increases.

The localized valence electron density of a target atom may be crudely represented by the concept of effective charge.[29] A variety of methods are available for obtaining values for effective charge[1] including theoretical integrals over the electron density, orbital population analysis, the use of electronegativities, the measurement of isomer shifts by Mössbauer spectroscopy and Knight shift by nuclear magnetic

resonance spectroscopy. Isomer shift and Knight shift sample only s-like electrons at the nucleus, while x-ray and electron line shifts are sensitive to the entire electron density in the region of core orbitals.

In the present study, the simple method of Pauling is used.[52] Accordingly, the effective charge is taken to be the product of the oxidation number and the bond ionicity, I, which is defined as

$$I = 1 - e^{-0.25\Delta^2} \tag{4.27}$$

where Δ is the electronegativity difference between the two atoms involved. Thus in a totally ionic bond $1 >> e^{-0.25\Delta^2}$ and the oxidation number represents the number of electrons transferred. Shown in Fig. 25 is the correlation of p_L versus effective charge for compounds of silicon, sulfur and chlorine. In each of the chemical series it is seen that p_L decreases smoothly with increasing effective charge. The p_L values for the gases SO_2, SF_6, and Cl_2 and the liquid CCl_4 are consistent with the observed variation of solid compounds with effective charge. The p_L value for SiF_4 seems to be too high. A more accurate determination of effective charge would likely decrease Pauling's value and bring it into better agreement. What is strikingly apparent is that the p_L value for the hydrated gases lie well above the other values.

The trend of p_L with effective charge can be understood by considering where the valence electrons reside during the collision process. At low effective charge the valence electrons are localized about the target atom and are probably ionized in the ion atom collision. This valence electron ionization results in a high p_L value since the total valence electron population is thereby depleted. At more positive values for effective charge the valence electrons spend less time in the

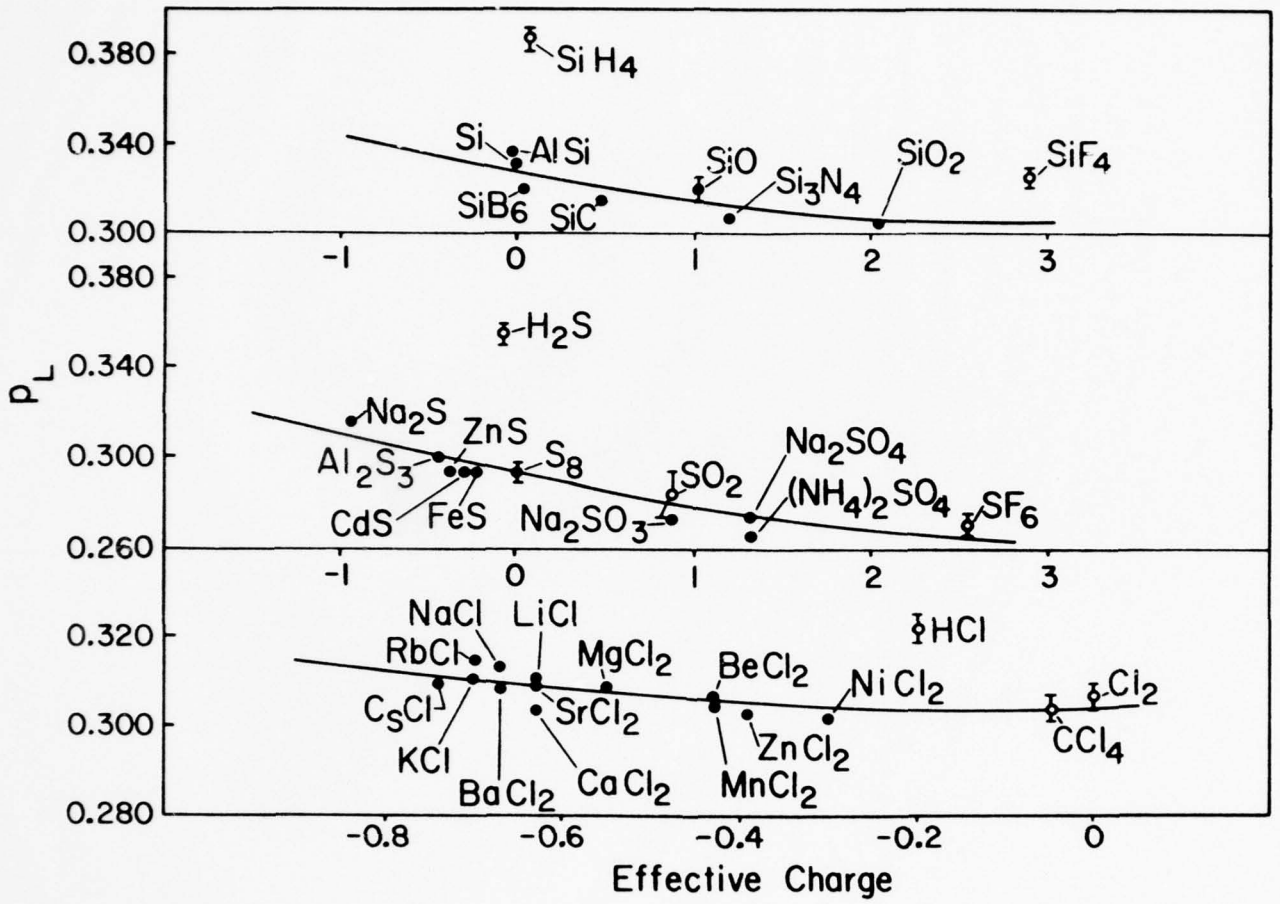

FIG. 25. The variation of p_L with effective charge for compounds of silicon, sulfur, and chlorine excited by 32 MeV O ions.

vicinity of the target atom and more time displaced toward neighboring atoms, in which case they are not as likely to be ionized in the collision. Following the collision, these valence electrons become readily available to participate in K- and L-vacancy filling transitions which leads to a lower p_L value. The decrease in p_L with increasing effective charge appears to level off at high positive values which indicates that interatomic transitions reach a saturation point beyond which an increase in available valence electron density has no contributory effect.

Finally, since the heavy gases and liquid have p_L values that closely fit the trend established by the data for solids, it is concluded that the rearrangement processes in general do not depend upon physical state, but rather upon the availability of electrons from neighboring atoms.

3. Correlation of p_L with electron binding energy shift

As mentioned previously, electron binding energy shifts are sensitive to the valence electron density in the region of the core orbitals. Therefore experimental binding energy shifts of inner shell electrons as measured by ESCA provide another test of the correlation of p_L with local valence electron density. In fact, a comparison of p_L with ESCA binding energy shifts compensates for inaccuracies that may exist in the simple effective charge model. Shown in Fig. 26 is a comparison of p_L with 2p electron binding energy shifts. The references for the binding energies shown in Fig. 26 are as follows: sulfur and silicon compounds and CCl_4 Ref. 14, chlorine solids Ref. 53, and HCl Ref. 54.

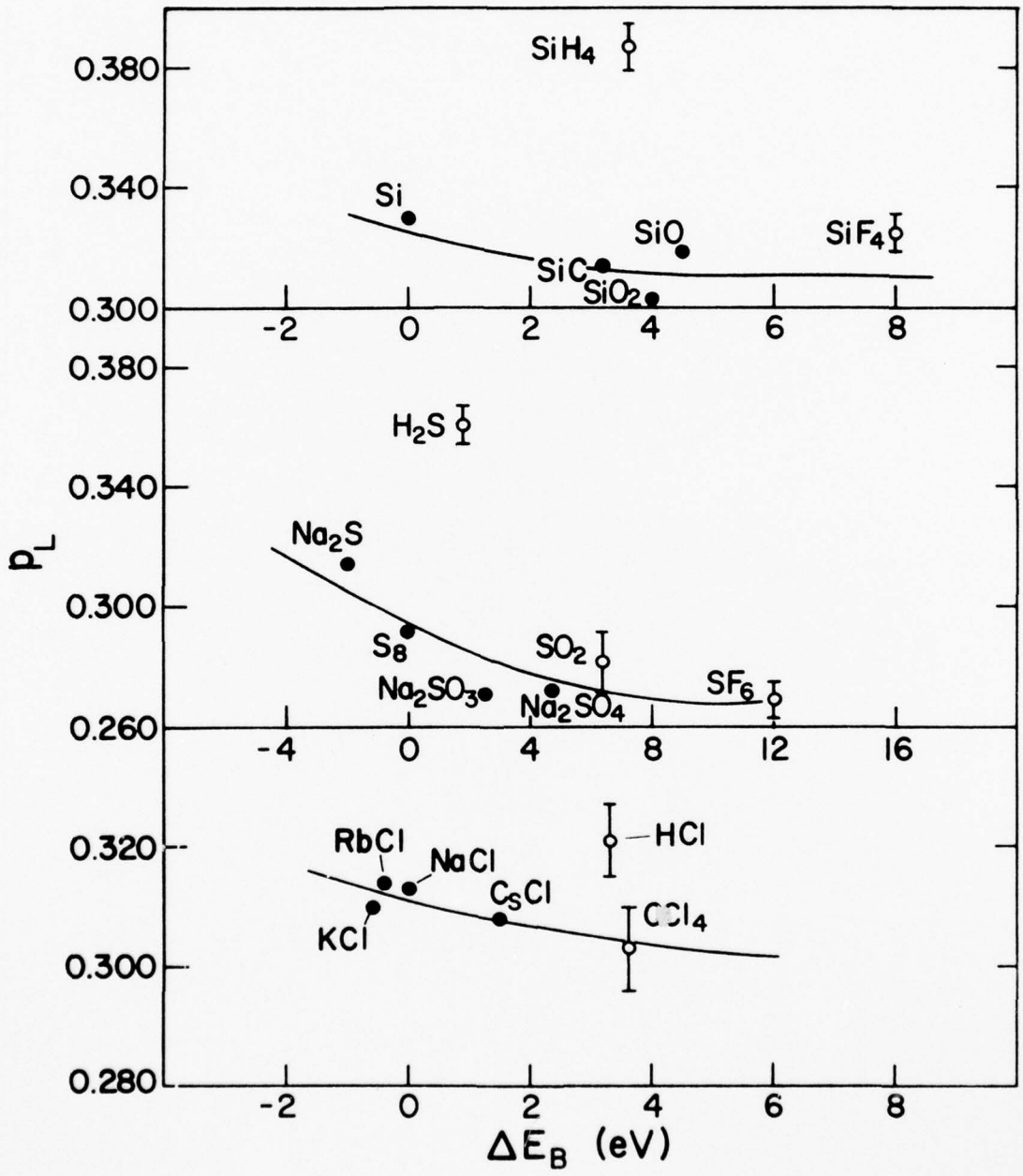

FIG. 26 Comparison of p_L with ESCA binding energy shifts.

A correction was applied to the binding energy values for solids to allow for their comparison with binding energy values for gases. This correction was necessary since the binding energies of electrons in solids are normally measured relative to the Fermi level. The difference in binding energy between the gas and solid is the work function, w. Values for w have not been measured for many solid compounds but a survey of the reported values of w[55] for the nonconducting elements in the portion of the periodic table that includes the elements of interest resulted in the choice of 4.5 eV for Si and 4.6 eV for S and Cl. Evaluation of Fig. 25 reinforces the validity of the comparison of p_L with effective charge.

In summary, it has been discovered that the observed differences in the apparent degree of L-shell ionization for the gases SiF_4, SO_2, SF_6, and Cl_2, and the liquid CCl_4 are all consistent with what is expected based on the observed variation of the solid compound p_L values with local valence electron density. In fact, the observed p_L values are associated with the availability of electrons from neighboring atoms and not with physical state (i.e. solid, liquid or gas). Moreover, the much higher p_L values for the light gases are indicative of the importance of interatomic transitions in solids, liquids, and gases having ligands with available valence electrons. Furthermore, the results indicate that the Kα satellite intensity distributions for elements beyond argon should not be significantly affected by chemical environment.

D. Theoretical determination of p_L

To the extent that the hydrated gases (SiH_4, H_2S, and HCl) can be considered free atoms, experimental determinations of p_L for these gases should provide a means for testing the Z dependence of theoretical predictions of p_L. The theory chosen for this test is the impact-parameter formulation of the binary encounter approximation (BEA) as developed by Hansen.[56] The BEA method was chosen since it closely reproduces the excitation functions for K-shell ionization by alpha particles over a wide range of projectile velocities and target atomic numbers.[27]

The BEA treats the collision process as an interaction of two free particles - the incident ion and the specified electron. Hansen modified the BEA as originally presented by Gerjuoy[57] and Vriens[58] from a calculation performed in momentum space to a calculation performed in configuration space by relating the velocity of the electron to its distance from the nucleus The calculations involve screened hydrogenic wavefunctions, a hyperbolic projectile ion path, a fully stripped projectile ion and a single value for the electron binding energy.

Previous investigations have found that high-resolution Kα x-ray spectra resulting from ion-atom collisions could be well represented by binomial distributions.[59,27] Therefore, to a good approximation, multiple ionization can be expressed as a binomial distribution in the single ionization probability which can be calculated by a number of recent theoretical methods. The ionization cross section for a particular

KL^n state is accordingly given by

$$\sigma_{KL^n} = 2\pi \int_0^\infty b\, 2\, P_K(b)[1 - P_K(b)]\, \binom{N_L}{n} P_L(b)^n [1 - P_L(b)]^{N_L - n}\, db \qquad (4.29)$$

where b represents the impact parameter, $P_K(b)$ is the probability of ionizing a K shell electron, $\binom{N_L}{n}$ is the binomial coefficient expressed by $N_L!/(N_L-n)!n!$, N_L is the total number of L shell electrons in the ground state and $P_L(b)$ is the weighted average of the 2s and 2p ionization probabilities per electron as calculated from the BEA.

The parameter p_L is then calculated in terms of σ_{KL^n} by

$$p_L = \frac{1}{N_L} \frac{\sum_{n=1}^{7} n\omega_n \sigma_{KL^n}}{\sum_{n=0}^{7} \omega_n \sigma_{KL^n}} \qquad (4.30)$$

where ω_n is the fluorescence yield for the n^{th} satellite peak interpolated from the theoretical values given in Ref. 31 and 32 [see Fig. 11 (p. 24) in Chapter II]. The results of these calculations for 23.5 MeV oxygen on Si, S, Cl and Ar are listed in Table 16 under the column labeled Theory A. When the fluorescence yield is assumed to be constant in Eq. (4.30), slightly lower values for p_L result and these values are listed in Table 16 under the column labeled Theory B. It has been noted before that the theoretical p_L values are much larger than the experimental values.[60,31] However, if the values of Theory A are normalized to the experimental values at SiH_4 only a small disagreement in the Z dependence results and is illustrated by a dashed-dot line on Fig. 27. Also illustrated in Fig. 27 are Theory A, Theory B, p_L values for the light gases (open circles), heavy gases (open triangles), and the reference solids (solid squares).

TABLE 16. Theoretical p_L values for Kα x-ray satellite production by 23.5 MeV oxygen ions.

Compound	BEA predicted p_L		
	Expt.[a]	Theory A[b]	Theory B[c]
SiH_4	0.410	0.865	0.857
H_2S	0.370	0.859	0.844
HCl	0.335	0.856	0.837
Ar	0.324	0.853	0.829

[a] p_L values corrected to the energy of the ion beam after penetration through the Kapton foil.

[b] Calculated using fluorescence yields interpolated from the theoretical values given in ref. 31 and 32.

[c] Calculated assuming a constant fluorescence yield for peaks KL^0 to KL^7.

Two factors may account for a small portion of the disagreement between theory and experiment. The first factor concerns the fact that the projectile ion is not fully stripped but carries an average charge state of $6.5^{+}.^{61}$ Changes in projectile charge state play an important role in affecting target p_L values (see Ref. 62). The second factor concerns the fact that theory does not account for any intra-atomic electron rearrangement (a process which becomes increasingly more important as the population of the M-shell is filled). It will be demonstrated in Chapter V that even the light gases are not fully stripped of M-shell electrons and hence intra-atomic rearrangement cannot be discounted. A true test of the BEA necessitates a collision system consisting of a fully stripped projectile and a free atom target that has only K- and

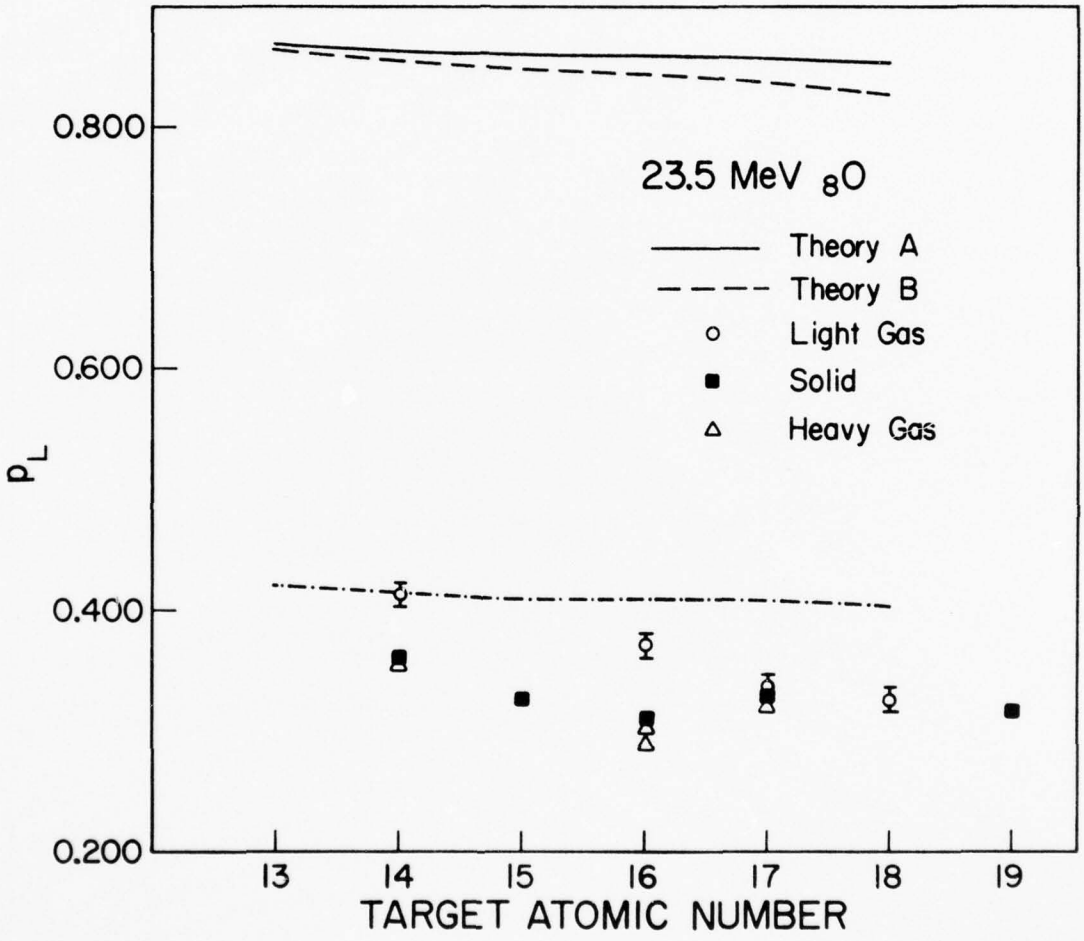

FIG. 27. Comparison of theoretical and experimental p_L values using 23.5 MeV oxygen ions. The dashed-dot line represents Theory A normalized to the experimental values at SiH_4.

L-shell electrons remaining after the collision such that electron rearrangement via interatomic processes and vacancy transfer to higher shells cannot occur.

E. Comparison of Kα satellite distribution of gases and solids produced by 6.7 MeV He ion bombardment

The study of Kα spectra of third row gases and solids were extended to bombardment by 6.7 MeV He ions in order to judge the significance of fast electron rearrangement on systems that display a low degree of L-shell ionization. In addition, a more valid test of the Z dependence of the BEA theory is provided since the projectile is fully stripped and the relatively low states of L-shell ionization exhibited in the spectra are not expected to be greatly influenced by variations in fluorescence yield or by fast electron rearrangement processes.

Displayed in Fig. 28 are the Kα satellite intensity distributions of Si, SiH_4, S_8, SF_6, H_2S, KCl and HCl produced by 6.7 MeV He ions. The spectra reveal remarkably little change in any of the features that were identified in the 32.4 MeV oxygen ion data. In fact, there is little change in the relative satellite distributions despite the differences in molecular environment, physical state, and atomic number. The relative satellite intensities, fn, are listed in Table 17 along with the calculated beam energy for the detection of Kα x-rays, the p_L values determined directly from fn and the p_L values corrected for projectile energy loss.

A surprising observation from this data is that within the margin of error noted, the light gases consistently display a slightly lower p_L value than the solids. This is just the opposite behavior observed in

AD-A050 006 AIR FORCE INST OF TECH WRIGHT-PATTERSON AFB OHIO F/G 7/4
COMPARISON OF HEAVY ION-INDUCED K-ALPHA X-RAY SATELLITE SPECTRA--ETC(U)
DEC 77 J A DEMAREST

UNCLASSIFIED AFIT-CI-78-31 NL

2 OF 2
AD
A050006

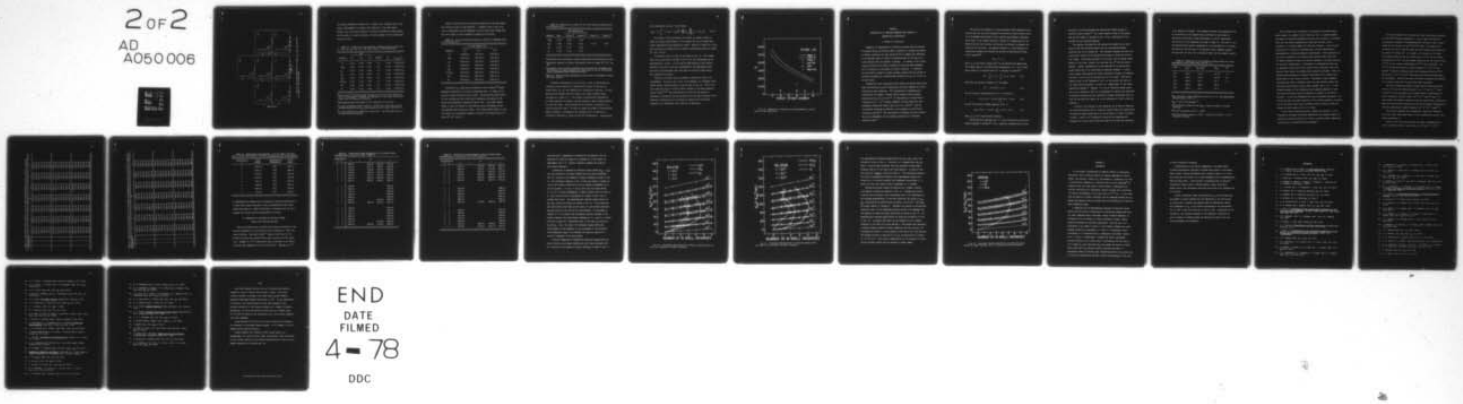

END
DATE
FILMED
4-78
DDC

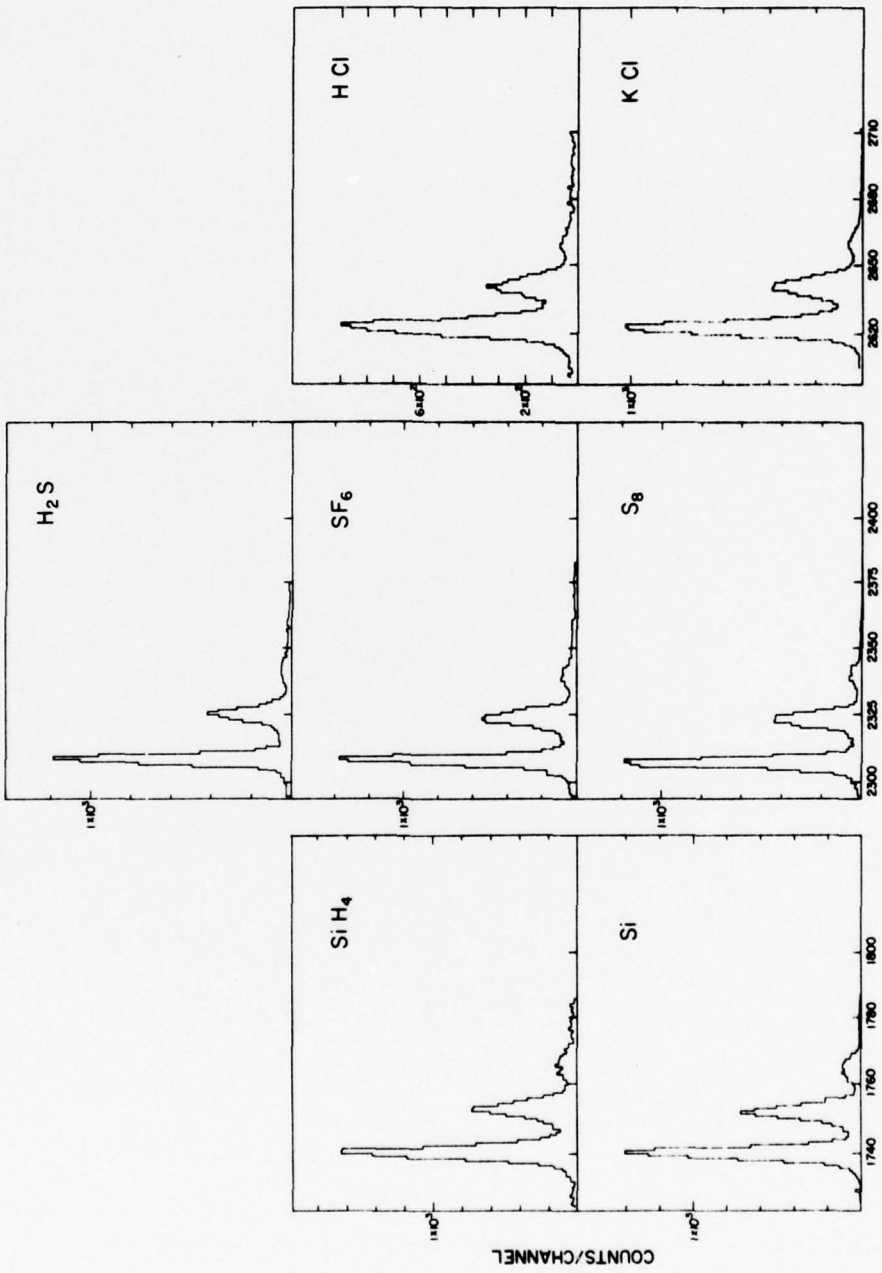

FIG. 28. Kα x-ray spectra for Si, SiH_4, S_8, SF_6, H_2S, KCl and HCl using 6.7 MeV helium ions.

the spectra produced by oxygen ions. Possibly this indicates that intra-atomic rearrangement is slightly more effective in the light gases. However, due to the small amount of ionization displayed by these spectra and the margin of errors indicated, a strong argument for this explanation cannot be given.

TABLE 17. Relative Kα x-ray satellite intensities and p_L values for Si, SiH_4, S_8, SF_6, H_2S, KCl, HCl and Ar using 6.7 MeV helium ions.

Compound	fn[a]			$\bar{E}$(MeV)[b]	p_L[c]	$p_{L(corr)}$[d]
	n=0	n=1	n=2			
Si	0.572	0.366	0.062	4.9	0.061	0.051±0.002
SiH_4	0.616	0.327	0.057	4.8	0.055	0.044±0.003
S_8	0.623	0.333	0.044	4.9	0.053	0.043±0.002
SF_6	0.611	0.345	0.044	5.1	0.054	0.045±0.002
H_2S	0.652	0.312	0.036	4.8	0.049	0.038±0.003
KCl(Cl)	0.627	0.315	0.058	5.0	0.052	0.042±0.002
HCl	0.654	0.295	0.051	4.9	0.050	0.039±0.003
Ar	0.687	0.272	0.042	4.9	0.044	0.033±0.003

[a] Ratio of the n^{th} satellite peak intensity to the sum of the intensities of all the Kα peaks - corrected for absorption in the target and detector window, and for detector efficiency.

[b] Calculated average beam energy for the detection of Kα x-rays.

[c] p_L value determined directly from fn. In the case of KCl the p_L value has been corrected for $K\alpha_{1,2}$ photoionization by Kα x-rays (see Ref. 29).

[d] p_L value corrected for projectile energy loss. The indicated errors are root-mean-square deviations.

Table 18 lists the Kα x-ray satellite energies for the three peaks that could be fitted in each spectrum. A chemical shift in the x-ray lines is observable for the compounds of silicon and sulfur though they are not as great as those observed in oxygen ion collisions.

TABLE 18. Kα x-ray satellite energies of third row compounds using 6.7 MeV helium ions.

	Kα x-ray Energy (eV)		
Compound	KL^0	KL^1	KL^2
Si	1739.8±0.4	1751.5±0.4	1764.1±0.6
SiH_4	1739.9±0.4	1752.3±0.4	1764.9±0.6
S_8	2308.1±0.5	2323.7±0.4	2339.9±0.4
SF_6	2308.8±0.5	2324.0±0.4	2339.4±0.4
H_2S	2308.1±0.5	2324.5±0.6	2341.0±0.8
KCl(Cl)	2621.9±0.5	2639.6±0.5	2656.1±1.0
HCl	2621.8±0.5	2639.6±0.5	2656.1±1.0
Ar	2957.0±0.5	2977.7±0.7	2997.1±1.2

Theoretical p_L values were calculated by use of Hansen's[56] impact parameter formulation of the BEA as described above. In Table 19 the results of these calculations are listed. The projectile energy chosen for the calculations was 5.8 MeV which represents the energy of the helium ions penetrating through the Kapton foil. The column labeled Theory A lists the results of calculations using fluorescence yields interpolated from theoretical values. The column labeled Theory B lists the results of calculations assuming a constant fluorescence yeild for peaks KL^0, KL^1, and KL^2.

TABLE 19. Theoretical p_L values for Kα x-ray satellite production by 5.8 MeV helium ions.

		BEA predicted p_L			
Compound	Expt.	Theory A[a]	Theory B[b]	Theory C[c]	Theory D[d]
SiH_4	0.049	0.425	0.370		
H_2S	0.043	0.283	0.247	0.127	0.116
HCl	0.045	0.230	0.200		
Ar	0.039	0.180	0.157		

[a] Calculated using fluorescence yields interpolated from theoretical values.

[b] Calculated assuming a constant fluorescence yield for peaks KL^0, KL^1, and KL^2.

[c] Calculated using L-electron probabilities accounting for increased binding energies as L-shell electrons are removed and by use of fluorescence yields interpolated from theoretical values.

[d] Same as c except constant fluorescence yield values are assumed for peaks KL^0, KL^1, and KL^2.

One major shortcoming of the use of Eq. (4.29) in calculating the ionization cross section for a particular KL^n state is the use of a single value, P_L, for the probability of ionizing an L-electron. As more electrons are ionized from the L-shell, the L-shell binding energy increases by a factor of 3. The results of Hartree-Fock calculations of sulfur reported in Chapter V provide accurate L-shell binding energies for each KL^n state. These energies may be utilized to calculate a P_L value for each KL^n state. In order to assess the effect of these binding energy increases, a calculation was carried out for 5.8 MeV He on S utilizing a different P_L value for each KL^n configuration. Incorporating

this modification into Eq. (4.29) yields

$$\sigma_{KL^n} = 2\pi \int_0^\infty b\, 2\, P_K(1 - P_K)\binom{N_L}{n} \prod_{i=0}^{n} P_{L_i} \prod_{j=n+1}^{N_L} (1 - P_{L_j})\, db \qquad (4.31)$$

The result of this calculation for sulfur is listed in Table 19 under the column labeled Theory C and includes the use of fluorescence yields interpolated from theoretical values. Theory D in Table 19 is this same calculation accomplished with constant fluorescence yields for peaks KL^0, KL^1, and KL^2.

The results listed in Table 19 are shown in Fig. 29. The Z dependence of p_L predicted by the BEA is not at all well represented by the experimental p_L values. In this case the BEA predicts a much greater decrease in p_L with Z than that represented by the experimental data. This fact is discouraging since this type of collision system should best represent the theory.

Obviously the theory must be refined to account for some of its shortcomings. The use of Eq. (4.31) is one example of a refinement which yields greatly improved results as can be seen in Fig. 29. This is the first reported result of such an effort although it has been suggested several times.[60,63] More calculations of this type are needed to ascertain if accounting for the increase in the L-binding energies of the remaining L-electrons as an L-electron is removed will also better represent the Z dependence of p_L observed by experiment.

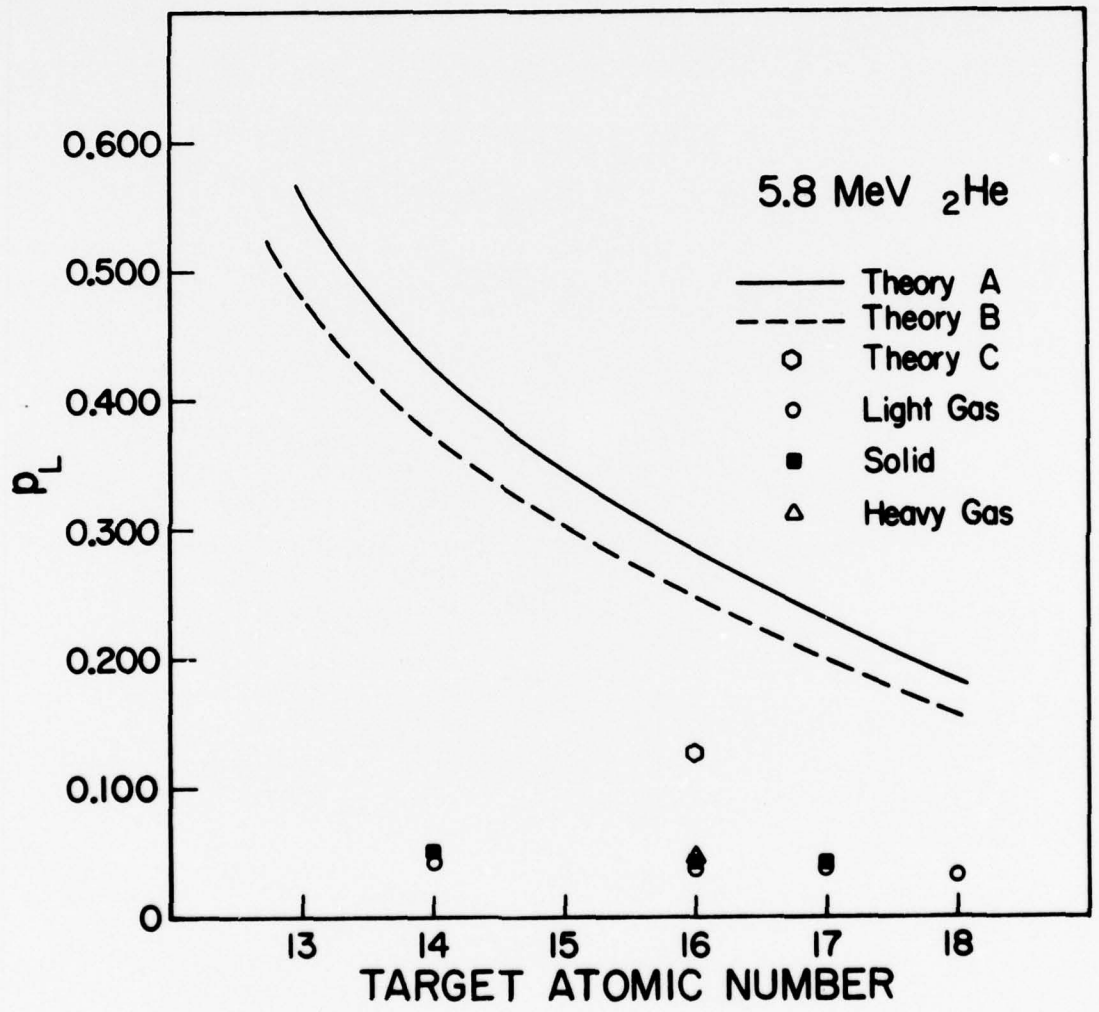

FIG. 29. Comparison of theoretical and experimental p_L values using 5.8 MeV helium ions.

CHAPTER V

COMPARISON OF Kα SATELLITE ENERGIES WITH RESULTS OF HARTREE-FOCK CALCULATIONS

A. Method of Calculation

Comparison of experimental Kα satellite energies with the results of accurate energy calculations make it possible to estimate the degree of M-shell ionization for each satellite and to compare the difference in the average number of M-shell vacancies present at the time of Kα x-ray emission from one compound to another. In Chapter IV the M-shell vacancy fractions were used to estimate Kα satellite peak broadening due to variations in the number of M-shell vacancies. In addition, the calculated increase of L-shell binding energies with an increase in ionization allowed for a modified BEA calculation of p_L for 5.8 MeV He on free sulfur.

Hartree-Fock (HF) calculations were chosen over Hartree-Fock-Slater (HFS) calculations since HF calculations have been reported to be more accurate for many situations. HFS calculations of hypersatellite transitions, for example, (double K-shell vacancy initial states) produced errors of up to 40 eV.[64] HF calculations of Coster-Kronig transitions ($2s^{-1} \rightarrow 2p^{-1}$ vacancy transfer) of argon agree well with experiment whereas HFS results were 10-15 eV in error.[65] Also HF calculations reproduce the absolute x-ray energies of silicon more accurately than HFS.[20] HFS calculations of energies are less accurate due to the replacement of the exchange potential by a localized potential term.[27]

The Hartree-Fock method is a self-consistent field calculation that follows from the variation principle by setting up a wave function which is an antisymmetrized produce of one electron spin-orbitals (determinantal form) of the various electrons, finding the average value of the Hamiltonian for this function, and varing the orbitals to minimize the energy of this function. The spatial orbitals, ϕ_i, that minimize the variational integral are obtained by solving the Hartree-Fock differential equations[66]

$$\bar{H}\,\phi_i = \varepsilon_i\ \phi i \qquad (5.1)$$

where ε_i is the orbital energy and $\bar{H}$ is the Hartree-Fock Hamiltonian. The average value of the Hartree-Fock Hamiltonian, <H> , for a closed shell system of N electrons and N/2 = n orbitals is given by[67]

$$\langle H\rangle = \sum_{i=1}^{n} 2\,\varepsilon_i^{\,0} + \sum_{i,j}^{n} (2\,Jij - Kij) \qquad (5.2)$$

where the one electron integrals $\varepsilon_i^{\,0}$ are simply

$$\varepsilon_i^{\,0} = \langle \phi i\,|H^0(i)|\ \phi i\rangle \quad , \qquad (5.3)$$

the two electron Coulomb operator Ji(1) is defined by

$$Ji(1)\ \phi j(1) = \langle \phi i(2)|\ \frac{1}{r_{12}}\ |\phi i(2)\rangle\ \phi j(1) \qquad (5.4)$$

and the two electron exchange operator Ki(1) is

$$K_i(1)\ \phi j(1) = \langle\ \phi i(2)\ |\ \frac{1}{r_{12}}\ |\ \phi j(2)\rangle\ \phi i(1) \qquad (5.5)$$

where r_{12} is the inter-electron distance.

The Hartree-Fock equation (Eq. 5.1) can be solved by an analytical method proposed by Roothaan[68] or by a numerical procedure such as that

utilized in the multiconfiguration Hartree-Fock (MCHF) program of Charlotte Froese Fischer.[69] The latter method is used in the present work and the reader is referred to Ref. 69 for a description of the program and the equations employed.

The energies calculated by the Hartree-Fock method are not exact since the HF wave functions account for the interactions between electrons only in an average way. The difference between the exact non-relativistic energy and the Hartree-Fock energy is called the correlation energy. Correlation energies of the K-shell for the target atomic numbers in this work, however, are less than one eV[70] and can thus be ignored. Another consideration is the magnitude of the relativistic energy correction to the calculated Kα satellite energies. A relativistic energy contribution for K-shell ionization energies is estimated from Ref. 70 to be 3 eV for silicon and 6 eV for sulfur. MCHF calculations result in KL^0 energies of 1737.1 eV for silicon and 2301.8 eV for sulfur which are within 3 eV and 6 eV, respectively, of the values reported by Bearden.[33] However, it is the Kα satellite energy shifts that are of interest so that it is unnecessary to correct the calculated Kα satellite energies for the relativistic energy contribution since it will for the most part cancel out in the difference of the Kα satellite energies.

A check on the accuracy of this assertion can be made by comparing the calculated Hartree-Fock Kα satellite energy shifts with experimental Kα satellite energy shifts where the exact degree of M-shell ionization is known. Panke et al.[71] reported Kα satellite and hypersatellite energies for 92 MeV sulfur projectiles where the M-shell was determined

to be completely stripped. The difference between the experimental and HF calculated Kα x-ray energy shifts indicates the error made in neglecting relativistic energy differences in the KL^n transitions. The results of this comparison are shown in Table 20. The error in the HF computed energy shifts corresponds to an overestimate of 0.8 M-shell vacancies for the KL^6 peak of the measured sulfur compound energies and thus will not alter the conclusions drawn from the present analysis.

TABLE 20. Comparison of HF Kα satellite energy shifts in eV with experimental sulfur beam x-rays from Ref. 71.

Peak	E_{KL^n}[a]	$E_{KL^n}-E_{KL^0}$[b]	ΔE_{HF}	Δm[c]
KL^6	2429.3	121.8	117.7[d]	1.1
KL^6	2429.3	121.8	118.8[e]	0.8
KL^7	2454.6	147.2	141.0	1.4
K^2L^6	2596.2	288.8	285.9	
K^2L^7	2621.6	314.2	310.4	

[a] Mean transition energy obtained by use of Eq. (4.2) from experimental energies given in Ref. 71.

[b] E_{KL^0} = 2307.4 from Bearden.[33]

[c] The difference between ΔE and ΔE_{HF} in terms of number of M-shell vacancies.

[d] From KL^6 transitions $1s^1 2p^2 \rightarrow 1s^2 2p^1$.

[e] From statistical average of $1s^1 2p^2 \rightarrow 1s^2 2p^1$ and $1s^1 2s^1 2p^1 \rightarrow 1s^2 2s^1$ transition energies.

The following input information is required by the MCHF program: atomic number, the number of wave functions, the n, ℓ quantum numbers, the number of electrons associated with each wave function, an estimated value for the orbital eigenvalue for each wave function, and an estimate of a screening number for each wave function. In the initial calculation of a series of configurations, the wave functions were approximated by screened hydrogenic wavefunctions. After completion of the first calculation, the resulting wave functions were often left in computer memory and used as an initial estimate of the wave functions for the next configuration. Calculations of configurations with open or completely vacant inner shells having M-shell electrons often took several trials before the minimum total energy was obtained. Often the program would converge on a solution that would be of a larger total energy than for the correct solution. Fortunately, these erroneous solutions were easy to recognize since the outer electron radial wave functions would contain too many nodes (greater than $n-\ell-1$). A more accurate estimate of the eigenvalues and screening numbers for these cases would eventually allow the program to converge to the correct solution. It was also determined that once the program converged to the correct solution any other alteration of the initial estimates (including use of the output values from a previous correct solution) would only change the final answer by 0.01 eV or less.

In the case of some particularly stubborn calculations, it was necessary to estimate the orbital eigenvalues and screening numbers by removing one type of electron at a time or by using orbital eigenvalues calculated by a Hartree-Fock-Slater program.[72]

The total energies for the inital and final states were calculated for each KL^nM^m vacancy configuration. For all cases the option of calculating an average of configurations was utilized so that a single energy was calculated for the KL^0 and KL^7 peaks, two energies were calculated for the KL^1 and KL^6 peaks and three energies were calculated for peaks KL^2 through KL^5. For example, in the case of a KL^1 peak, the average energy for the two initial states (^1S, ^3S) for the vacancy configuration $1s^{-1}2s^{-1}$ and the average energy for the two initial states (^1P, ^3P) for the vacancy configuration $1s^{-1}2p^{-1}$ were calculated. The $1s^{-1}2s^{-1}$ states may decay by Kα x-ray emission to ^1P and ^3P final states[27] for which an average energy was calculated and the $1s^{-1}2p^{-1}$ may decay to ^1S or ^1D, and ^3P final states for which an average energy was calculated. Thus for each state of M-shell ionization the energies of 21 initial states and 21 final states were calculated.

The total energies calculated by MCHF were converted from atomic units to eV using the conversion factor 1 au = 27.2107 eV.[70] Table 21 lists the total energies for the various defect configurations of sulfur containing a filled K-shell [$2s^{-\ell}\ 2p^{-n}\ (3s3p)^{-m}$] where ℓ, n, and m denote the number of vacancies from the ground state configuration. Table 22 lists the total energies for the various defect configurations of sulfur containing a single K-vacancy [$1s^{-1}\ 2s^{-\ell}\ 2p^{-n}\ (3s3p)^{-m}$].

Kα satellite energies can be obtained by taking the difference of a final state energy from Table 21 and an appropriate initial state energy from Table 22.

Table 23 lists the total energies for defect configurations of sulfur containing vacant K- and M-shells [$1s^{-2}(2s2p)^{-n}\ 3s^{-2}3p^{-4}$].

TABLE 21. Hartree-Fock total energies in eV for defect configurations of sulfur $[2s^{-\ell}2p^{-n}\ (3s3p)^{-m}]$.

Configuration		m						
ℓ	n	0	1	2	3	4	5	6
0	0	10815.70	10804.99	10783.64	10750.34	10703.88	10633.28	10545.93
0	1	10643.54	10619.61	10583.03	10532.67	10467.42	10375.85	10266.19
0	2	10433.54	10393.92	10339.55	10269.78	10183.52	10069.22	9935.58
0	3	10181.29	10123.90	10049.92	9958.46	9849.09	9710.40	9551.14
0	4	9884.97	9806.08	9710.39	9595.64	9461.10	9296.39	9109.93
0	5	9540.10	9438.72	9318.19	9178.00	9016.56	8824.26	8609.06
0	6	9143.62	9017.57	8870.96	8702.92	8512.54	8291.09	8045.65
1	0	10579.26	10555.32	10518.72	10468.33	10403.07	10312.15	10203.17
1	1	10375.02	10335.16	10280.90	10211.18	10125.00	10011.50	9878.68
1	2	10129.70	10071.80	9997.52	9906.29	9797.11	9659.36	9501.06
1	3	9839.23	9761.39	9665.44	9550.54	9416.34	9252.73	9067.38
1	4	9502.00	9400.63	9281.02	9140.95	8979.73	8788.70	8574.75
1	5	9113.67	8987.88	8841.55	8674.22	8484.33	8264.30	8020.29
1	6	8671.27	8518.95	8344.73	8147.78	7927.22	7676.72	7401.12
2	0	10306.56	10266.72	10212.46	10142.74	10056.60	9943.73	9811.73
2	1	10067.32	10009.17	9935.06	9843.94	9734.88	9597.92	9440.59
2	2	9784.08	9705.75	9609.53	9494.95	9360.98	9198.31	9014.08
2	3	9452.99	9352.70	9232.89	9092.76	8931.94	8741.98	8529.34
2	4	9072.58	8946.87	8801.53	8634.41	8444.90	8225.03	7983.46
2	5	8638.63	8486.64	8312.79	8116.65	7896.67	7647.56	7373.59
2	6	8148.21	7967.91	7764.44	7536.96	7282.21	7003.72	6696.86

TABLE 22. Hartree-Fock total energies in eV for defect configurations of sulfur $[1s^{-1}2s^{-\ell}2p^{-n}(3s3p)^{-m}]$.

Configuration		m						
ℓ	n	0	1	2	3	4	5	6
0	0	8341.72	8317.24	8279.83	8228.26	8161.45	8068.42	7957.02
0	1	8118.60	8077.80	8022.25	7950.87	7862.61	7746.51	7610.75
0	2	7852.40	7793.11	7717.04	7623.61	7511.77	7370.91	7209.15
0	3	7539.11	7459.33	7361.05	7243.37	7105.90	6938.67	6749.33
0	4	7176.99	7073.18	6950.65	6807.19	6642.08	6446.87	6228.41
0	5	6761.80	6632.98	6483.13	6311.78	6117.36	5892.64	5643.53
0	6	6290.53	6134.57	5956.22	5754.60	5528.93	5273.12	4991.89
1	0	8060.69	8019.94	7964.43	7893.10	7804.91	7689.64	7554.71
1	1	7801.33	7741.85	7665.98	7572.70	7461.04	7321.16	7160.38
1	2	7495.99	7415.81	7317.33	7200.00	7062.84	6896.73	6708.53
1	3	7140.83	7038.13	6915.47	6772.00	6607.38	6413.45	6196.29
1	4	6734.32	6605.63	6456.83	6285.75	6091.71	5868.43	5620.79
1	5	6272.27	6116.71	5938.78	5738.04	5512.96	5258.82	4979.22
1	6	5751.78	5567.27	5359.08	5126.36	4868.26	4581.77	4268.75
2	0	7739.38	7679.98	7604.20	7511.01	7399.49	7260.41	7100.64
2	1	7441.15	7360.83	7262.61	7145.51	7008.60	6843.44	6656.40
2	2	7094.27	6991.21	6868.41	6725.37	6561.13	6368.31	6152.46
2	3	6695.00	6567.48	6418.63	6247.63	6054.15	5832.14	5585.97
2	4	6241.93	6086.58	5909.78	5709.40	5484.78	5232.07	4954.11
2	5	5730.94	5546.92	5339.26	5107.50	4850.15	4565.26	4254.05
2	6	5159.19	4944.48	4704.84	4439.43	4146.05	3828.89	3482.97

TABLE 23. Hartree-Fock total energies in eV for defect configurations of sulfur [$1s^{-2}(2s2p)^{-n}\ 3s^{-2}3p^{-4}$] and Hypersatellite x-ray energies.

Configuration n	Total Energy	Hypersatellite Designation	X-ray Energy
0	5140.38	K^2L^0	2470.37
1	4674.10	K^2L^1	2486.28
2	4153.54	K^2L^2	2502.86
3	3630.48	K^2L^3	2521.98
4	3043.47	K^2L^4	2542.50
5	2389.70	K^2L^5	2564.41
6	1666.39	K^2L^6	2587.66
7	870.74	K^2L^7	2612.23

Kα hypersatellite energies can be obtained by taking the difference of a final state energy from Table 22 and an appropriate initial state energy from Table 23. Table 24 and Table 25 similarly list the total energies for various defect configurations of silicon.

B. Comparison of calculated Kα satellite energy shifts with solid and gas data

Many investigators have concluded that multiple ionization of the M-shell accompanies K- plus multiple L-shell ionization in heavy ion-atom collisions. Burch and Richard[73] reported that three to five M-shell electrons were removed from Ca when ionized by 15 MeV oxygen ions. Kaufmann et al.[22] claimed that SiH_4 is stripped of all M-shell electrons when bombarded by 45 MeV chlorine ions. Madison et al.[74]

TABLE 24. Hartree-Fock total energies in eV for various defect configurations of silicon [$2s^{-\ell}2p^{-n}$ $(3s3p)^{-m}$].

Configuration		m				
ℓ	n	0	1	2	3	4
0	0	7859.41		7836.59	7804.64	7760.00
0	1	7751.24		7704.37	7656.57	7594.58
0	2	7610.89		7534.69	7469.13	7388.00
0	3	7434.62		7324.33	7239.20	7137.23
0	4	7218.46		7070.13	6963.76	6839.32
0	5	6959.43		6769.06	6639.82	6491.34
0	6	6655.11		6418.12	6264.43	6090.37
1	0	7698.66				7542.73
1	1	7562.57				7340.78
1	2	7391.12				7095.35
1	3	7180.95				6803.48
1	4	6928.25				6462.24
1	5	6630.21			6241.61	6068.72
1	6	6284.49		5998.21	5819.87	5620.07
2	0	7506.06				7285.15
2	1	7339.17				7044.70
2	2	7134.11				6758.52
2	3	6887.74				6423.67
2	4	6596.34				6037.26
2	5	6257.23			5794.84	5596.40
2	6	5868.10		5529.25	5324.91	5098.23

TABLE 25. Hartree-Fock total energies in eV for various defect configurations of silicon [$1s^{-1}$ $2s^{-\ell}$ $2p^{-n}$ $(3s3p)^{-m}$].

Configuration		m				
ℓ	n	0	1	2	3	4
0	0	6014.11		5965.89	5917.22	5854.07
0	1	5862.97		5784.65	5717.88	5635.24
0	2	5674.41		5561.22	5474.54	5370.70
0	3	5445.05		5292.49	5184.20	5057.51
0	4	5171.10		4975.42	4843.89	4692.78
0	5	4849.76		4607.06	4450.72	4273.64
0	6					
1	0	5814.98				5588.39
1	1	5631.76				5329.63
1	2	5408.30				5022.93
1	3	5141.45				4665.39
1	4	4827.53				4254.15
1	5	4463.84		4170.88	3989.53	3786.35
1	6					
2	0	5580.01				5279.24
2	1	5362.20				4978.66
2	2	5101.54				4627.94
2	3	4795.02				4224.22
2	4	4439.06				3764.65
2	5	4031.02		3684.52	3476.81	3246.40
2	6	3568.65		3163.83	2927.13	2666.65

concluded from a comparison of Hartree-Fock calculations with the measured KL^1 satellite energy of Ti produced by 30 MeV oxygen ion bombardment that 2 to 3 M-shell vacancies accompany the single K- and L-shell vacancies.

A comparison of measured Kα satellite energy shifts ($E_{KL^n} - E_{KL^0}$) for solid sulfur and the gases studied here with those calculated (HF) as a function of the number of M-shell vacancies is shown in Fig. 30. The calculated energies in Fig. 30 show the spread in energy for a given KL^n vacancy configuration for the various arrangements of 2s and 2p electrons. In fact, it can be seen that the energy spread (3 to 5 eV) of these arrangements is nearly constant over the range of M. This fact was used to interpolate for values in the Si and Ar figures that follow. The experimentally observed energy shifts for H_2S, SF_6, and S_8 are plotted as curves in Fig. 30. It can easily be seen from these curves that H_2S has about 1.5 more M-shell vacancies than SF_6 and S_8 at the time of Kα x-ray emission. As concluded in Chapter IV, it is evident that interatomic electron transfer to the M-shell together with intra-atomic cascading of M → L and M → K transitions may account for a substantial part of the lower p_L values for SF_6 and S_8. Thus, the study of Kα satellite energy shifts add reinforcement to the arguments of the involvement of the electrons from neighboring atoms in the observed Kα satellite spectra of a series of compounds of the same element.

A similar comparison of measured Kα satellite energy shifts for solid silicon and the gases studied here with those calculated (HF) as a function of the number of M-shell vacancies is shown in Fig. 31.

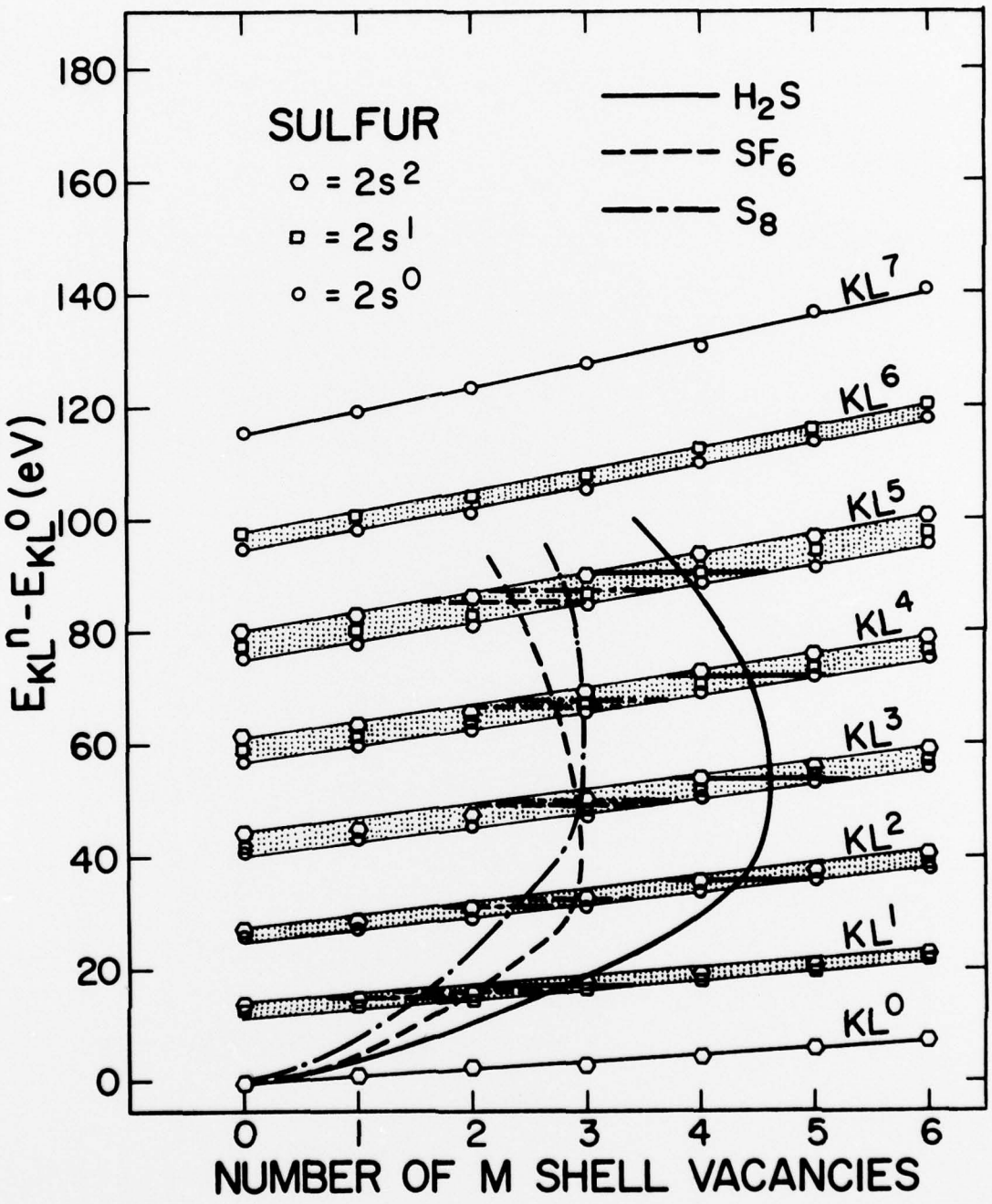

FIG. 30. Calculated (Hartree-Fock) Kα satellite energy shifts for sulfur as a function of M-shell vacancies.

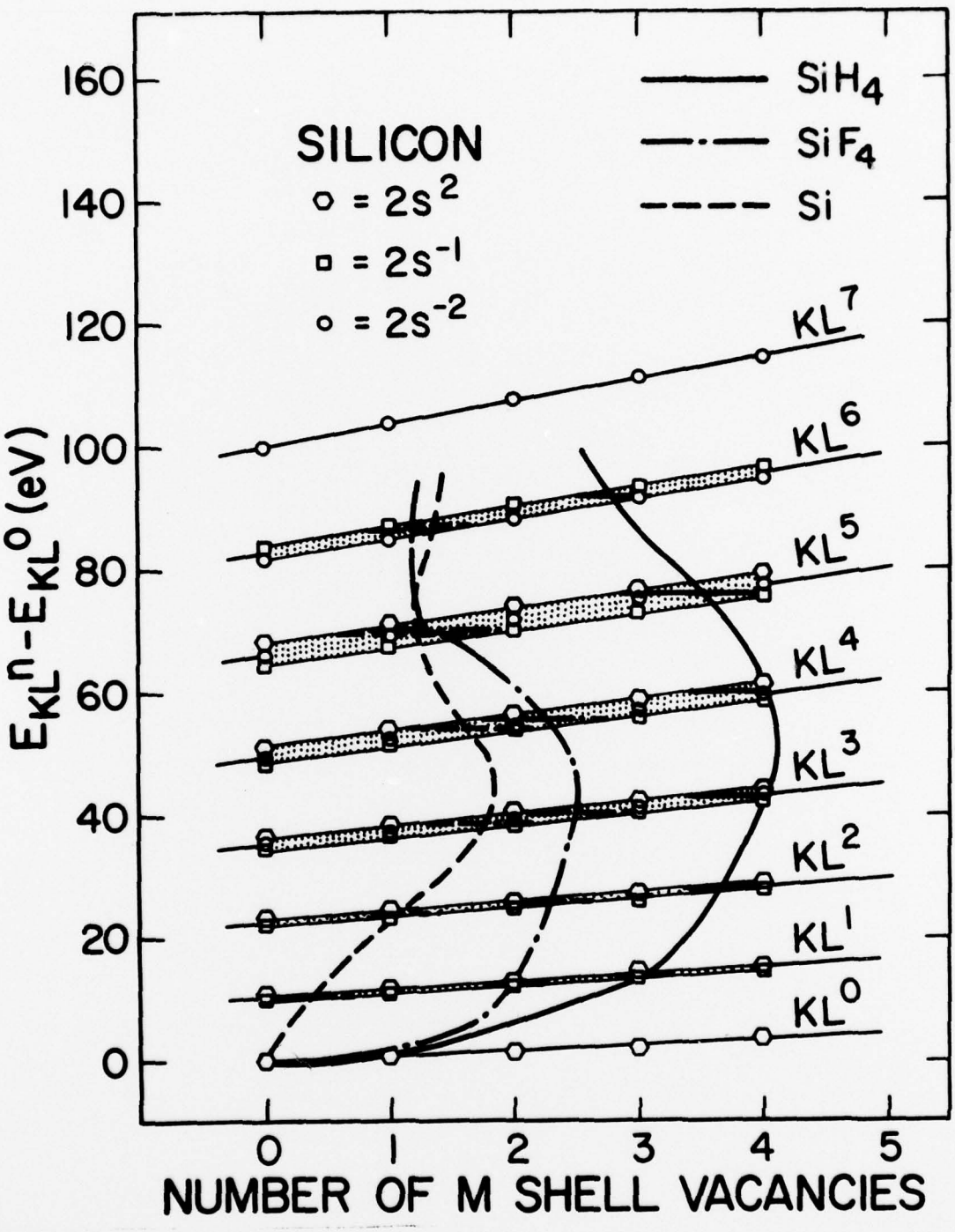

FIG. 31. Calculated (Hartree-Fock) Kα satellite energy shifts for silicon as a function of M-shell vacancies.

The experimentally observed energy shifts for SiH_4, SiF_4, and Si are plotted as curves in Fig. 31. From Fig. 31 it appears that SiH_4 has about 1.5 more M-shell vacancies than SiF_4 and about 2 more M-shell vacancies than Si at the time of Kα x-ray emission. In spite of this fact SiF_4 has a lower p_L value than does Si. This interesting observation may be interpreted as evidence that rearrangement cannot occur solely by M → M electron transfer with subsequent intra-atomic M → L decay, but must also involve direct interatomic M → L transfer.

Hartree-Fock-Slater energy calculations for a number of defect calculations of argon are reported in Ref. 32. Although HFS calculations are not as accurate as HF calculations due to the limitations of the exchange approximation, it has been found that the values of $E_{KL^n} - E_{KL^0}$ calculated by HF and HFS agree to within 2 eV for $KL^1 \rightarrow KL^4$ peaks for atomic numbers 13 through 19. Therefore the results of calculations reported in Ref. 32 are considered accurate enough to be compared with the measured Kα satellite energy shifts and are shown in Fig. 32. The experimentally observed energy shifts for argon are plotted as a curve in Fig. 32. It appears that argon has an average of 4 to 5 M-shell vacancies at the time of Kα x-ray emission. Even though this represents a slightly greater number of M-shell vacancies than SiH_4 and H_2S, the percentage of M-shell vacancies present at the time of Kα x-ray emission has dropped from 88% in SiH_4 and 67% in H_2S (as pointed out in Chapter IV) to 55% in Ar. This trend is expected due to the increase in M-shell electron binding energy with an increase in atomic number.

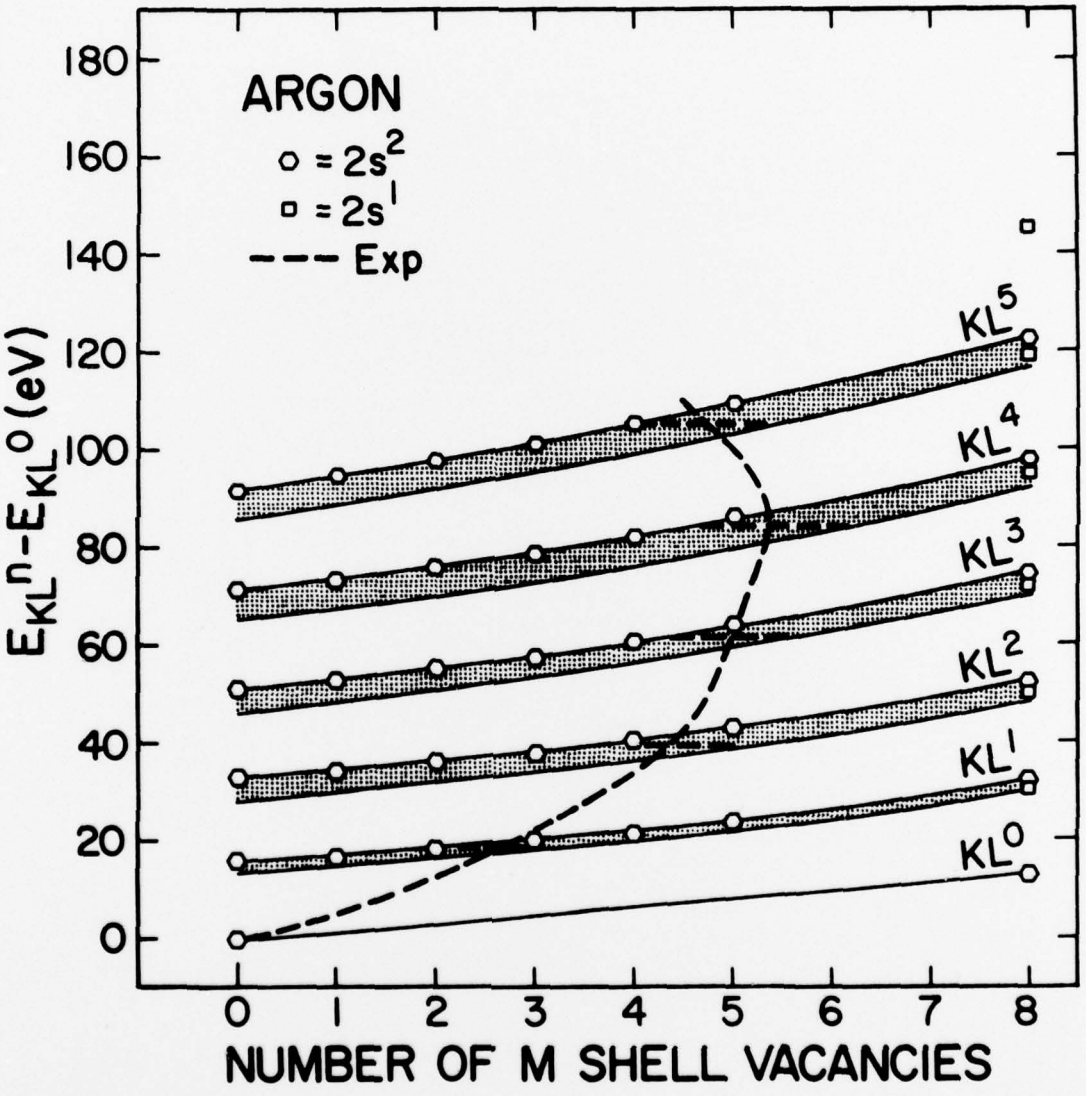

FIG. 32. Calculated (Hartree-Fock-Slater) Kα satellite energy shifts for argon from Ref. 32 as a function of M-shell vacancies.

CHAPTER VI

CONCLUSION

In the present investigation of chemical effects on inner-shell ionization, the Kα satellite spectra of gaseous compounds of silicon, sulfur, and chlorine, liquid CCl_4, and gaseous Ar, produced by 32.4 MeV O ions have been compared to a previous study of solid compounds[29] of elements within the same range of atomic number to demonstrate the relative contribution of interatomic vacancy transfer that contributes to electron rearrangement on the time scale of 10^{-14} sec. It was found that the degree of L-shell ionization for the compounds studied did not depend upon physical state but rather upon the availability of electrons from neighboring atoms.

A comparison of the experimentally measured Kα satellite energy shifts with the results of Hartree-Fock calculations demonstrated that for those compounds where interatomic vacancy transfer dominates (as indicated by the low degree of L-shell ionization) M-shell vacancy transfer processes are even more significant. What has yet to be determined is the extent to which L- and K-vacancy transfer are accomplished directly by interatomic M → L and M → K transitions versus interatomic M → M transitions with a subsequent intra-atomic cascade of M → L and M → K transitions. Evidence for direct interatomic electron transfer to all three levels is provided by the fact that Si has a higher p_L value than does SiF_4 even though the satellite energy shifts show that SiF_4 has more M-shell vacancies than does Si. Experiments aimed at studying Auger transitions and Kβ x-ray transitions in these two compounds may provide a clearer understanding of the role

of these interatomic processes.

A determination of the various components of the peak widths including spectrometer resolution, extended path length in low density gases, M-shell vacancy distribution and a residual factor (i.e. multiplet structure) was shown to be in good agreement with the experimentally observed peak widths. Other sources of broadening such as molecular dissociation Doppler shift, lifetime effects, target atom recoil Doppler shift, and vibrational excitation were shown to be insignificant in this work.

Finally, theoretical (BEA) calculations of p_L for the projectiles and targets utilized revealed that the magnitudes of the theoretical p_L values were in general much greater than the experimental values. The Z dependence of p_L is much better represented by the calculations for 23.5 MeV O ions than those for 5.8 MeV He ions. Accounting for the increase in the L-binding energies of the remaining L-electrons as each L-electron is removed brings the theoretical results into much better agreement with experiment.

REFERENCES

1. D. J. Nagel and W. L. Baun, in X-ray Spectroscopy, edited by L. V. Azaroff (McGraw-Hill, New York, 1974), p. 445.

2. J. A. Bearden and A. F. Burr, Rev. Mod. Phys. 39, 78 (1967).

3. A. Rosen and I. Lindgren, Phys. Rev. 176, 114 (1968).

4. A. Fahlman, K. Hamrin, J. Hedman, R. Nordberg, C. Nordling, and K. Siegbahn, Nature 210, 4 (1966).

5. R. L. Watson and J. O. Rasmussen, J. Chem. Phys. 47, 778 (1967).

6. A. Faessler and M. Goehring, Naturwiss, 39, 169 (1952).

7. M. Siegbahn and W. Stenström, Physikal Z 17, 318 (1916).

8. G. Wentzel, Ann. d. Physik 66, 437 (1921).

9. D. W. Fischer and W. L. Baun, J. Appl. Phys. 36, 534 (1965).

10. E. H. Kennard and L. Ramberg, Phys. Rev. 46, 1040 (1934).

11. U. Chun, in Proceedings of the International Conference on Inner Shell Ionization Phenomena, Atlantic (USAEC Report No. CONF-720404, Oak Ridge, TN, 1973).

12. V. F. Demekhin and V. P. Sachenko, Bull. Acad. Sci. USSR 31, 921 (1967).

13. K. Läuger, J. Phys. Chem. Solids 33, 1343 (1972).

14. T. A. Carlson, Photoelectron and Auger Spectroscopy (Plenum Press, New York, 1975).

15. T. Åberg, in Proceedings of the International Symposium on X-ray Spectra and Electronic Structure of Matter, Munich, 1972 (unpublished).

16. C. P. Bhalla, Phys. Rev. A 12, 122 (1975).

17. D. L. Matthews, B. M. Johnson, and C. F. Moore, Phys. Rev. A 10, 451 (1974).

18. P. Richard, J. Bolger, D. K. Olsen, and C. F. Moore, Phys. Lett. 41A, 269 (1972).

19. P. G. Burkhalter, A. R. Knudson, D. J. Nagel, and K. L. Dunning, Phys. Rev. A 6, 2093 (1972).

20. J. McWherter, D. K. Olsen, H. H. Wolter and C. F. Moore, Phys. Rev. A 10, 200 (1974).

21. R. L. Watson, T. Chiao, and F. E. Jenson, Phys. Rev. Lett. 35, 254 (1975).

22. R. L. Kauffman, K. A. Jamison, T. J. Gray, and P. Richard, Phys. Rev. Lett. 36, 1074 (1976).

23. F. Hopkins, A. Little, N. Cue, and V. Dutkiewicz, Phys. Rev. Lett. 37, 1100 (1976).

24. H. A. Liebhafsky, A. G. Pfeiffer, E. H. Winslow, and P. D. Zemany in X-rays, Electrons, and Analytical Chemistry (John Riley & Sons, Inc., New York, 1972).

25. E. P. Bertin, in Principles and Practice of X-Ray Spectrometric Analysis, (Plenum Press, New York, 1975).

26. E. Storm and H. I. Isreal, Nucl. Data A7, 565 (1970).

27. R. L. Watson, F. E. Jenson, and T. Chiao, Phys. Rev. A 10, 1230 (1974).

28. R. L. Watson, H. R. Bowman, and S. G. Thompson, Phys. Rev. 162, 1169 (1967).

29. R. L. Watson, A. K. Leeper, B. I. Sonobe, T. Chiao, and F. E. Jenson, Phys. Rev. A 15, 914 (1977).

30. C. P. Bhalla, N. O. Folland, and M. A. Hein, Phys. Rev. A 8, 649 (1973).

31. F. Hopkins, D. O. Elliott, C. P. Bhalla, and P. Richard, Phys. Rev. A 8, 2952 (1973).

32. C. P. Bhalla, Phys. Rev. A 8, 2877 (1973).

33. J. A. Bearden, Rev. Mod. Phys. 39, 78 (1967).

34. D. G. McCrary and P. Richard, Phys. Rev. A 5, 1249 (1972).

35. T. L. Hardt, Ph.D. thesis, Texas A&M University, 1975 (unpublished).

36. K. A. Jamison, J. M. Hill, J. Oltjen, C. W. Woods, R. L. Kauffman, T. J. Gray, and P. Richard, Phys. Rev. A 14, 937 (1976).

37. J. Valasek, Phys. Rev. 53, 274 (1938).

38. P. E. Best, Phys. Rev. B 3, 4377 (1971).

39. P. H. Citrin, J. Electron Spect. and Rel. Phenom. 5, 273 (1974).

40. P. H. Citrin, J. E. Rowe, and S. B. Christman, Phys. Rev. B 14, 2642 (1976).

41. P. H. Citrin, Phys. Rev. Lett. 31, 1164 (1973).

42. R. Mann, F. Folkmann, and K.-O. Groeneveld, Phys. Rev. Lett. 37, 1674 (1976).

43. R. D. Evans, The Atomic Nucleus (McGraw-Hill, New York, 1972).

44. J. P. Desclaux, At. Data Nucl. Data Tables 12, 311 (1973).

45. E. J. McGuire, Phys. Rev. 185, 1 (1969).

46. E. J. McGuire, Phys. Rev. A 2, 273 (1970).

47. H. D. Betz, F. Bell, H. Panke, G. Kalkoffen, M. Welz, and D. Evers, Phys. Rev. Lett. 33, 807 (1974).

48. U. Gelius, J. Electron Spect. and Rel. Phenom. 5, 985 (1974).

49. G. Friedlander, J. W. Kennedy, and J. M. Miller, Nuclear and Radiochemistry (John Wiley & Sons, New York, 1964).

50. J. P. Desclaux and P. Pyykko, Chem. Phys. Lett. 29, 534 (1974).

51. O. Keski-Rahkonen and M. O. Krause, J. Electron Spect. and Rel. Phenom. 9, 371 (1976).

52. L. Pauling, The Nature of the Chemical Bond (Cornell U.P., Ithaca, N.Y., 1960).

53. C. K. Jorgensen and H. Berthou, Mat. fys. Medd. Danske Vidensk Selskab 38 no 15 (1972).

54. D. B. Adams, J. Electron Spect. and Rel. Phenom. 10, 247 (1977).

55. Handbook of Chemistry and Physics, edited by R. C. Weast (Chemical Rubber Publishing Co., Cleveland, Ohio, 1975-1976), 56th ed.

56. J. S. Hansen, Phys. Rev. A 8, 822 (1973).

57. E. Gerjuoy, Phys. Rev. 148, 54 (1966).

58. L. Vriens, Proc. Phys. Soc. Lond. 90, 935 (1967).

59. R. L. Kauffman, J. H. McGuire, P. Richard, and C. F. Moore, Phys. Rev. A 8, 1233 (1973).

60. J. H. McGuire and P. Richard, Phys. Rev. A 8, 1374 (1973).

61. A. B. Wittkower and H. D. Betz, Atomic Data 5, 113 (1973).

62. R. L. Kauffman, F. Hopkins, C. W. Woods, and P. Richard, Phys. Rev. Lett. 31, 621 (1973).

63. K. W. Hill, B. L. Doyle, S. M. Shafroth, D. H. Madison, and R. D. Deslattes, Phys. Rev. A 13, 1334 (1976).

64. D. K. Olsen and C. F. Moore, Phys. Rev. Lett. 33, 194 (1974).

65. F. P. Larkins, Aust. J. Phys. 27, 177 (1974).

66. I. N. Levine, Quantum Chemistry (Allyn and Bacon, Inc., Boston, 1974).

67. A. G. Turner, Methods in Molecular Orbital Theory (Prentice-Hall, Inc., Englewood Cliffs, N.J., 1974).

68. C. C. J. Roothaan, Rev. Mod. Phys. 32, 179 (1960).

69. C. Froese Fischer, Comput. Phys. Commun. 1, 151 (1969).

70. T. Åberg, Phys. Rev. 162, 5 (1967).

71. H. Panke, F. Bell, H. D. Betz, and W. Stehling, Nucl. Instr. 132, 25 (1976).

72. F. Herman and S. Skillman, Atomic Structure Calculations (Prentice-Hall, Englewood Cliffs, N.J., 1963).

73. D. Burch and P. Richard, Phys. Rev. Lett. 25, 983 (1970).

74. D. H. Madison, K. W. Hill, B. L. Doyle, and S. M. Shafroth, Phys. Lett. 48A, 249 (1974).

VITA

John Allen Demarest was born the son of Beatrice and Burdette Demarest on June 30, 1945 in East Chicago, Indiana. His father currently resides in Caldwell, New Jersey where Captain Demarest graduated from James Caldwell High School in 1963. He was commissioned an officer in the United States Air Force upon graduation from Syracuse University in 1967 where he earned a B.S. degree in Chemical Engineering. He has since served on active duty as a fighter pilot. In 1971-1972 he served in the Vietnam War as an F-4E aircraft commander and flight commander.

He was selected in 1975 by the Air Force Institute of Technology for education in the present degree program. He is a member of the Phi Lambda Upsilon Chemical Honorary.

Captain Demarest will reside at 10410 Sierra Bonita, N.E., Albuquereque, N.M. with his wife, Teddy, and children, Tina and Stephen. He will conduct research in the Nuclear Systems Branch of the Air Force Weapons Laboratory at Kirtland AFB, N.M.

The typist for this thesis was Molly Allen.